Report No.339

epaResearch
Climate - Water - Sustainability
Identifying pressures • Informing policy • Developing solutions

High-resolution Climate Projections for Ireland – A Multi-model Ensemble Approach

Authors: Paul Nolan and Jason Flanagan

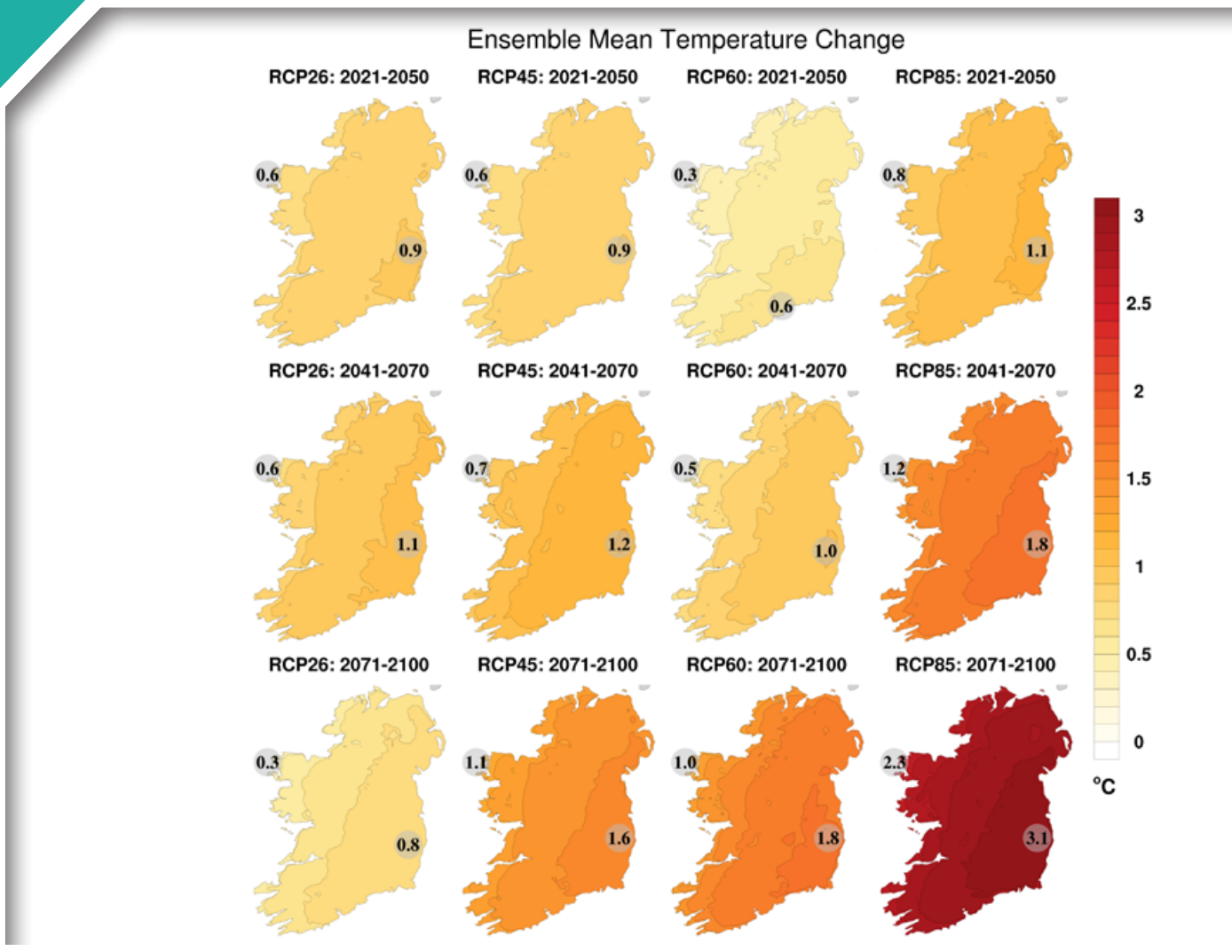

www.epa.ie

Rialtas na hÉireann
Government of Ireland

ENVIRONMENTAL PROTECTION AGENCY

The Environmental Protection Agency (EPA) is responsible for protecting and improving the environment as a valuable asset for the people of Ireland. We are committed to protecting people and the environment from the harmful effects of radiation and pollution.

The work of the EPA can be divided into three main areas:

Regulation: *We implement effective regulation and environmental compliance systems to deliver good environmental outcomes and target those who don't comply.*

Knowledge: *We provide high quality, targeted and timely environmental data, information and assessment to inform decision making at all levels.*

Advocacy: *We work with others to advocate for a clean, productive and well protected environment and for sustainable environmental behaviour.*

Our Responsibilities

Licensing

We regulate the following activities so that they do not endanger human health or harm the environment:

- waste facilities *(e.g. landfills, incinerators, waste transfer stations)*;
- large scale industrial activities (*e.g. pharmaceutical, cement manufacturing, power plants)*;
- intensive agriculture *(e.g. pigs, poultry)*;
- the contained use and controlled release of Genetically Modified Organisms *(GMOs)*;
- sources of ionising radiation *(e.g. x-ray and radiotherapy equipment, industrial sources)*;
- large petrol storage facilities;
- waste water discharges;
- dumping at sea activities.

National Environmental Enforcement

- Conducting an annual programme of audits and inspections of EPA licensed facilities.
- Overseeing local authorities' environmental protection responsibilities.
- Supervising the supply of drinking water by public water suppliers.
- Working with local authorities and other agencies to tackle environmental crime by co-ordinating a national enforcement network, targeting offenders and overseeing remediation.
- Enforcing Regulations such as Waste Electrical and Electronic Equipment (WEEE), Restriction of Hazardous Substances (RoHS) and substances that deplete the ozone layer.
- Prosecuting those who flout environmental law and damage the environment.

Water Management

- Monitoring and reporting on the quality of rivers, lakes, transitional and coastal waters of Ireland and groundwaters; measuring water levels and river flows.
- National coordination and oversight of the Water Framework Directive.
- Monitoring and reporting on Bathing Water Quality.

Monitoring, Analysing and Reporting on the Environment

- Monitoring air quality and implementing the EU Clean Air for Europe (CAFÉ) Directive.
- Independent reporting to inform decision making by national and local government *(e.g. periodic reporting on the State of Ireland's Environment and Indicator Reports)*.

Regulating Ireland's Greenhouse Gas Emissions

- Preparing Ireland's greenhouse gas inventories and projections.
- Implementing the Emissions Trading Directive, for over 100 of the largest producers of carbon dioxide in Ireland.

Environmental Research and Development

- Funding environmental research to identify pressures, inform policy and provide solutions in the areas of climate, water and sustainability.

Strategic Environmental Assessment

- Assessing the impact of proposed plans and programmes on the Irish environment *(e.g. major development plans)*.

Radiological Protection

- Monitoring radiation levels, assessing exposure of people in Ireland to ionising radiation.
- Assisting in developing national plans for emergencies arising from nuclear accidents.
- Monitoring developments abroad relating to nuclear installations and radiological safety.
- Providing, or overseeing the provision of, specialist radiation protection services.

Guidance, Accessible Information and Education

- Providing advice and guidance to industry and the public on environmental and radiological protection topics.
- Providing timely and easily accessible environmental information to encourage public participation in environmental decision-making *(e.g. My Local Environment, Radon Maps)*.
- Advising Government on matters relating to radiological safety and emergency response.
- Developing a National Hazardous Waste Management Plan to prevent and manage hazardous waste.

Awareness Raising and Behavioural Change

- Generating greater environmental awareness and influencing positive behavioural change by supporting businesses, communities and householders to become more resource efficient.
- Promoting radon testing in homes and workplaces and encouraging remediation where necessary.

Management and structure of the EPA

The EPA is managed by a full time Board, consisting of a Director General and five Directors. The work is carried out across five Offices:

- Office of Environmental Sustainability
- Office of Environmental Enforcement
- Office of Evidence and Assessment
- Office of Radiation Protection and Environmental Monitoring
- Office of Communications and Corporate Services

The EPA is assisted by an Advisory Committee of twelve members who meet regularly to discuss issues of concern and provide advice to the Board.

EPA RESEARCH PROGRAMME 2014-2020

High-resolution Climate Projections for Ireland – A Multi-model Ensemble Approach

(2014-CCRP-MS.23)

EPA Research Report

Prepared for the Environmental Protection Agency

by

Irish Centre for High-End Computing (ICHEC) and Met Éireann

Authors:

Paul Nolan and Jason Flanagan

ENVIRONMENTAL PROTECTION AGENCY
An Ghníomhaireacht um Chaomhnú Comhshaoil
PO Box 3000, Johnstown Castle, Co. Wexford, Ireland

Telephone: +353 53 916 0600 Fax: +353 53 916 0699
Email: info@epa.ie Website: www.epa.ie

ACKNOWLEDGEMENTS

This report is published as part of the EPA Research Programme 2014–2020. The EPA Research Programme is a Government of Ireland initiative funded by the Department of Communications, Climate Action and Environment. It is administered by the Environmental Protection Agency, which has the statutory function of co-ordinating and promoting environmental research.

The authors would like to acknowledge the members of the project steering committee, namely Ray McGrath (University College Dublin), Philip O'Brien (EPA), Margaret Desmond (EPA), Frank McGovern (EPA), Saji Varghese (Met Éireann), Alice Wemaere (EPA), Keith Lambkin (Met Éireann), John O'Neill (Department of Communications, Climate Action and Environment) and Patrick Fournet (Met Éireann). In addition, we thank Basanta Kumar Samala (ICHEC) for preparing the CMIP5 data for driving the WRF climate simulations.

The authors wish to acknowledge the Irish Centre for High-End Computing (ICHEC) for the provision of computational facilities and support.

Cover image: 21st century regional climate model (RCM) ensemble projections of 2-m temperature for the four Representative Concentration Pathways: RCP2.6, RCP4.5, RCP6.0 and RCP8.5. All RCM ensemble members were run with 4-km grid spacing. In each case, the future 30-year period is compared with the past period 1976–2005. The numbers included on each plot are the minimum and maximum projected changes, displayed at their locations.

DISCLAIMER

This report is based on research carried out/data from January 2017 to December 2020. More recent data may have become available since the research was completed.

The EPA Research Programme addresses the need for research in Ireland to inform policymakers and other stakeholders on a range of questions in relation to environmental protection. These reports are intended as contributions to the necessary debate on the protection of the environment.

EPA RESEARCH PROGRAMME 2014–2020
Published by the Environmental Protection Agency, Ireland

ISBN: 978-1-84095-934-5 September 2020

Price: Free Online version

Project Partners

Dr Paul Nolan
Irish Centre for High-End Computing (ICHEC)
NUI Galway
Grand Canal Quay
Dublin 2
Ireland
Tel.: + 353 1 529 1032
Email: paul.nolan@ichec.ie

Dr Jason Flanagan
ICHEC
NUI Galway
Co. Galway
Ireland
Tel.: + 353 91 397 824
Email: jason.flanagan@ichec.ie

Contents

List of Figures

List of Tables

Executive Summary

The method of regional climate modelling was employed to assess the impacts of a warming climate on the 21st-century climate of Ireland. The regional climate model (RCM) simulations were run at high spatial resolution (3.8 and 4 km), the first systematic study of its kind at this scale, thus allowing a better evaluation of the local effects of climate change. To address the issue of uncertainty, a multi-model ensemble approach was employed. Through the ensemble approach, the uncertainty in the projections can be partly quantified, thus providing a measure of confidence in the projections. Simulations were run for the reference period 1981–2000 and the future period 2041–2060. Differences between the two periods provide a measure of climate change. The Consortium for Small-scale Modeling–Climate Limited-area Modelling (COSMO-CLM) and Weather Research and Forecasting (WRF) RCMs were used to downscale the following Coupled Model Intercomparison Project – Phase 5 (CMIP5) global climate model (GCM) datasets: CNRM-CM5, EC-EARTH (four ensemble members), HadGEM2-ES, MIROC5 and MPI-ESM-LR. To account for the uncertainty in future greenhouse gas emissions, the future climate was simulated under both the Representative Concentration Pathway 4.5 (RCP4.5) and RCP8.5 scenarios.

The RCMs were validated by downscaling ERA-Interim global reanalyses and the GCM datasets for the period 1981–2000 and comparing the output with observational data. Extensive validations were carried out to test the ability of the RCMs to accurately model the climate of Ireland. Results confirm that the output of the RCMs exhibit reasonable and realistic features, as documented in the historical data record, and consistently demonstrate improved skill over the GCMs. Moreover, an increase in the spatial resolution of the RCMs resulted in a general increase in skill. However, it was found that although RCM accuracy increased with higher spatial resolution, reducing horizontal grid spacing below 4 km provided relatively little added value. The validation analysis confirms that the RCM configurations and domain size of the current study are capable of accurately simulating the current and past climate of Ireland.

The climate projections of the current report are in broad agreement with previous research, which adds a measure of confidence to the projections. Moreover, the current report presents projections of additional climate fields and derived variables that are of vital importance to sectors such as agriculture, health, energy, biodiversity and transport. It is envisaged that the research will inform policy and further the understanding of the potential environmental impacts of climate change in Ireland at a local scale.

Temperature Projections

Mid-century mean annual temperatures are projected to increase by 1–1.2°C and 1.3–1.6°C for the RCP4.5 and RCP8.5 scenarios, respectively. Temperature projections show a clear west-to-east gradient, with the largest increases in the east. Warming is enhanced for the extremes (i.e. hot days and cold nights), with the warmest 5% of daily maximum temperatures projected to increase by 1.0–2.2°C compared with the baseline period. The coldest 5% of daily minimum temperatures are projected to rise by 1–2.4°C. Heatwave events are expected to increase by the middle of the century; over the 20-year period (2041–2060), increases in heatwave events range from 1 to 8 for the RCP4.5 scenario and from 3 to 15 for the RCP8.5 scenario, with the largest increases in the south-east. Averaged over the whole country, the number of frost days (days when the minimum temperature is lower than 0°C) is projected to decrease by 45% and 58% for the RCP4.5 and RCP8.5 scenarios, respectively. Similarly, the number of ice days (days when the maximum temperature is lower than 0°C) is projected to decrease by 68% and 78% for the RCP4.5 and RCP8.5 scenarios, respectively. It is worth noting that periods of frost and ice are important environmental drivers that trigger phenological phases in many plant and animal species. Changes in the occurrence of these weather types may disrupt the life cycles of these species. The projected increase in heatwaves will have a direct impact on public health and mortality but this may be offset by the projected decrease in frost and ice days.

Precipitation, Snow and Surface Humidity Projections

Substantial decreases in precipitation are projected for the summer months, with reductions ranging from ≈0% to 11% for the RCP4.5 scenario and from 2% to 17% for the RCP8.5 scenario. Other seasons, and over the full year, show small projected changes in precipitation. However, the mid-century precipitation climate is expected to become more variable with substantial projected increases in both dry periods and heavy precipitation events.

The frequencies of heavy precipitation events show notable increases over the year as a whole and in the winter and autumn months, with "likely" projected increases of 5–19%.[1] The projected increase in evapotranspiration, noted for all seasons, may offset flooding events caused by the expected increases in heavy rainfall. However, it is recommended that additional hydrological modelling be undertaken to improve understanding of the potential impact on flooding. The number of extended dry periods (defined as at least 5 consecutive days for which the daily precipitation is less than 1 mm) is also projected to increase substantially by the middle of the century over the full year and for all seasons except spring. The projected increases in dry periods are largest for summer, with "likely" values of +11% and +48% for the RCP4.5 and RCP8.5 scenarios, respectively. The precipitation projections, summarised previously, were found to be generally robust with over 66% of the ensemble members in agreement.

Snowfall is projected to decrease substantially by the middle of the century with "likely" reductions of 51% and 60% for the RCP4.5 and RCP8.5 scenarios, respectively.

Specific humidity is projected to increase substantially (≈10%) for all seasons by the middle of the century. Relative humidity is projected to increase slightly (or show ≈0% change) for all seasons except summer. The largest increases are noted for spring (both RCP scenarios) and winter (RCP8.5). For summer, relative humidity is expected to decrease in the south-east and increase in the north-west (both RCP scenarios).

Wind Speed, Storm Tracks and Mean Sea Level Pressure Projections

Mid-century mean 10-m wind speeds are projected to decrease for all seasons. The decreases are largest for summer months under the RCP8.5 scenario. The summer reductions in 10-m wind speed range from 0.3% to 3.4% for the RCP4.5 scenario and from 2% to 5.4% for the RCP8.5 scenario. The frequency of "driving rain" events is projected to decrease for all seasons with the exception of the winter months (RCP8.5), when small increases are projected.

The projections indicate that the mean sea level pressure (MSLP) is projected to increase by ≈1 hPa by the middle of the century, with similar increases noted for all seasons. To assess the potential impact of climate change on extreme cyclonic activity in the North Atlantic, an algorithm was developed to identify and track cyclones as simulated by an ensemble of EURO-CORDEX 12-km downscaled CMIP5 RCMs. The results show an overall reduction of ≈10% in the numbers of storms affecting Ireland and suggest an eastward extension of the more severe wind storms over Ireland and the UK from the middle of the century. It should be noted that because extreme storms are rare events, the storm projections should be considered with a level of caution. Future work will focus on analysing a larger ensemble of downscaled CMIP6 data, thus allowing a more robust statistical analysis of extreme storm track projections.

Agricultural Impacts

The projections, outlined previously, of increases in temperature, heatwaves, heavy precipitation and dry periods/droughts along with decreases in frost and ice days will have direct and substantial effects on agriculture in Ireland by the middle of the century. In addition, the projections indicate an average increase in the length of the growing season by the middle of the century of 12% and 16% for the RCP4.5 and RCP8.5 scenarios, respectively. Similarly, the grazing season, crop heat units (CHUs) and growing degree days (GDDs) for a range of crops are projected to increase substantially by the middle of the century. The results suggest a warming climate may present some

1 A "likely" projection is defined as a projection for which at least 66% of the RCM ensemble members are in agreement. In this case, 66% of the ensemble members project increases in heavy precipitation events of at least 5–19% (spatially) over Ireland. See section 1.2.5 for a full description.

positive opportunities for farming. However, the results should be viewed in the context that a warming climate will also result in an increase in pests as a result of an increase in pest-GDDs and a decrease in frost and ice days, as cold conditions are a key control mechanism for the survival of pests. Furthermore, the projected increase in the frequency of both droughts and heavy rainfall events could be detrimental to the potential gains of a warming climate to the agricultural sector.

Energy Impacts

The energy content of the 120-m wind is projected to decrease for all seasons by the middle of the century. The decreases are largest for summer, with reductions ranging from 2.8% to 8.7% for the RCP4.5 scenario and from 6.5% to 14.1% for the RCP8.5 scenario. To assess the impacts of climate change on solar power in Ireland, projections of solar photovoltaic (PV) power were analysed. Results show a small expected decrease in PV by the middle of the century ranging from ≈0 to 4%. The largest decreases are noted in the north of the country and for the RCP8.5 scenario. The projected change in heating degree days (HDDs) shows that by the middle of the century there will be a greatly reduced requirement for heating in Ireland, with HDDs projected to decrease by 12–17% and 15–21% for the RCP4.5 and RCP8.5 scenarios, respectively. A clear north-to-south gradient is evident for both RCP scenarios, with the largest decreases in the south. The projections show that cooling degree days (CDDs) are expected to slightly increase, suggesting a small increase in air conditioning requirements by the middle of the century. However, the amounts are small compared with HDDs and therefore have a negligible effect on the projected changes in the total energy demand, calculated using the first-order approximation: energy degree days (EDD) = HDD + CDD.

1 Introduction

The objective of this study is to evaluate the effects of climate change on the future climate of Ireland using the method of high-resolution regional climate modelling. There is a lack of research in dynamically downscaled high-resolution (finer than 7-km grid spacing) climate modelling of Ireland, for projections in the medium term. Existing studies have either focused on analysing relatively small ensembles of regional climate model (RCM) simulations at a relatively low spatial resolution (7–12 km) (e.g. McGrath *et al*., 2005; McGrath and Lynch, 2008; Nolan *et al*., 2012, 2014, 2017; Gleeson *et al*., 2013; Nolan, 2015; O'Sullivan *et al*., 2015) or analysed a large ensemble of low-resolution RCM simulations (van der Linden and Mitchell, 2009; Jacob *et al*., 2014). The analysis presented in this study was undertaken to address this lack of research by analysing the output of three high-resolution (≈4 km) RCMs of Ireland, driven by an ensemble of eight global climate model (GCM) datasets, under the Representative Concentration Pathway 4.5 (RCP4.5) and RCP8.5 emission scenarios. Simulations were run for a reference period, 1981–2000, and a future period, 2041–2060. Differences between the two periods are used to provide a measure of the projected climate change.

The current research consolidates and expands on previous national RCM research (e.g. McGrath *et al*., 2005; McGrath and Lynch, 2008; Nolan *et al*., 2012, 2014, 2015, 2017; Gleeson *et al*., 2013; O'Sullivan *et al*., 2015) by running a large ensemble of downscaled simulations, using the most up-to-date RCMs and the RCP4.5 and RCP8.5 scenarios to simulate the future climate of Ireland. Additionally, the accuracy and usefulness of the model predictions are enhanced by increasing the model grid spacings to ≈4 km. Although uncertainty can never be eliminated in climate projections (see sections 1.1 and 1.2.5 for further comments), the large ensemble size (using different RCMs, GCMs and RCPs) allows for a robust quantification of climate projection uncertainty and a measure of confidence to be assigned to the projections. Nevertheless, RCM-downscaling studies will always be limited by the available resources to process large ensembles and will likely underrepresent the full range of possible climate futures.

The climate projections of the current report are in broad agreement with previous research, which adds another measure of confidence to the projections. Moreover, the current report presents projections of additional climate fields and derived variables that are of vital importance to sectors such as agriculture, health, energy, biodiversity and transport. It is envisaged that the research will inform policy and further the understanding of the potential environmental impacts of climate change in Ireland at a local scale.

1.1 Regional Climate Models

The impact of increasing greenhouse gases and changing land use on climate change can be simulated using GCMs. However, on account of computational constraints, long climate simulations using GCMs are currently feasible only with horizontal resolutions of ≈50 km or coarser. Because climate fields such as precipitation, wind speed and temperature are closely correlated to the local topography, this is inadequate to simulate the detail and pattern of climate change and its effects on the future climate of Ireland. Furthermore, and of particular relevance to Ireland, numerous studies have shown that, even at 50-km grid spacing, GCMs severely underresolve both the number and intensity of cyclones (e.g. Zhao *et al*., 2009; Camargo, 2013; Zappa *et al*., 2013).

To overcome these limitations, the RCM method dynamically downscales the coarse information provided by the global models and provides high-resolution information on a subdomain covering Ireland. The computational cost of running the RCM, for a given resolution, is considerably less than that of a global model. The approach has its flaws: all models have errors, which are cascaded in this technique, and new errors are introduced via the flow of data through the boundaries of the regional model. Nevertheless, numerous studies have demonstrated that high-resolution RCMs improve the simulation of fields, such as precipitation (Lucas-Picher *et al*., 2012; Kendon *et al*., 2012, 2014; Bieniek *et al*., 2015; Nolan, 2015, 2017) and topography-influenced phenomena and extremes with relatively small

spatial or short temporal character (Feser *et al*., 2011; Feser and Barcikowska, 2012; Shkol'nik *et al*., 2012; IPCC, 2013a). An additional advantage is that the physically based RCMs explicitly resolve more small-scale atmospheric features and provide a better representation of convective precipitation (Rauscher *et al*., 2010) and extreme precipitation (Kanada *et al*., 2008; Nolan *et al*., 2017). Other examples of the added value of RCMs are improved simulations of near-surface temperature (Feser, 2006; Di Luca *et al*., 2016), European storm damage (Donat *et al*., 2010), strong mesoscale cyclones (Cavicchia and Storch, 2011), North Atlantic tropical cyclone tracks (Daloz *et al*., 2015) and near-surface wind speeds (e.g. Kanamaru and Kanamitsu, 2007; Nolan *et al*., 2014; Nolan, 2015), particularly in coastal areas with complex topography (Feser *et al*., 2011; Winterfeldt *et al*., 2011). The added value of RCMs in the simulation of cyclones is particularly important for the current study, as low pressure systems are the main delivery mechanism for precipitation and wind in Ireland. Furthermore, numerous studies have demonstrated that increased RCM spatial resolution results in a more accurate representation of the climate system. Low-resolution RCMs use parameterised convection schemes, meaning that the heaviest precipitation events (e.g. convective systems on hot summer days) may not be adequately represented in the simulations (Prein *et al*., 2013; Kendon *et al*., 2014). Zängl *et al*. (2015) investigated heavy rainfall events over the North-Alpine region and found that increasing the mesh size (9, 3 and 1 km) resulted in a stepwise improvement in skill. Similarly, Nolan *et al*. (2017) found that RCM accuracy increased with higher spatial resolution; however, reducing the horizontal grid spacing below 4 km provided relatively little added value.

The Intergovernmental Panel on Climate Change (IPCC) has concluded that there is "high confidence that downscaling adds value to the simulation of spatial climate detail in regions with highly variable topography (e.g., distinct orography, coastlines) and for mesoscale phenomena and extremes" (IPCC, 2013a).

1.2 Methods and Climate Models of the Current Study

1.2.1 Climate models and emission scenarios

The future climate of Ireland was simulated at high spatial resolution (3.8 and 4 km) using the Consortium for Small-scale Modeling–Climate Limited-area Modelling (COSMO-CLM; v4.0 and 5.0) and Weather Research and Forecasting (WRF; v3.8) RCMs. The COSMO-CLM RCM is the COSMO weather forecasting model in climate mode (Rockel *et al*., 2008).[2] The COSMO model[3] is the non-hydrostatic operational weather prediction model used by the German weather service (*Deutscher Wetterdienst*; DWD). A detailed description of the COSMO model is given by Doms and Schättler (2002) and Steppeler *et al*. (2003). The WRF model[4] is a numerical weather prediction system designed to serve atmospheric research, climate and operational forecasting needs. The WRF simulations of the present study adopted the Advanced Research WRF (ARW, v3.8.1) dynamical core, with development led by the US National Center for Atmospheric Research (NCAR) (Skamarock *et al*., 2008; Powers *et al*., 2017).

Projections for the future Irish climate were generated by downscaling the following Coupled Model Intercomparison Project Phase 5 (CMIP5; Taylor *et al*., 2012) global datasets:

- the UK Met Office's Hadley Centre Global Environment Model version 2 Earth System (HadGEM2-ES) configuration GCM (W.J. Collins *et al*., 2011);
- four realisations of the EC-Earth consortium GCM (Hazeleger *et al*., 2011);
- the CNRM-CM5 GCM developed by the Centre National de Recherches Météorologiques–Groupe d'études de l'Atmosphère Météorologique (CNRM-GAME) and the Centre Européen de Recherche et de Formation Avancée (Cerfacs) (Voldoire *et al*., 2013);
- the Model for Interdisciplinary Research on Climate (MIROC5) GCM developed by the MIROC5 Japanese research consortium (Watanabe *et al*., 2010);

2 www.clm-community.eu (accessed 29 May 2020).

3 www.cosmo-model.org (accessed 29 May 2020).

4 www.wrf-model.org (accessed 29 May 2020).

- the MPI-ESM-LR Earth System Model developed by the Max Planck Institute for Meteorology (Giorgetta *et al*., 2013).

To account for the uncertainty arising from the estimation of future global emission of greenhouse gases, downscaled GCM simulations based on two RCPs (RCP4.5 and RCP8.5) (Moss *et al*., 2010; van Vuuren *et al*., 2011) were used to simulate the future climate of Ireland.

1.2.2 Model domains and experiment setup

The RCMs were driven by GCM boundary conditions with the following one-way nesting strategies: GCM to 50 km to 18 km to 4 km (COSMO v4); GCM to 18 km to 4 km (COSMO v5); and GCM to 19 km to 3.8 km (WRF). The COSMO v4 50-, 18- and 4-km model domains are shown in Figure 1.1. The COSMO v5 (18 and 4 km) and WRF (19 and 3.8 km) domains are similar to the d02 and d03 domains of Figure 1.1. The advantage of high-resolution RCM simulations is highlighted in Figure 1.2, which shows how the

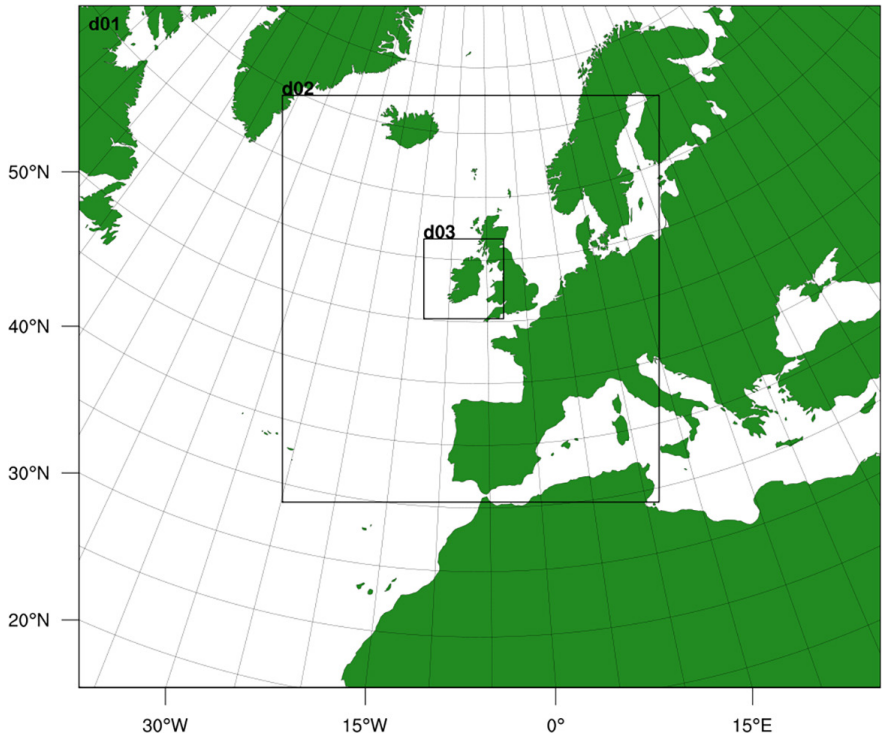

Figure 1.1. The COSMO4-CLM model domains. The d01, d02 and d03 domains have 50-, 18- and 4-km grid spacings, respectively.

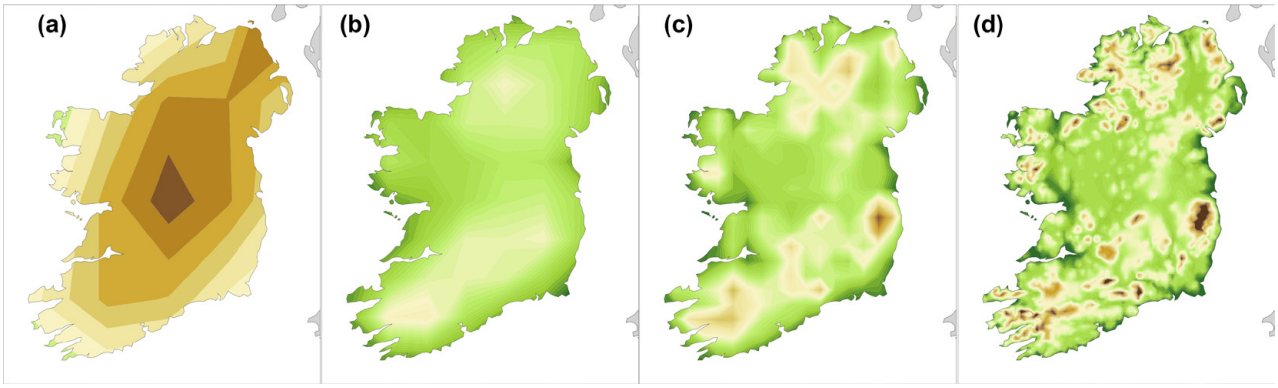

Figure 1.2. The topography of Ireland as resolved by the EC-Earth GCM and the COSMO4-CLM RCM for different spatial resolutions: (a) EC-Earth 125-km grid spacing, (b) COSMO4-CLM 50-km grid spacing, (c) COSMO4-CLM 18-km grid spacing and (d) COSMO4-CLM 4-km grid spacing.

surface topography is better resolved by the higher resolution data. For the current study, only 3.8-km and 4-km grid spacing RCM data are considered. The higher resolution data allow improved estimates of the regional variations of climate projections. The climate fields of the RCM simulations were archived at 3-h intervals. An overview of the COSMO-CLM archived fields are provided in Table 1.1. The WRF archived fields are similar.

The RCM simulations were run on the Irish Centre for High-End Computing (ICHEC) supercomputers. Running such a large ensemble of high-resolution RCMs was a substantial computational task and required extensive use of the ICHEC supercomputer systems over a period of 3–4 years. This archive of data will be made available to the wider research community and general public through the EPA and the Climate Ireland platform.[5]

Table 1.1. Archived data of the COSMO RCM simulations

Variable	Units	Variable	Units
Surface pressure	Pa	Surface lifted index	K
Mean sea level pressure	Pa	Showalter index	K
Surface temperature	K	Surface net downward SW radiation	$W m^{-2}$
2-m temperature	K	Average surface net downward SW radiation	$W m^{-2}$
2-m dew point temperature	K	Direct surface downward SW radiation	$W m^{-2}$
U-component of 10-m wind	$m s^{-1}$	Averaged direct surface downward SW radiation	$W m^{-2}$
V-component of 10-m wind	$m s^{-1}$	Averaged surface diffuse downward SW radiation	$W m^{-2}$
Surface roughness length	m	Averaged surface diffuse upward SW radiation	$W m^{-2}$
Maximum 10-m wind speed	$m s^{-1}$	Averaged downward LW radiation at the surface	$W m^{-2}$
Surface-specific humidity	$kg kg^{-1}$	Averaged upward LW radiation at the surface	$W m^{-2}$
2-m specific humidity	$kg kg^{-1}$	Averaged surface net downward LW radiation	$W m^{-2}$
2-m relative humidity	%	Averaged surface photosynthetic active radiation	$W m^{-2}$
Snow surface temperature	K	Surface albedo	0–1 (fraction)
Thickness of snow	m	Surface latent heat flux	$W m^{-2}$
Height of freezing level	m	Surface sensible heat flux	$W m^{-2}$
Total precipitation amount	$kg m^{-2}$	Surface evaporation	$kg m^{-2}$
Precipitation rate	$kg m^{-2} s^{-1}$	Soil temperature (eight levels)	K
Large-scale rainfall	$kg m^{-2}$	Soil water content (eight levels)	m
Convective rainfall	$kg m^{-2}$	Daily average 2-m temperature	K
Large-scale snowfall	$kg m^{-2}$	Daily maximum 2-m temperature	K
Convective snowfall	$kg m^{-2}$	Daily minimum 2-m temperature	K
Large-scale graupel	$kg m^{-2}$	Daily duration of sunshine	s
Surface runoff	$kg m^{-2}$	Daily relative duration of sunshine	s
Subsurface runoff	$kg m^{-2}$	Daily evapotranspiration	mm
Vertical integrated water vapour	$kg m^{-2}$	U-component of wind[a]	$m s^{-1}$
Vertical integrated cloud ice	$kg m^{-2}$	V-component of wind[a]	$m s^{-1}$
Vertical integrated cloud water	$kg m^{-2}$	Air density[a]	$kg m^{-3}$
Total cloud cover	0–1 (fraction)	Wind speed[a]	$m s^{-1}$
Low cloud cover	0–1 (fraction)	Cube wind speed[a]	$m^3 s^{-3}$
Medium cloud cover	0–1 (fraction)	Wind direction[a]	degree
High cloud cover	0–1 (fraction)	Monthly (1–48) Standardized Precipitation Index	–3 to 3
CAPE 3 km	$J kg^{-1}$		

Note: with the exception of the daily and monthly data, all variables are archived at 3-h intervals.

[a]Variables archived at 20, 40, ..200 m.

LW, longwave; SW, shortwave; U-component, zonal velocity; V-component, meridional velocity.

5 www.climateireland.ie (accessed 29 May 2020).

The choice of domain size, nesting downscaling ratio and grid spacing was decided upon following the recommendations of previous studies. For example, several studies found that the parent–grid ratio should be no larger than approximately 1:12 (e.g. Denis *et al*., 2003; Antic *et al*., 2006). Brisson *et al*. (2015) investigated the sensitivity of simulating precipitation over Belgium by downscaling ERA-Interim data. They concluded that an intermediate nesting ratio of approximately 3 was essential for the correct representation of precipitation. Rummukainen (2010) recommended that an RCM domain should be "large enough to allow for desired phenomena related to topographic influence and small-scale atmospheric processes to develop, but still sufficiently small so that the flow solution does not deviate too much from the driving model". The 50- and 18-km domains of the current study are large enough to allow changes to synoptic scales. Ideally, the domain for the finest grid size would be larger in order to allow the RCM to fully develop small-scale dynamical structures in the interior of the domain, superposed on the coarse-scale information that enters through the lateral boundaries. However, the size of the inner domains was constrained by available computational resources. Finally, the choice of grid spacing was determined by both computational constraints and a careful preliminary validation experiment (e.g. Nolan *et al*., 2017; Flanagan *et al*., 2019). A number of 1-month validation simulations were run using different physics schemes in order to determine the most accurate physics options to use for the current study. It was found that although the RCM accuracy increased with a higher spatial resolution, reducing the horizontal grid spacing below 4 km provided relatively little added value (Nolan *et al*., 2017). The results of the preliminary experiments determined the model configurations of the current study (Nolan *et al*., 2017; Flanagan *et al*., 2019).

An overview of the simulations is presented in Table 1.2. The GCM realisations result from running the same GCM with slightly different initial conditions, i.e. the starting date of historical simulations. Data from two time slices, 1981–2000 (the reference period) and 2041–2060 (the future period), were used for analysis of projected changes in the middle of the 21st-century Irish climate. These periods were chosen because they are the longest decadal time periods common to all RCM simulations. The historical period was compared with the corresponding future period for all simulations within the same RCM-GCM group. This results in future anomalies for each model run,

Table 1.2. Details of the ensemble RCM simulations

RCM	GCM (no. of ensemble members, realisations)	Nesting strategy (km)	Historical period	RCP4.5 (no. of ensemble comparisons)	RCP8.5 (no. of ensemble comparisons)
COSMO4	HadGEM2-ES (r1i1p1)	50, 18, 4	1980–2000	2020–2060 (1)	2020–2060 (1)
COSMO4	EC-Earth x3 (r1i1p1, r13i1p1 & r14i1p1)	50, 18, 4	1980–2005	2020–2060 (9)	2020–2060 (9)
COSMO5	EC-Earth (r12i1p1)	18, 4	1975–2005	2006–2100 (1)	2006–2100 (1)
COSMO5	MPI-ESM-LR (r1i1p1)	18, 4	1975–2005	2006–2100 (1)	2006–2100 (1)
COSMO5	CNRM-CM5 (r1i1p1)	18, 4	1975–2005	2006–2100 (1)	2006–2100 (1)
COSMO5	HadGEM2-ES (r1i1p1)	18, 4	1975–2005	2006–2100 (1)	2006–2100 (1)
COSMO5	MIROC5 (r1i1p1)	18, 4	1975–2005	2006–2100 (1)	2006–2100 (1)
WRF	MIROC5 (r1i1p1)	19, 3.8	1975–2005	2006–2100 (1)	2006–2100 (1)

The rows present information on the RCM used, corresponding downscaled GCM and number of realisations, nesting strategy, historical simulated period, future simulated period, RCP details and the number of ensemble comparisons.

i.e. the difference between future and past. In this study the ensemble members of the downscaled GCM simulations are treated as independent estimates of the climate system and are given equal weight. Only the differences between the simulations of the past and future climate for each model will be used in the analysis. While model biases may not be invariant under future scenarios of greenhouse gas emissions, this approach may reduce the impact of model bias.

1.2.3 Regional climate model validation

The RCMs were validated by downscaling ERA-Interim reanalyses and the GCM datasets for the period 1981–2000 and comparing the output with observational data. Extensive validations were carried out to test the ability of the RCMs to accurately model the climate of Ireland. Results confirm that the output of the RCMs exhibit reasonable and realistic features as documented in the historical data record (Nolan *et al*., 2017; Flanagan *et al*., 2019; Werner *et al*., 2019).

1.2.4 Model domains and experiment setup

Simulations were run for a reference period, 1981–2000, and a future period, 2041–2060. Differences between the two periods provide a measure of climate change. To provide a more comprehensive examination of climate change, projected changes in the standard deviation are considered in context with changes in the mean. Analyses of changes in the standard deviation provide information on projected changes in the shape (or variability) of the distribution of a climate field. In particular, analyses of changes in the mean and standard deviation provide a more comprehensive understanding of projections of extreme events.

To illustrate this concept, Figure 1.3 presents a schematic of past and future probability distributions of precipitation.[6] Figure 1.3a presents a future with increases in mean precipitation and no change in the standard deviation. In this future world, the total amount of precipitation increases, the amount of dry events decreases and the amount of wet events increases. Figure 1.3b presents a future with no change in mean precipitation and an increase in the standard deviation. In this future world, the total amount of precipitation remains constant, with an increase in both dry and wet events (i.e. increased variability). Conversely, Figure 1.3c shows that a decrease in variability, coupled with no change in mean precipitation, results in a decrease in both dry and wet events. Finally, Figure 1.3d illustrates how an increase in the mean and variability results in large increases in wet events.

To create a large ensemble, all RCM outputs were regridded to a common 4-km grid over Ireland using the method of bilinear interpolation. This results in 16 RCP4.5 and 16 RCP8.5 ensemble comparisons. The relatively large number of comparisons allows for the uncertainty of the projections to be partly quantified, providing a measure of confidence in the predictions.

1.2.5 Overview of climate projection uncertainty

Climate change projections are subject to uncertainty, which limits their utility. Fronzek *et al*. (2012) suggest that there are four main sources of uncertainty: (1) the natural variability of the climate system; (2) uncertainties on account of the formulation of the models themselves; (3) uncertainties in future regional climate because of the coarse resolution of GCMs; and (4) uncertainties in the future atmospheric composition, which affects the radiative balance of the Earth. The uncertainties arising from (1) and (2) can be addressed, in part, by employing a multi-model ensemble approach (Déqué *et al*., 2007; van der Linden and Mitchell, 2009; Jacob *et al*., 2014). The ensemble approach of the current project analyses the output of three RCMs, driven by several GCMs, to simulate climate change (see Table 1.2). Through the ensemble approach, the uncertainty in the projections can be partly quantified, providing a measure of confidence in the predictions. The uncertainty arising from (3) is addressed in the current work by running the RCM simulations at the high spatial resolution of ≈4-km grid spacings. To account for the uncertainty

6 Note: the figures are schematic representations of the distribution of standardised precipitation data. The distribution of raw precipitation data does not generally follow a normal distribution. The purpose of Figure 1.3 is simply to illustrate the concepts of how projected changes in the mean and variance can lead to substantial changes in the extremes.

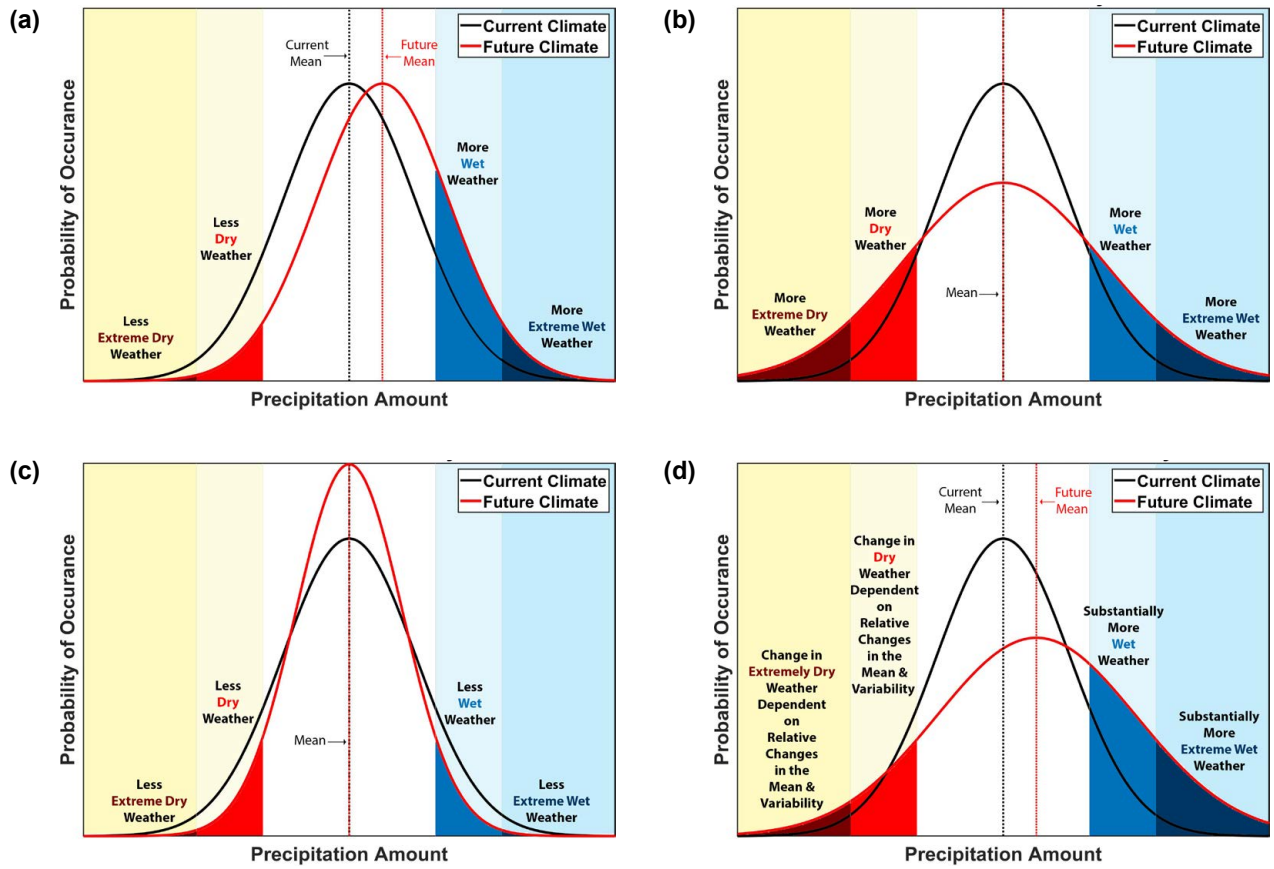

Figure 1.3. Schematic illustrating the effects of changes in the mean and standard deviation on the probability of low and high precipitation: (a) an increase in the mean with no change in the standard deviation, (b) an increase in the standard deviation with no change in the mean, (c) a decrease in the standard deviation with no change in the mean and (d) an increase in both the mean and standard deviation.

arising from (4), the future climate is simulated under both the RCP4.5 and RCP8.5 emission scenarios.

A disagreement between RCM ensemble projections can result in large individual outliers,[7] skewing the mean ensemble projection. For this reason, it can be informative to also consider percentiles when analysing an ensemble of future projections. The relatively large ensemble size of the current study allows the construction of a probability density function (pdf) of climate projections. Likelihood values can then be assigned to the projected changes. For example, if the mean (and median) ensemble projection is positive for a particular climate field, the 33rd percentile of the ensemble of projected changes is considered and is defined as the "likely" projected increase. This is a projection such that over 66% of the RCM ensemble members project greater increases. Similarly, if the mean (and median) ensemble projection is negative, the 66th percentile of the ensemble of projections is considered and is defined as the "likely" projected decrease. In this case, over 66% of the RCM ensemble members project greater decreases. In a similar manner, a "very likely" projection is defined as a projection for which at least 90% of the RCM ensemble members are in agreement; the "as likely as not" projection is defined as the 50th percentile (median) projection.

This method of analysing percentiles allows for a better understating of climate change uncertainty and allows for a quantification of conservative and robust ("likely") projections. Conversely, the likelihood method allows for policymakers to consider more "unlikely"

7 However, there is information in the outliers that may be of relevance in specific circumstances and so they cannot be entirely discounted. For example, analysis of the outliers allows policymakers to plan for "low-probability, high-impact" climate projections.

(and possibly high-impact) climate projections. These definitions, based on an ensemble of 16 members for each RCP, provide a statistically based descriptive measure of the climate change projection uncertainty.

Note that the accuracy of these statistical descriptions is based on the assumption that the ensemble members represent an unbiased sampling of the (unknown) future climate. It is also important to stress that the likelihood values presented in the current study (and similarly in studies such as Murphy *et al.*, 2009; IPCC, 2013b; and Lowe *et al.*, 2018) are derived from the most up-to-date evidence currently available. Therefore, the "likelihood" values only apply to the specific sets of high-resolution models and experimental design of the current study. Future improvements in modelling may alter the projections, as uncertainty is expected to be further reduced. Future work will focus on reducing this uncertainty by increasing the ensemble size and employing more up-to-date RCMs (including fully coupled atmosphere–ocean–wave models) to downscale recently completed CMIP6 GCMs under the full range of the Scenario Model Intercomparison Project (ScenarioMIP) "tier 1" Shared Socioeconomic Pathways (SSPs), namely SSP1-2.6, SSP2-4.5, SSP3-7.0 and SSP5-8.5 (Riahi *et al*., 2017).

2 Regional Climate Model Validations

The RCMs were validated by running 20-year simulations of the past Irish climate for the time period 1981–2000, driven by both ERA-Interim reanalysis (Dee *et al*., 2011) and the GCM datasets, and comparing the output against observational data. Uncertainty estimates (bias, absolute error and root mean square error – RSME) have been calculated for precipitation and 2-m temperature, utilising gridded datasets of observations made available by Met Éireann and the UK Met Office. The results of these analyses are presented in sections 2.1 and 2.2. The equivalent uncertainty estimates for 10-m winds and 2-m relative humidity have been calculated utilising station observations and are presented in sections 2.3 and 2.4.

2.1 RCM Precipitation Validations

Gridded datasets of (observed) accumulated daily precipitation, at 1-km resolution, covering Ireland (Walsh, 2012) for the period 1981–2000 were obtained from Met Éireann. Additionally, equivalent UK Met Office datasets covering Northern Ireland were acquired from the Centre for Ecology and Hydrology (Tanguy *et al*., 2016). The gridded datasets are available in monthly comma-separated values (CSV) files and require several processing steps before they can be used in any later analyses. These steps involve solutions that vary in complexity: the precipitation files contain spurious negatives that must be masked; easting and northing coordinates must be transformed to longitude and latitude pairs; and the gridded datasets are at 1-km resolution, whereas the modelled datasets are at 4 km (COSMO4 and 5) and 3.8 km (WRF). The latter step requires a degree of care, as there are differences in how the observed values and the model values have been calculated; the observed values are calculated for a given point, whereas the model values represent accumulations over the model grid cell. A routine has been developed that overlays the observed grid with the model grid. For each cell on the model grid, an average precipitation amount is calculated from those observed values that fall within the cell. This routine has been applied to the gridded observations for each model grid and the transformed observed datasets stored for comparison with the appropriate model outputs.

Figure 2.1a presents the annual observed precipitation averaged over the period 1981–2000. Figure 2.1b presents the downscaled ERA-Interim data as simulated by the COSMO5-CLM model with 4-km grid spacings. Note that the majority of the future

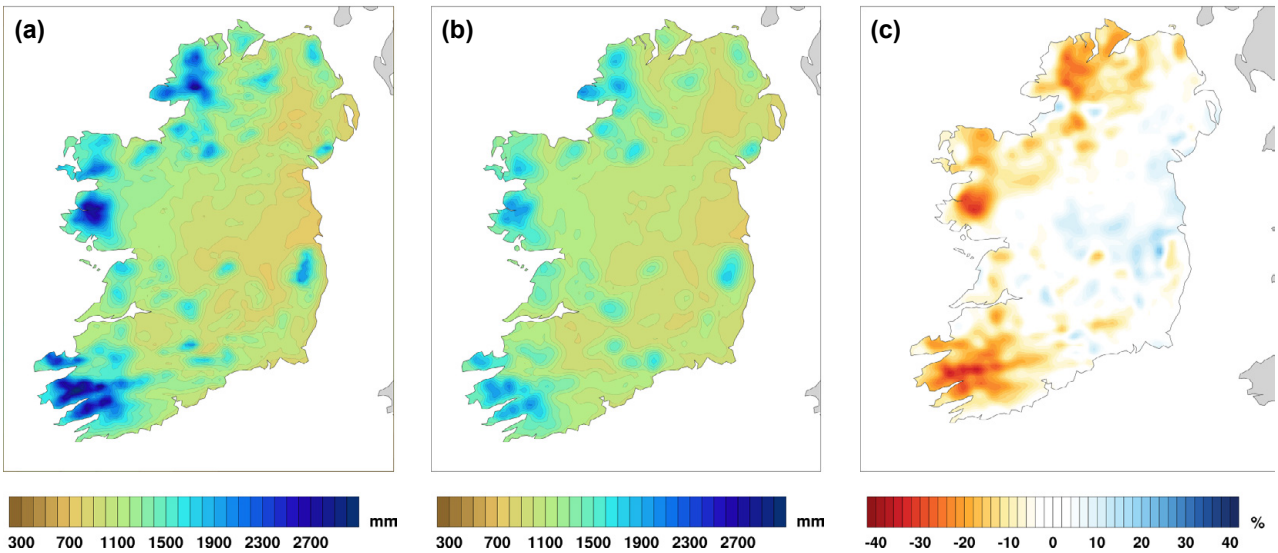

Figure 2.1. Mean annual precipitation for 1981–2000: (a) observations, (b) COSMO5-CLM-ERA-Interim 4-km data and (c) COSMO5-CLM-ERA-Interim error (%).

projections analysed for the current study use this configuration (see Table 1.2). It is noted that the RCM accurately captures the magnitude and spatial characteristics of the historical precipitation climate, e.g. higher rainfall amounts in the west and over mountains. The COSMO4-CLM RCM was found to give similar results (not shown). The WRF 3.8-km RCM was found to generally overestimate precipitation, whereas both COSMO4-CLM and COSMO5-CLM underestimate.

Figure 2.1c shows that the percentage errors range from approximately −30% to approximately +15% for COSMO5-CLM downscaled ERA-Interim data. The percentage error at each grid point (*i, j*) is given by:

$$per\_bias_{(i,j)} = 100 \times \left(\frac{bias_{(i,j)}}{\overline{OBS}_{(i,j)}} \right) \quad (2.1)$$

where

$$bias_{(i,j)} = \overline{RCM}_{(i,j)} - \overline{OBS}_{(i,j)} \quad (2.2)$$

and the $\overline{RCM}_{(i,j)}$ and $\overline{OBS}_{(i,j)}$ terms represent the RCM and observed values, respectively, at grid point (*i*, *j*), averaged over the period 1981–2000.

Figure 2.1c highlights a clear underestimation of precipitation over the mountainous regions. This is probably because the RCMs underestimate heavy precipitation; previous validations studies (e.g. Nolan *et al*., 2017) have demonstrated a decrease in RCM skill with increasing magnitude of heavy precipitation events. To quantify the overall bias evident in Figure 2.1c, the mean was calculated over all grid points covering Ireland, resulting in an overall bias of −4.7%. The bias metric allows for the evaluation of the systematic errors of the RCMs but this can hide large errors, as positive and negative values can cancel each other out. For this reason, the percentage mean absolute error (MAE) metric was also used to evaluate the RCM precipitation errors:

$$per\_MAE_{(i,j)} = 100 \times \frac{MAE_{(i,j)}}{\overline{OBS}_{(i,j)}} \quad (2.3)$$

where

$$MAE_{(i,j)} = \left| \overline{RCM}_{(i,j)} - \overline{OBS}_{(i,j)} \right| \quad (2.4)$$

Again, the mean was calculated over all grid points covering Ireland, resulting in an overall MAE value of 8.3%. Additionally, the percentage RMSE metric was calculated:

$$per\_RMSE = 100 \times \left(\frac{RMSE}{\overline{OBS}} \right) \quad (2.5)$$

where

$$RMSE = \sqrt{\frac{1}{N} \sum_{i,j} \left(\overline{RCM}_{(i,j)} - \overline{OBS}_{(i,j)} \right)^2} \quad (2.6)$$

where N is the number of grid points covering Ireland. The COSMO5-CLM-ERA-Interim precipitation data, presented in Figure 2.1, has a *per_RSME* value of 14%.

The validations described previously were repeated for each RCM ensemble member (with 3.8- and 4-km horizontal grid spacings) outlined in Table 1.2. The mean bias (daily), absolute error (MAE) and RMSE (in both mm and as a percentage of observations) for each ensemble member has been calculated over the period 1981–2000. The results found for each ensemble member are presented in Table 2.1.

Percentage bias values found range from −0.26% (COSMO4-CLM-HadGEM2-ES) to 15.9% (COSMO5-CLM-MPI-ESM-LR), the percentage MAE values range from 8.75% (COSMO5-CLM-EC-Earth) to 17.99% (COSMO5-CLM-MPI-ESM-LR) and the percentage RMSE values range from 11.17% (COSMO5-CLM-EC-Earth) to 21% (COSMO5-CLM-MPI-ESM-LR).

It should be noted that the observed precipitation dataset has a margin of error of approximately ± 10%, so the RCM validations should be considered within this context.

To assess the added value of high-resolution RCM models, and to quantify the improved skill of RCMs over the GCMs, precipitation data were compared with both RCM and GCM data for the period 1976–2005. The analysis was limited to Ireland and the COSMO5-CLM RCM simulations as outlined in Table 1.2. Results, presented in Table 2.2, demonstrate improved skill of the RCMs over the GCMs. Moreover, an increase in grid resolution of the RCMs (from 18- to 4-km grid spacings) results in a general increase in skill. Nolan *et al*. (2017) analysed a larger ensemble of RCMs (both COSMO-CLM and WRF) with different grid spacings (18, 7, 6, 4, 2 and 1.5 km) and found that the RCMs demonstrated a general stepwise increase in skill with increased model resolution. Furthermore, it was shown that heavy precipitation events are more accurately resolved by the higher spatial resolution RCM data. However, it was found that although the RCM accuracy increased with higher spatial

Table 2.1. Precipitation uncertainty estimates found for each RCM ensemble member through comparison with gridded observations

Precipitation (daily) validation statistics 1981–2000						
RCM ensemble member	Bias (mm)	Bias (%)	MAE (mm)	MAE (%)	RMSE (mm)	RMSE (%)
COSMO4-CLM-EC-Earth (r1i1p1)	0.01	2.61	0.33	9.48	0.47	12.0
COSMO4-CLM-EC-Earth (r13i1p1)	0.24	9.40	0.39	12.25	0.51	15.17
COSMO4-CLM-EC-Earth (r14i1p1)	0.11	5.33	0.33	9.91	0.47	12.57
COSMO4-CLM-HadGEM2-ES	–0.11	–0.26	0.40	11.21	0.61	14.05
COSMO5-CLM-CNRM-CM5	–0.20	–3.16	0.42	11.26	0.61	14.15
COSMO5-CLM-EC-Earth (r12i1p1)	–0.14	–1.98	0.32	8.57	0.49	11.17
COSMO5-CLM-HadGEM2-ES	–0.54	–14.48	0.56	15.17	0.74	17.30
COSMO5-CLM-MIROC5	0.15	8.08	0.45	14.09	0.57	17.04
COSMO5-CLM-MPI-ESM-LR	0.44	15.9	0.56	17.99	0.65	21.0
WRF-MIROC5	0.18	7.5	0.31	9.7	0.38	11.56

For each metric, the best- and worst-performing scores are highlighted in green and red, respectively.

Table 2.2. GCM and COSMO5-CLM MAE (%) uncertainty estimates through comparison with gridded observations for the period 1976–2005

30-year average annual rainfall MAE % error			
		COSMO5-CLM-GCM	
GCM	GCM Data	18 km	4 km
CNRM-CM5	16.5	14.1	11.8
EC-Earth (r12i1p1)	17.3	14.0	10.0
HadGEM2-ES	20.8	14.6	15.1
MIROC5	26.0	18.2	15.6
MPI-ESM-LR	25.1	24.8	21.6

For each metric, the best- and worst-performing scores are highlighted in green and red, respectively.

resolution, reducing the horizontal grid spacing below 4 km provided relatively little added value (Nolan *et al.*, 2017).

2.2 RCM 2-m Temperature Validations

Daily 1-km gridded observations of 2-m temperature for Ireland for the period 1981–2000 were obtained from Met Éireann and processed for comparison with each ensemble member. As with the gridded precipitation observations, the (observed) temperature data require coordinate transformation (easting and northing to longitude and latitude) and regridding (1-km model grids to 3.8-km/4-km model grids). Unlike precipitation, however, no spurious values needed to be masked and the calculation of temperature at specific grid points is relatively straightforward; a bilinear interpolant was used.

Figure 2.2a presents the observed 2-m temperature averaged over the 20-year period 1981–2000. Figure 2.2b presents the downscaled ERA-Interim data as simulated by the COSMO5-CLM model at 4-km resolution. It is noted that the COSMO5-CLM data accurately capture the magnitude and spatial characteristics of the observed temperature climate. This is confirmed by Figure 2.2c, which shows a small negative bias of a mean value of −0.32°C over Ireland. The corresponding MAE statistic has a value of 0.34°C.

In Table 2.3, we present the results (bias, MAE and RMSE) found for each RCM ensemble member (with 3.8- and 4-km horizontal grid spacings) outlined in Table 1.2. Bias values found range from −0.05°C (COSMO4-CLM-HadGEM2-ES) to −2.1°C (COSMO5-CLM-CNRM-CM5), MAE values range from 0.25°C (COSMO4-HadGEM2-ES) to 2.1°C

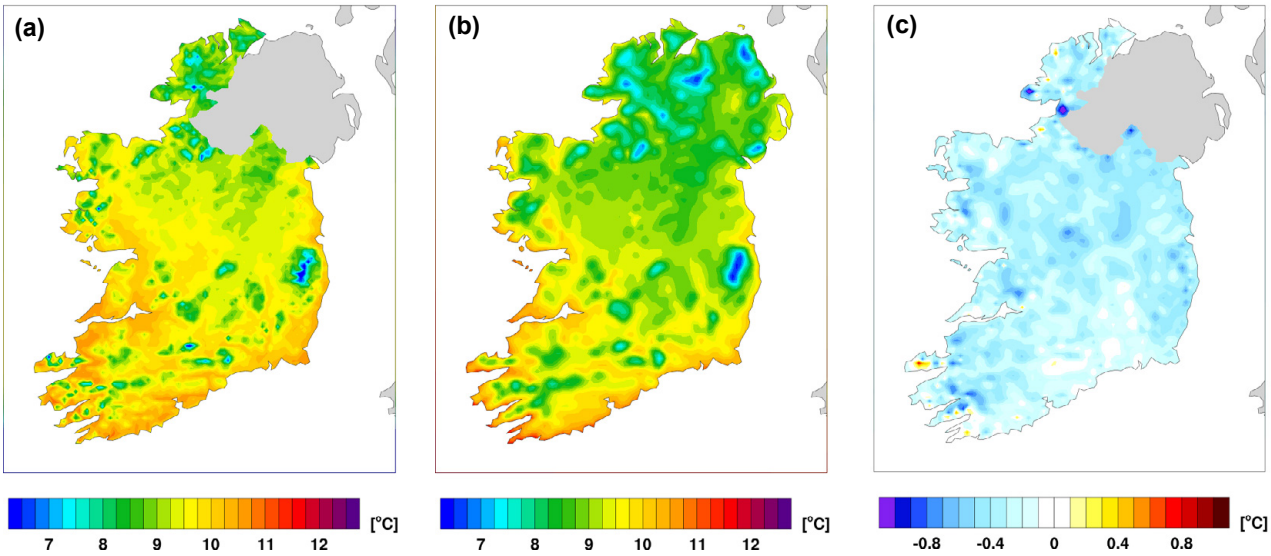

Figure 2.2. Mean annual 2-m temperature for 1981–2000: (a) observations, (b) COSMO5-CLM-ERA-Interim 4-km data and (c) COSMO5-CLM-ERA-Interim bias.

Table 2.3. 2-m temperature uncertainty estimates found for each RCM ensemble member through comparison with gridded observations

2-m temperature validation statistics 1981–2000			
RCM ensemble member	**Bias (°C)**	**MAE (°C)**	**RMSE (°C)**
COSMO4-CLM-EC-Earth (r1i1p1)	–1.52	1.52	1.56
COSMO4-CLM-EC-Earth (r13i1p1)	–1.93	1.93	1.96
COSMO4-CLM-EC-Earth (r14i1p1)	–1.62	1.62	1.66
COSMO4-CLM-HadGEM2-ES	–0.05	0.25	0.36
COSMO5-CLM-CNRM-CM5	–2.1	2.1	2.12
COSMO5-CLM-EC-Earth (r12i1p1)	–1.60	1.60	1.63
COSMO5-CLM-HadGEM2-ES	–0.49	0.53	0.59
COSMO5-CLM-MIROC5	–0.29	0.37	0.44
COSMO5-CLM-MPI-ESM-LR	–0.73	0.75	0.80
WRF-MIROC5	–1.0	1.05	1.10

For each metric, the best- and worst-performing scores are highlighted in green and red, respectively.

(COSMO5-CLM-CNRM-CM5) and RMSE values range from 0.36°C (COSMO4-CLM-HadGEM2-ES) to 2.12°C (COSMO5-CLM-CNRM-CM5).

The observed gridded 2-m temperature dataset has an estimated MAE of 0.19°C and an RMSE of 0.41°C, so the RCM validations should be considered within this context.

2.3 RCM 10-m Wind Speed Validations

Daily (00.00 Coordinated Universal Time – UTC) 10-m wind speed data from nine Met Éireann weather stations were utilised to validate model outputs. The data obtained were from Shannon Airport (Co. Clare), Roches Point (Co. Cork), Malin Head (Co. Donegal), Casement Aerodrome (Co. Dublin), Dublin Airport (Co. Dublin), Valentia Observatory (Co. Kerry), Belmullet (Co. Mayo), Claremorris (Co. Mayo) and Mullingar (Co. Westmeath) and covered time periods longer than 1981–2000. Although other Met Éireann station data exist, they typically do not extend back to 1981 and were therefore not used. The observed time series were trimmed to cover the required period (1981–2000) and units were converted from knots to $m\,s^{-1}$ for comparison with ensemble member values.

Before this latter step could be completed, time series of (daily) 10-m wind speeds were generated from each ensemble member at each station location. This was achieved by first estimating the (3-hourly) 10-m (zonal velocity – U, meridional velocity – V) wind components at each station location through bilinear interpolation and then calculating (3-hourly) 10-m wind speeds through the simple formula $W = \sqrt{U^2 + V^2}$.

For each ensemble member (m), mean (daily) 10-m wind speeds (both modelled – M – and observed – O) for the period 1981–2000 were calculated from each of the (nine in total) station (s) time series. The errors at each station location $\left(e_{s,m} = M - O\right)$ were then used to calculate:

overall bias $\left(\sum_{s=1}^{9} e_{s,m} / 9\right)$,

MAE $\left(\sum_{s=1}^{9} \left|e_{s,m}\right| / 9\right)$ and

RMSE $\left(\sqrt{\sum_{s=1}^{9} \left(e_{s,m}\right)^2 / 9}\right)$

for each ensemble member. The results of these calculations are given in Table 2.4; bias values range from −0.09 m s^{-1} (COSMO4-CLM-EC-Earth, r13i1p1) to −0.94 m s^{-1} (WRF-MIROC5); MAE ranges from 0.58 m s^{-1} (COSMO5-CLM-CNRM-CM5) to 1.09 m s^{-1} (WRF-MIROC5); and RMSE ranges from 0.73 m s^{-1} (COSMO4-CLM-EC-Earth, r13i1p1) to 1.32 m s^{-1} (WRF-MIROC5).

Initial test simulations showed that the WRF data exhibited a consistent overestimation in the wind speed. This overestimation was corrected by adapting the *topo_wind* parameterising scheme – a topographic correction for surface winds to represent extra drag from subgrid topography and enhanced flow at hill tops (Jimenez and Dudhia, 2012). However, adapting this parameterising scheme resulted in an underestimation of the WRF-MIROC5 wind speed (–0.94 m s^{-1} bias; see Table 2.4).

2.4 RCM 2-m Relative Humidity Validations

Hourly 2-m relative humidity data from the nine Met Éireann weather stations listed in section 2.3 were used for model validation. The data obtained have an earliest starting date of 1 January 1987, 01:00, and cover periods that extend beyond 2000. As with the daily data described in section 2.3, other Met Éireann station data exist but do not extend back to 1987 and were therefore not used. The observed time series were therefore systematically trimmed to cover the common period 1987–2000.

Bilinear interpolation was used to generate time series of 3-hourly 2-m relative humidity from each ensemble member at each station location. For each ensemble member (m), mean (3-hourly) 2-m relative humidities (both modelled – M – and observed – O) for the period 1987–2000 were calculated from each of the (nine in total) station (s) time series. As in section 2.3, the errors at each station location were then used to calculate overall bias, MAE and RMSE for each ensemble member. The results of

Table 2.4. 10-m wind speed validations calculated utilising Met Éireann daily station observations and estimations from each of the 10 ensemble members

Daily (mean) 10-m wind speed 1981–2000			
Model	**Bias (m s^{-1})**	**MAE (m s^{-1})**	**RMSE (m s^{-1})**
COSMO4-CLM-EC-Earth (r1i1p1)	-0.29	0.77	0.79
COSMO4-CLM-EC-Earth (r13i1p1)	-0.09	0.69	0.73
COSMO4-CLM-EC-Earth (r14i1p1)	-0.20	0.73	0.76
COSMO4-CLM-HadGEM2-ES	-0.57	0.86	0.93
COSMO5-CLM-CNRM-CM5	0.31	0.58	0.77
COSMO5-CLM-EC-Earth (r12i1p1)	0.72	0.86	0.97
COSMO5-CLM-HadGEM2-ES	0.59	0.74	0.86
COSMO5-CLM-MIROC5	0.36	0.61	0.76
COSMO5-CLM-MPI-ESM-LR	0.85	0.99	1.10
WRF-MIROC5	-0.94	1.09	1.32

For each metric, the best- and worst-performing scores are highlighted in green and red, respectively.

Table 2.5. 2-m relative humidity validations calculated utilising Met Éireann hourly station observations and estimations from each of the 10 ensemble members

2-m relative humidity validation statistics 1987–2000			
RCM ensemble member	**Bias (%)**	**MAE (%)**	**RMSE (%)**
COSMO4-CLM-EC-Earth (r1i1p1)	–4.07	4.07	4.25
COSMO4-CLM-EC-Earth (r13i1p1)	–3.94	3.94	4.16
COSMO4-CLM-EC-Earth (r14i1p1)	–3.77	3.77	3.99
COSMO4-CLM-HadGEM2-ES	–4.11	4.11	4.25
COSMO5-CLM-CNRM-CM5	–1.60	1.70	2.33
COSMO5-CLM-EC-Earth (r12i1p1)	–2.26	2.26	2.74
COSMO5-CLM-HadGEM2-ES	–2.75	2.75	3.12
COSMO5-CLM-MIROC5	–0.57	1.11	1.49
COSMO5-CLM-MPI-ESM-LR	–0.53	1.33	1.73
WRF-MIROC5	–0.15	1.37	1.62

For each metric, the best- and worst-performing scores are highlighted in green and red, respectively.

these calculations are given in Table 2.5; bias values range from −0.15% (WRF-MIROC5) to −4.11% (COSMO4-CLM-HadGEM2-ES); MAE ranges from 1.11% (COSMO5-CLM-MIROC5) to 4.11% (COSMO4-CLM-HadGEM2-ES); and RMSE ranges from 1.49% (COSMO5-CLM-MIROC5) to 4.25% (COSMO4-CLM-EC-Earth, r1i1p1 and COSMO4-CLM-HadGEM2-ES).

2.5 RCM Validation Summary

The RCMs were validated by downscaling ERA-Interim reanalyses and the GCM datasets for the period 1981–2000, and comparing the output with observational data. Extensive validations were carried out to test the ability of the RCMs to accurately model the temperature, precipitation, wind and humidity climate of Ireland. Results confirm that the output of the RCMs exhibit reasonable and realistic features as documented in the historical data record. The skill of the individual RCM datasets was dependent on the field under analysis (e.g. WRF performed well for precipitation but less well for wind speed). This variation in RCM skill stresses the importance of using an ensemble of RCMs to simulate climate change.

For an in-depth validation of additional climate fields, please refer to Nolan *et al*. (2014, 2015, 2017) and Flanagan *et al*. (2019). Additional experiments were carried out to assess the added value of high-resolution RCM models, the results of which demonstrated improved skill of RCMs over the GCMs. Moreover, an increase in the spatial resolution of the RCMs was found to result in a general increase in skill (e.g. Nolan *et al*., 2017). However, it was found that although the RCM accuracy increased with higher spatial resolution, reducing the horizontal grid spacing below 4-km provided relatively little added value (Nolan *et al*., 2017). Werner *et al*. (2019) completed a validation of agri-climate fields derived from downscaled ERA-Interim COSMO5-CLM5 and WRF datasets. The authors compared derived fields, such as evapotranspiration and soil moisture deficits, with observations and found that both RCMs exhibit high skill, with WRF slightly outperforming COSMO5-CLM.

The analysis presented in this chapter confirms that the RCM configurations and domain size of the current study are capable of accurately simulating the climate of Ireland.

Future validation work will focus on downscaling and analysing the more up-to-date and accurate ERA5 global reanalysis dataset from the European Centre for Medium-Range Weather Forecast (ECMWF), in place of ERA-Interim. ERA5 is the fifth generation of the ECMWF global climate reanalysis dataset (C3S, 2017). The ERA5 dataset was not available at the time that the current research was carried out. Furthermore, additional WRF historical simulations will be completed, which will allow for a robust quantification of the relative skill of the COSMO5-CLM and WRF RCMs.

3 Mid-century Climate Projections

3.1 Temperature Projections

Figure 3.1 presents the spatial distribution of annual temperature changes for 2041–2060 relative to 1981–2000. The mean annual temperature is projected to increase by 1–1.2°C and by 1.3–1.6°C for the RCP4.5 and RCP8.5 scenarios, respectively. Temperature projections show a clear west-to-east gradient, with the largest increases in the east.

The seasonal temperature projections are presented in Figure 3.2; winter temperatures show increases ranging from 0.9°C in the south-west to 1.2°C in the north-east for the RCP4.5 scenario (1.2°C in the south-west and 1.6°C in the north-east for RCP8.5). The patterns for spring are similar to winter, with a projected increase in temperature of 0.9°C to 1.0°C for RCP4.5 (1.0°C to 1.3°C for RCP8.5) with a south-west to north-east gradient. Summer temperatures show increases ranging from 1.0°C in the north-west to 1.3°C in the south-east for RCP4.5 (1.3°C in the north-west and 1.8°C in the south-east for RCP8.5). Autumn shows a west-to-east pattern with expected increases of 1.3°C to 1.5°C and 1.6°C to 1.9°C for the RCP4.5 and RCP8.5 scenarios, respectively. In summary, the temperature change gradient is from south-west to north-east in winter and spring, north-west to south-east in summer and from west to east in autumn and over the full year. These trends are consistent with previous studies (e.g. Gleeson *et al*., 2013; Nolan, 2015; O'Sullivan *et al*., 2015) and all RCM-GCM simulations, RCPs and future time periods assessed to date.

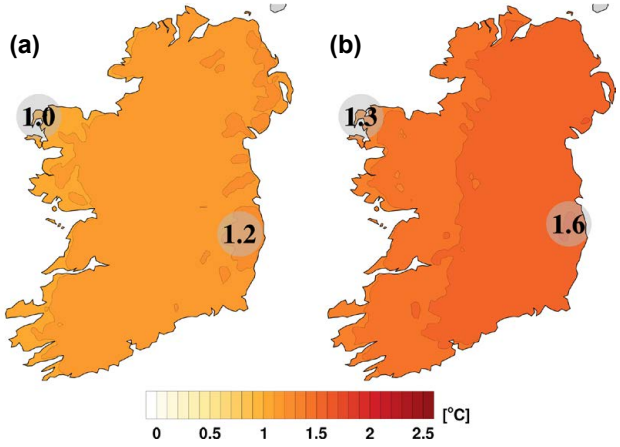

Figure 3.1. Ensemble mean of projections of 2-m temperature change for the (a) RCP4.5 and (b) RCP8.5 scenarios. In each case, the future period, 2041–2060, is compared with the past period, 1981–2000. The numbers included on each plot are the minimum and maximum projected changes, displayed at their locations.

As outlined in Chapter 1, a disagreement between RCM ensemble members can result in large individual outliers skewing the mean ensemble projection. For this reason, it can be more informative to consider percentiles when analysing an ensemble of future projections. The relatively large ensemble size of the current study allows the construction of a pdf of climate projections. Likelihood values can then be assigned to the projected changes. This method of analysing percentiles allows for a better understating of climate change uncertainty and it allows for a quantification of conservative and robust ("likely") projections. Conversely, the likelihood method allows for policymakers to consider more "unlikely" (and possibly high-impact) climate projections.

To this end, the 33rd, 50th and 66th percentiles of annual and seasonal mean 2-m temperature projections are presented in Figure 3.3. For example, the annual figures (top panels) show that over 67% (P33) of the ensemble members project an annual increase in temperatures of 0.8–1.1°C and 1.1–1.5°C for the RCP4.5 and RCP8.5 scenarios, respectively. That is to say, it is "likely" that increases in temperature will be greater than or equal to these values.[8] Similarly, the 50th percentile figures (P50) provides information on the "as likely as not" projection. The 66th percentile (P66) provides information on the "unlikely" projection and can be useful for the analysis of high-impact, low-probability projections.

8 Since all ensemble members project increases in temperature, the 33rd percentile is denoted the "likely" projection in this case (conversely, if projections are negative, the 66th percentile is denoted the "likely" projection).

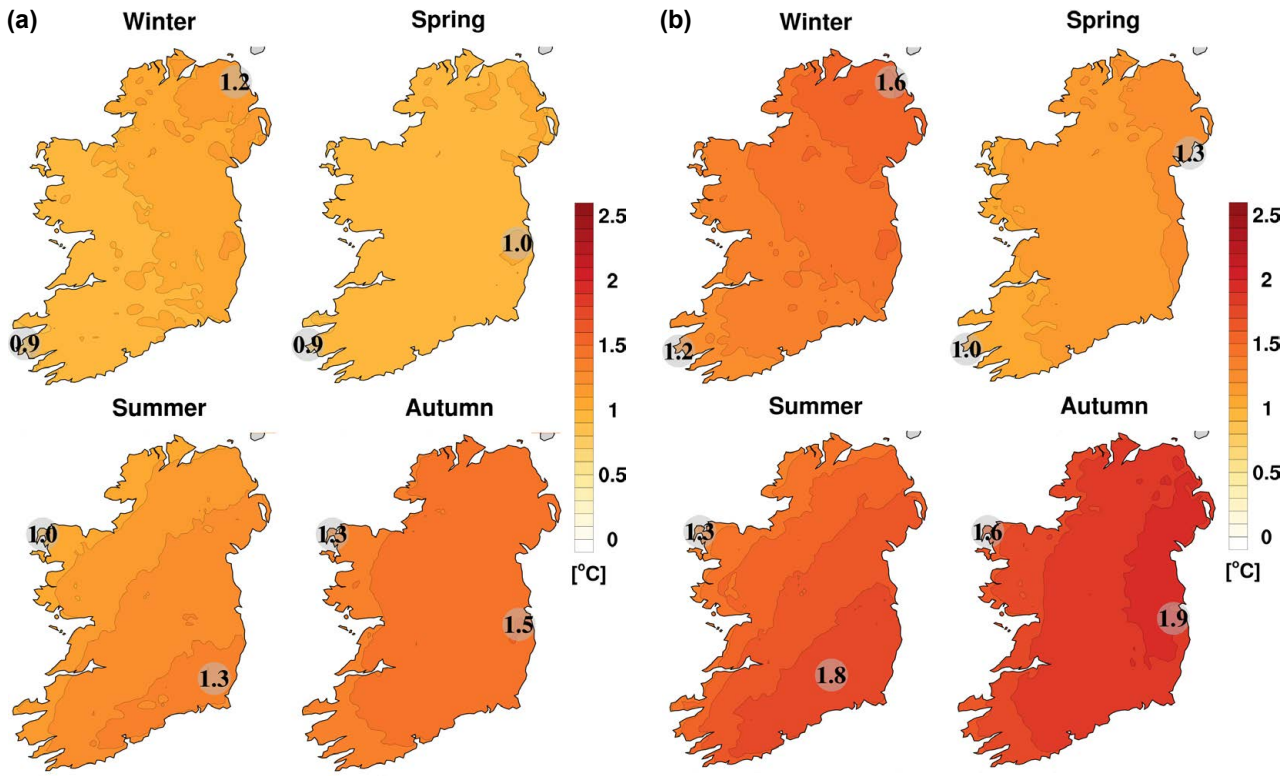

Figure 3.2. Mid-century seasonal projections of mean 2-m temperature change for the (a) RCP4.5 and (b) RCP8.5 scenarios. In each case, the future period, 2041–2060, is compared with the past period, 1981–2000. The numbers included on each plot are the minimum and maximum projected changes, displayed at their locations.

The warming gradient of the annual (Figure 3.1) and seasonal (Figure 3.2) mean projections are also evident in the percentile projections of Figure 3.3. Furthermore, there exists a small variation between the 33rd, 50th and 66th projection percentiles, which demonstrates good agreement (small spread) between ensemble members. Finally, the annual and seasonal warming gradients are similar for both the RCP4.5 and RCP8.5 scenarios. This agreement increases the confidence in the regional projections of temperature.

The annual change in the standard deviation (Figure 3.4) shows small changes of between ≈−0.1°C and ≈0.2°C for both the RCP4.5 and RCP8.5 scenarios.[9] Similarly, the seasonal projected changes in the standard deviation of temperature are small (Figure 3.5); small increases (decreases) are noted for summer (winter) for both RCPs and a mixed signal is noted for spring and autumn. It should be noted that large increases in the mean summer temperature (Figure 3.2) coupled with increases in the standard deviation will lead to enhanced increases in extreme high temperatures (refer to Figure 1.3d for a schematic example of such an outcome). Similarly, increases in mean winter temperature (Figure 3.2) coupled with a decrease in standard deviation will lead to enhanced decreases in extreme low temperatures. However, it should be noted that the projected changes in standard deviation are small for all seasons. The results suggest that although future temperatures will increase substantially for all seasons, the shape of the temperature distribution will remain broadly similar.

3.2 Extreme Temperature Projections

Changes in the daily maximum and daily minimum temperatures are arguably of more immediate importance, since extreme events have an abrupt and much larger impact on lives and livelihoods than a gradual change in mean values (Easterling *et al*., 2000; O'Sullivan *et al*., 2015). A sustained increase in the daily maximum temperature is associated

9 Please refer to section 1.2.4 for an overview of the effects of changes in the standard deviation on the distribution of a climate field.

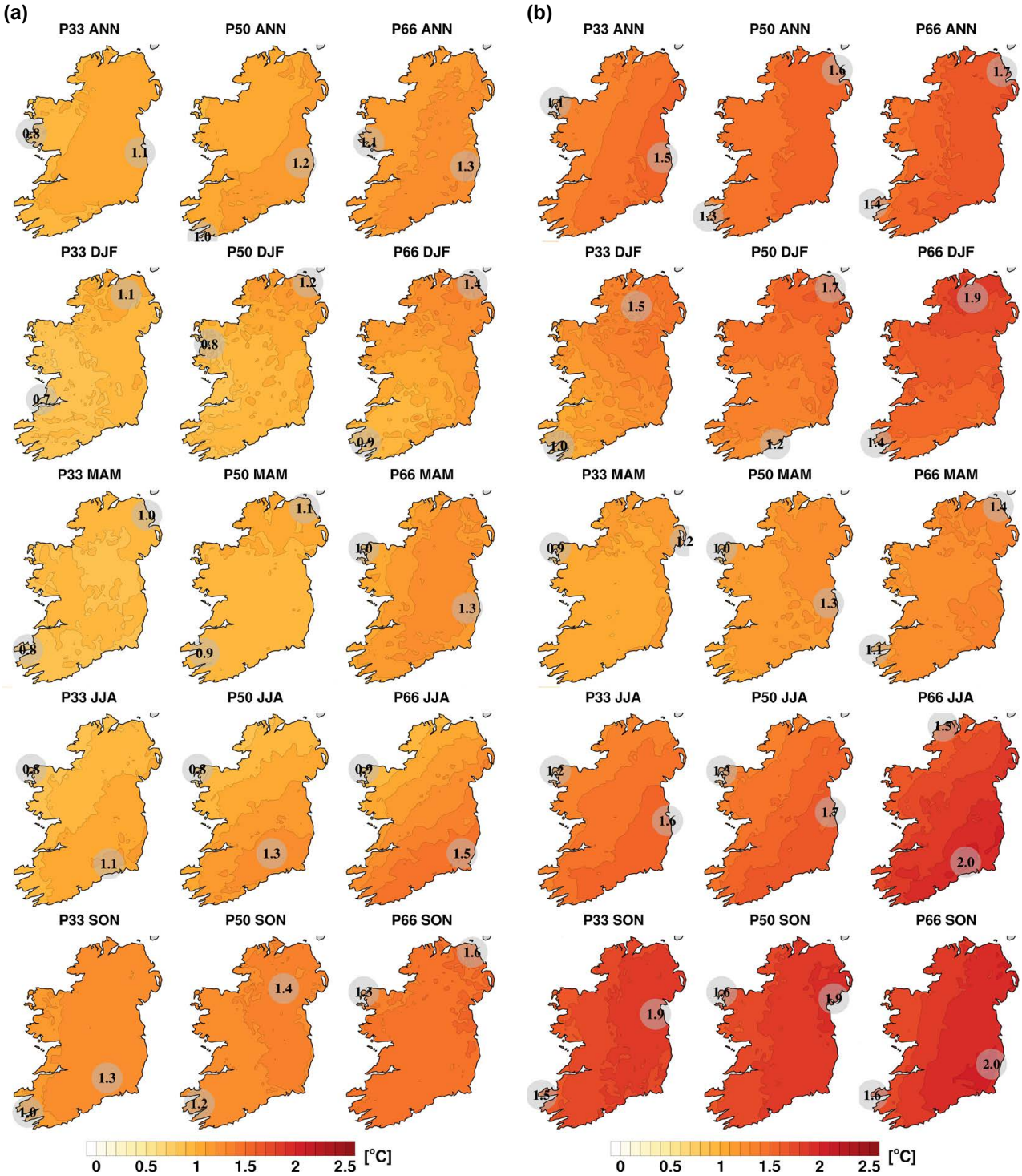

Figure 3.3. The 33rd, 50th and 66th percentiles of annual and seasonal mean 2-m temperature projections for the (a) RCP4.5 and (b) RCP8.5 scenarios. In each case, the future period, 2041–2060, is compared with the past period, 1981–2000. The numbers included on each plot are the minimum and maximum projected changes, displayed at their locations. ANN, annual; DJF, December, January, February; JJA, June, July, August; MAM, March, April, May; SON, September, October, November.

with heatwaves, whereas an increase in the daily minimum temperature will typically imply warmer nights. Figure 3.6a shows how the warmest 5% of daily maximum temperatures are projected to change (TMAX-95%). A strong warming is evident, which is greater than the projected mean summer increase (Figure 3.2), ranging from 1.0°C to 1.6°C for the RCP4.5 scenario and from 1.4°C to 2.2°C for the

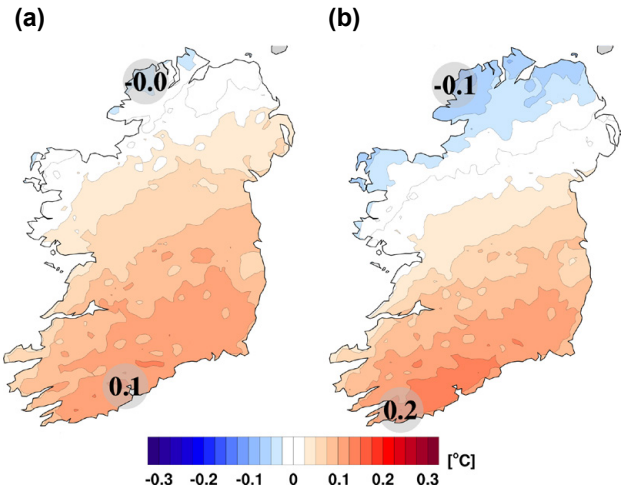

Figure 3.4. Annual projected change in the standard deviation of 2-m temperature for the (a) RCP4.5 and (b) RCP8.5 scenarios. In each case, the future period, 2041–2060, is compared with the past period, 1981–2000. The numbers included on each plot are the minimum and maximum projected changes, displayed at their locations.

RCP8.5 scenario. Warming is greater in the south than in the north.

Figure 3.6b shows how the coldest 5% of daily minimum temperatures are projected to change (TMIN-5%). Again, the projected increase of TMIN-5% is greater than the mean winter increase (Figure 3.2), ranging from 0.9°C to 1.8°C for the RCP4.5 scenario and from 1.2°C to 2.4°C for the RCP8.5 scenario. Warming is greater in the north than in the south.

3.3 Heatwaves

The large projected increase in high summer temperatures (TMAX-95%; Figure 3.6a) suggests an increase in the number of heatwave events by the middle of the century. This is confirmed by Figure 3.7, which presents the projected change in the number of heatwave events over the 20-year period 2041–2060. The increases range from 1 to 8 for the RCP4.5 scenario and from 3 to 15 for the RCP8.5 scenario. Both scenarios exhibit a north-west to south-east

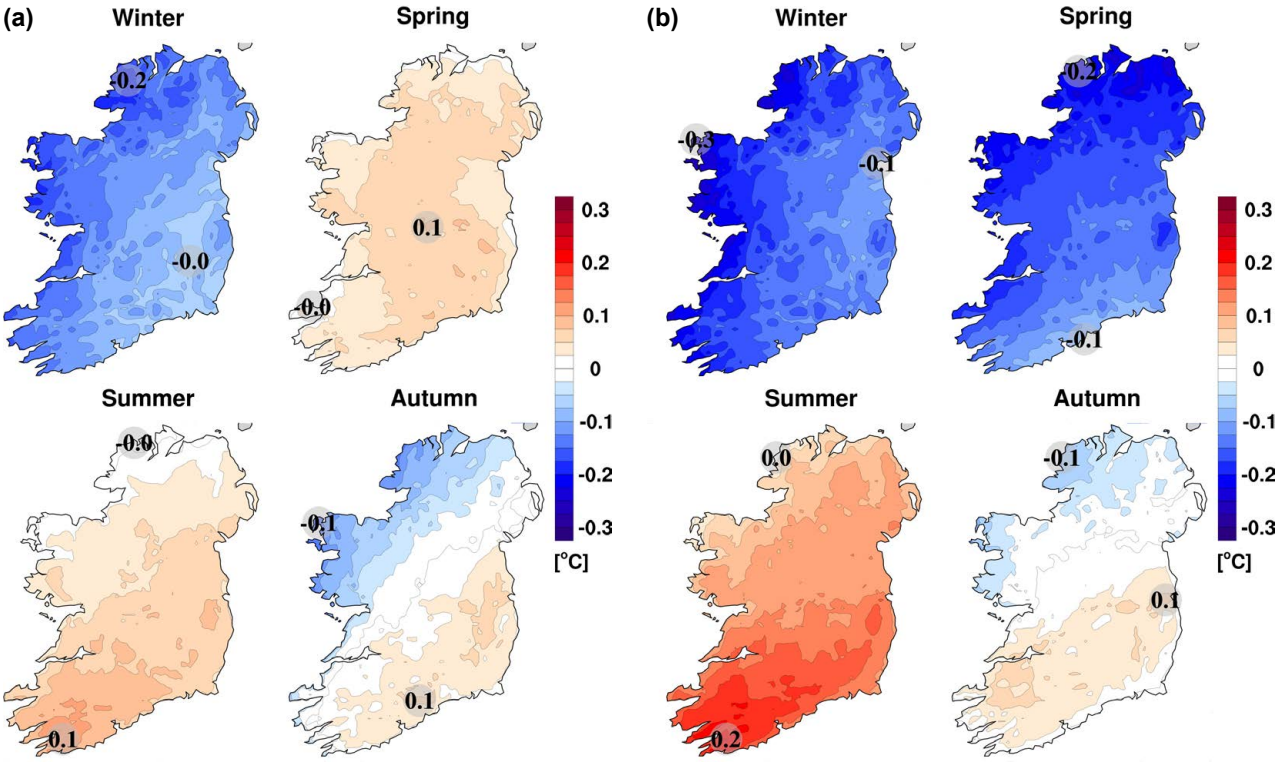

Figure 3.5. Seasonal projected change in the standard deviation of 2-m temperature for the (a) RCP4.5 and (b) RCP8.5 scenarios. In each case, the future period, 2041–2060, is compared with the past period, 1981–2000. The numbers included on each plot are the minimum and maximum projected changes, displayed at their locations.

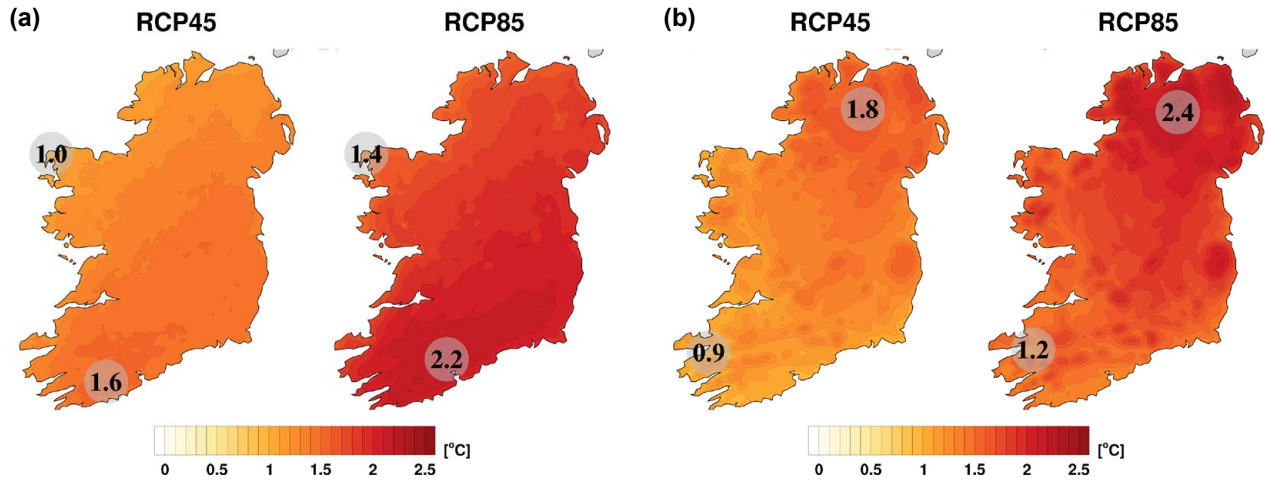

Figure 3.6. Projected changes in mid-century extreme 2-m temperature: (a) top 5% of daily maximum temperatures (warm summer days) and (b) bottom 5% of daily minimum temperatures (cold winter nights). In each case, the future period, 2041–2060, is compared with the past period, 1981–2000. The numbers included on each plot are the minimum and maximum projected changes, displayed at their locations.

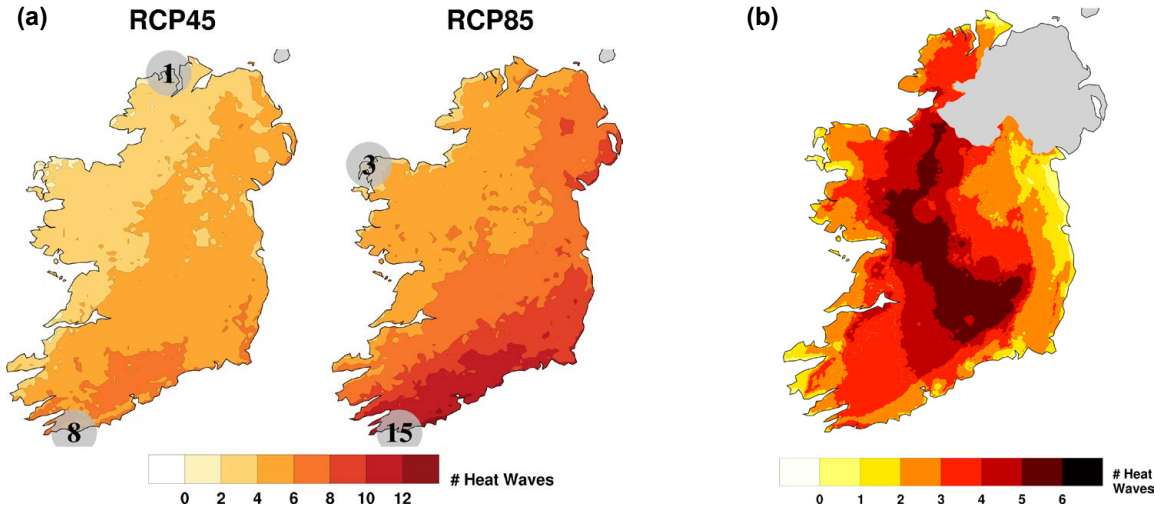

Figure 3.7. (a) The RCP4.5 and RCP8.5 projected change in the number of heatwave events over the 20-year period 2041–2060. In each case, the future period, 2041–2060, is compared with the past period, 1981–2000. The numbers included on each plot are the minimum and maximum increases, displayed at their locations. (b) The observed number of heatwave events over the period 1981–2000.

gradient. For comparison, the observed number of heatwave events over the period 1981–2000 is presented in Figure 3.7b (derived from daily maximum temperature data provided by Walsh, 2012). The projected increase in heatwaves will have a direct impact on public health and mortality, but this may be offset by the projected decrease in frost and ice days (see section 3.4).

For the analysis of the change in number of heatwaves, the following definition as described in Jacob *et al*. (2014) was used: heatwaves are considered as periods of more than 3 consecutive days exceeding the 99th percentile of the daily maximum temperature of the May-to-September season of the control period (1981–2000). Jacob *et al*. (2014) analysed a large ensemble of relatively low-resolution (12.5 km to 25 km) RCMs and showed small

projected increases in heatwave events over Ireland (2021–2050), with a slight north-west to south-east gradient evident over the country. These results are consistent with the findings of the current report.

3.4 Frost and Ice Days

The large projected decrease in cold nights (Figure 3.6b; TMIN-5%) implies a decrease in the number of frost and ice days by the middle of the century. This is confirmed by Figure 3.8a and b, which present the projected annual change in the number of frost and ice days, respectively. Averaged over the whole country, the number of frost days (days when the minimum temperature is < 0°C) is projected to decrease by 45% and 58% for the RCP4.5 and RCP8.5 scenario, respectively. Similarly, the number of ice days (days when the maximum temperature is < 0°C) is projected to decrease by 68% and 78% for the RCP4.5 and RCP8.5 scenarios, respectively. For comparison, the observed annual mean numbers of frost and ice days for 1981–2000 are presented in Figure 3.9a and b, respectively (data from Walsh, 2012). Note that the observed number of ice days is small, particularly in coastal regions. It is worth noting that periods of frost and ice are important environmental drivers that trigger phenological phases in many plant and animal species. Changes in the occurrence of these weather types may disrupt the life cycles of these species (e.g. Williams *et al*., 2015; Bigler and Bugmann, 2018).

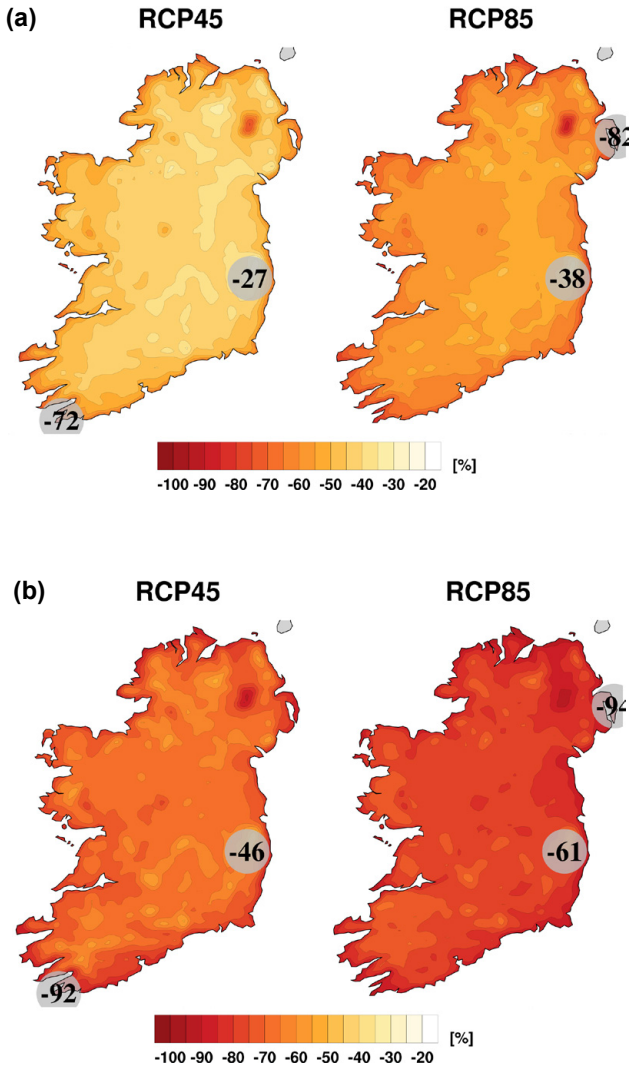

Figure 3.8. Projected changes in mid-century numbers of (a) frost days and (b) ice days. In each case, the future period, 2041–2060, is compared with the past period, 1981–2000. The numbers included on each plot are the minimum and maximum projected changes, displayed at their locations.

3.5 The Growing Season

Within a period of 12 months, the thermal growing season length is officially defined as the number of days between the first occurrence of at least 6 consecutive days with a daily mean temperature > 5°C and the first occurrence of at least 6 consecutive days with a daily mean temperature < 5°C.
Figure 3.10a shows a large projected increase in the average length of the growing season over Ireland by the middle of the century. There exists a clear south-to-north gradient, with values ranging from 5% to 18% and from 6% to 23% for the RCP4.5 and RCP8.5 scenarios, respectively. Averaged over the whole country, the length of the growing season is projected to increase by 12% and 16% for the RCP4.5 and RCP8.5 scenarios, respectively. Figure 3.10b, the projected change in the start of the growing season, shows that by the middle of the century the growing season is expected to start 10–31 days earlier for the RCP4.5 scenario and 10–36 days early for the RCP8.5 scenario. Averaged over the whole country, the growing season is projected to start 15 and 24 days early for the RCP4.5 and RCP8.5 scenarios, respectively.

For comparison, the observed length and start of the growing season over the period 1981–2000 (derived from daily mean temperature data provided by Walsh, 2012) are presented in Figure 3.11a and b, respectively.

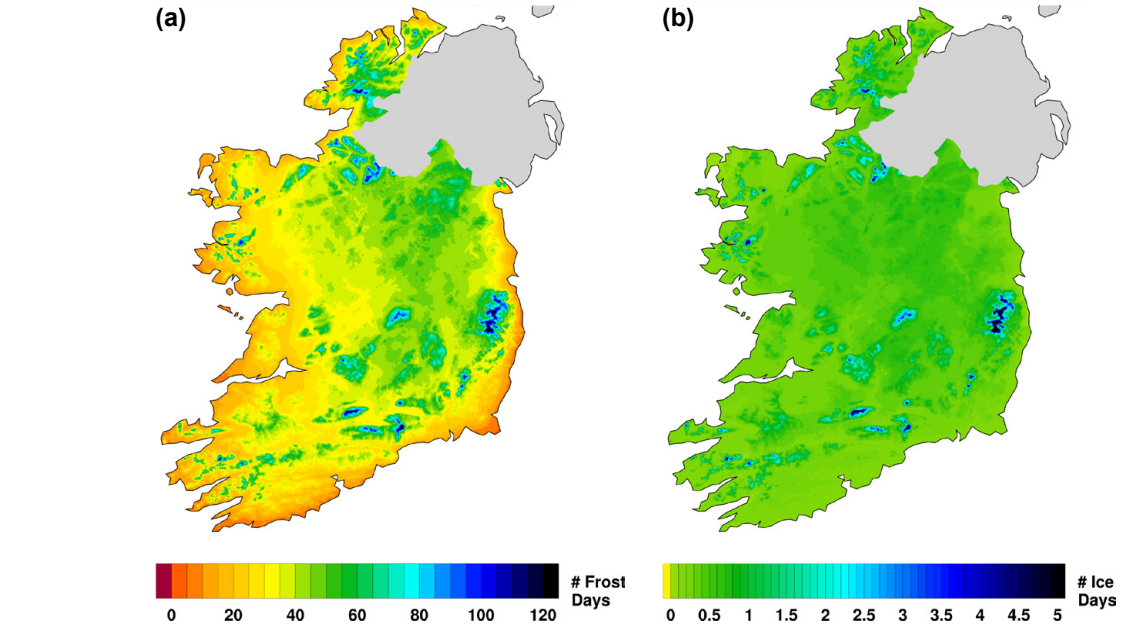

Figure 3.9. The observed mean annual number of (a) frost days and (b) ice days for the period 1981–2000.

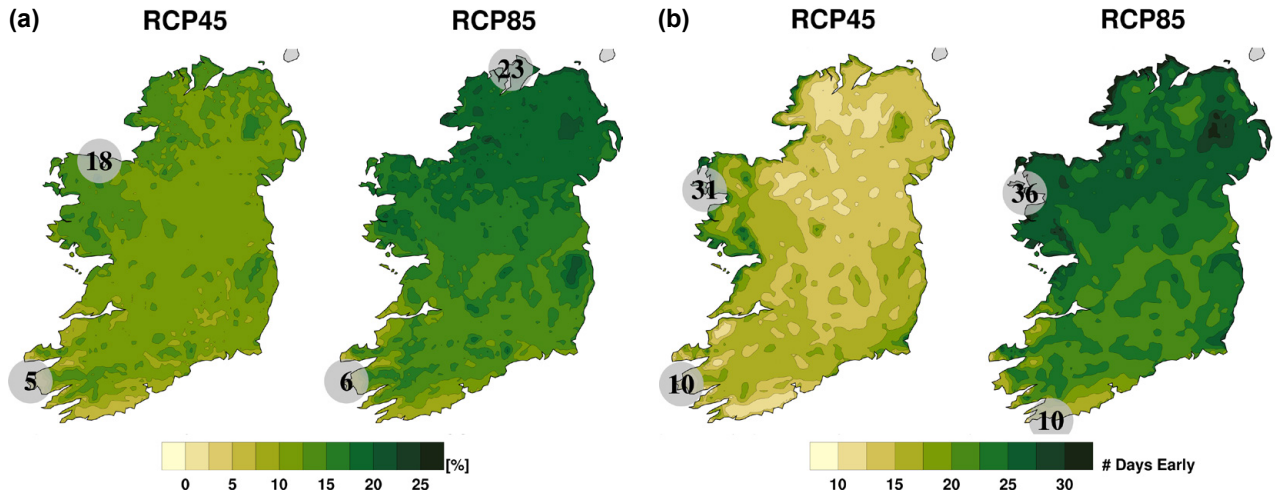

Figure 3.10. Mid-century projected changes in (a) the length of the growing season (%) and (b) the start of the growing season (number of days early). In each case, the future period, 2041–2060, is compared with the past period, 1981–2000. The numbers included on each plot are the minimum and maximum projected changes, displayed at their locations.

3.6 The Grazing Season

The growing season calculation is based solely on temperature and does not take into account the delay before sufficient plant cover is available to support grazing animals or the ability of animals and machinery to pass over land. The approximate length of the grazing season, in days per year, can be approximated from the following equation (Smith, 1976; Collins and Cummins, 1996):

$$GzS = 29.3T - 0.1R + 19.5 \quad (3.1)$$

where T is the mean annual 2-m temperature (°C) and R is the mean annual rainfall (mm year^{-1}).

Figure 3.12a shows that, by the middle of the century, the grazing season is projected to increase by 12–46 and 17–55 days per year for the RCP4.5 and RCP8.5 scenarios, respectively. Averaged over the whole country, the grazing season is projected to increase by

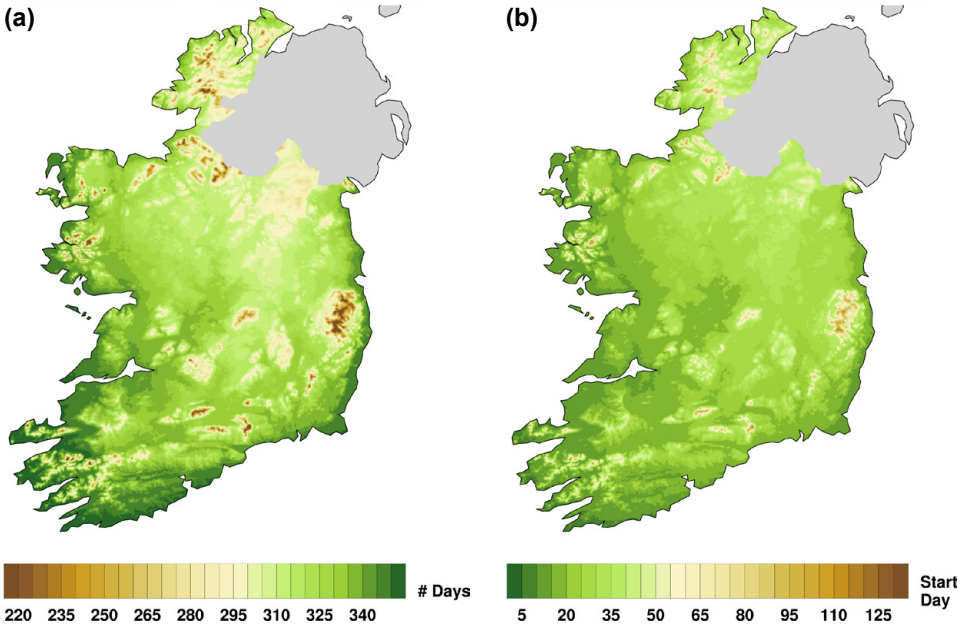

Figure 3.11. Observed growing season statistics for the period 1981–2000: (a) mean annual length and (b) mean start day of growing season (where day 1 is 1 January, day 2 is 2 January, etc.).

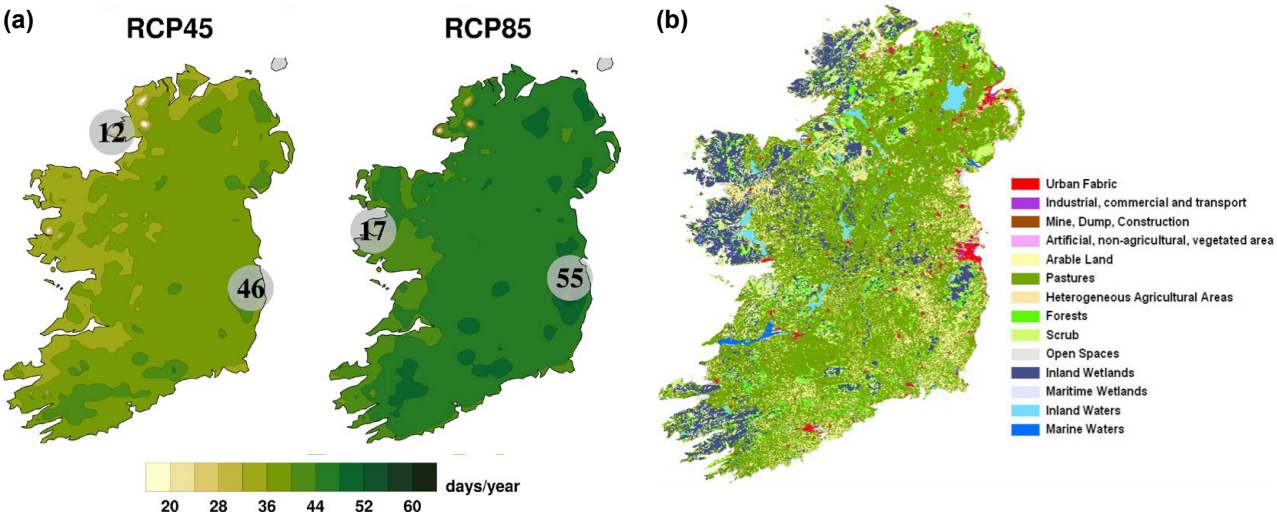

Figure 3.12. (a) Mid-century projected changes in the length of the grazing season and (b) the Coordination of Information on the Environment (Corine) land cover map of Ireland. The colours represent the land cover in 2006. Image reproduced with permission from Dwyer (2013).

37 and 45 days per year for the RCP4.5 and RCP8.5 scenarios, respectively.

It should be noted that not all areas presented in Figures 3.10 and 3.12a are suitable for agriculture and/or forestry. The projections should therefore be considered in the context of an observed soil/grass map, as presented in Figure 3.12b.

3.7 Growing Degree Days (Crops and Pests)

A degree day, an estimate of accumulated heat, is defined as the deviation (°C) from a reference temperature value (Fraisse *et al*., 2010; Project Team ECA&D, 2013; Kendon *et al*., 2015). Degree days represent the number of degrees by which the temperature has gone above or below a threshold.

Growing degree days (GDDs) are used to predict the growth and development of plants, insects and diseases of which the developments are very dependent on temperature and the daily accumulation of heat. The amount of heat required to advance a plant or pest to the next development stage remains constant from year to year; however, the actual amount of time (days) can vary considerably because of weather conditions. Each crop, insect and disease species has a minimum base temperature (T_b) or threshold below which development does not occur (Fraisse *et al*., 2010; OMAFRA, 2017). For example, in Europe, 5.5°C applies to wheat, barley, rye, oats and lettuce, 8°C to sunflowers and potatoes and 10°C to American maize, rice, corn, and tomato (McMaster and Wilhelm, 1997; Miller *et al*., 2001; Spinoni *et al*., 2015). See Table 3.1 for a list of base temperatures for crops and pests (McMaster and Wilhelm, 1997; Johnson *et al*., 1998; Miller *et al*., 2001; Spinoni *et al*., 2015).

The GDD was computed using the daily mean temperature (T_M) for different base temperatures (T_b), as described in Spinoni *et al*. (2015) and Project Team ECA&D (2013):

$$GDD_{daily} = \max\{(T_M - T_b), 0\} \quad (3.2)$$

$$GDD = \sum GDD_{daily} \quad (3.3)$$

Figure 3.13 shows that the GDDs for "crop base temperatures" 5.5°C, 8°C and 10°C are projected to increase substantially by the middle of the century. The projected increases are largest for the higher baseline temperatures. Averaged over the whole country, GDDs are projected to increase by 23% for RCP4.5 and 30% for RCP8.5 (T_b = 5.5°C); 32% for RCP4.5 and 42% for RCP8.5 (T_b = 8°C); and 45% for RCP4.5 and 59% for RCP8.5 (T_b = 10°C) (see Table 3.1). The results suggest a warming climate may present some positive opportunities for farming. However, the results should be viewed in the context that a warming climate will also result in an increase in pests as a result of an increase in heating and a decrease in frost and ice days (see section 3.4). Figure 3.14 and Table 3.1 show that the GDDs for "pest base temperatures" 6°C, 7°C, 9°C and 10°C are similarly projected to increase substantially by the middle of the century. Furthermore, projected increases in extreme temperatures (section 3.2), heatwaves (section 3.3), heavy precipitation (section 3.10) and dry periods/ droughts (section 3.11) will have substantial adverse effects on agriculture in Ireland by the middle of the century.

3.8 Ontario Crop Heat Units

The Ontario Crop Heat Unit (OCHU) is a variant of a degree day accumulation and is widely used to rate the suitability of regions for production of corn/ maize (Collins and Cummins, 1996; Bootsma *et al*., 1999, 2007; OMAFRA, 2017). The OCHU model uses separate calculations for maximum and minimum temperatures. The maximum or daytime relationship (Y_{max}) uses 10°C as the base temperature and has a curvilinear response to temperature with a maximum

Table 3.1. Growing degree days base temperature for various crops and pests, and mid-century projected change averaged over all land points of Ireland

	Base temperature (°C)	Projection (all Ireland)	
		RCP4.5 (%)	RCP8.5 (%)
Crops			
Wheat, barley, rye, oats and lettuce	5.5	+23	+30
Sunflower, potato	8	+32	+42
American maize, rice, corn and tomato	10	+45	+59
Pests			
Stalk borer	6	+25	+32
Corn rootworm[a]	7	+28	+36
Lucerne weevil	9	+38	+49
Black cutworm, European corn borer and standard baseline for insect and mite pests of woody plants	10	+45	+59

[a]**Reported in the UK but currently not present in Ireland.**

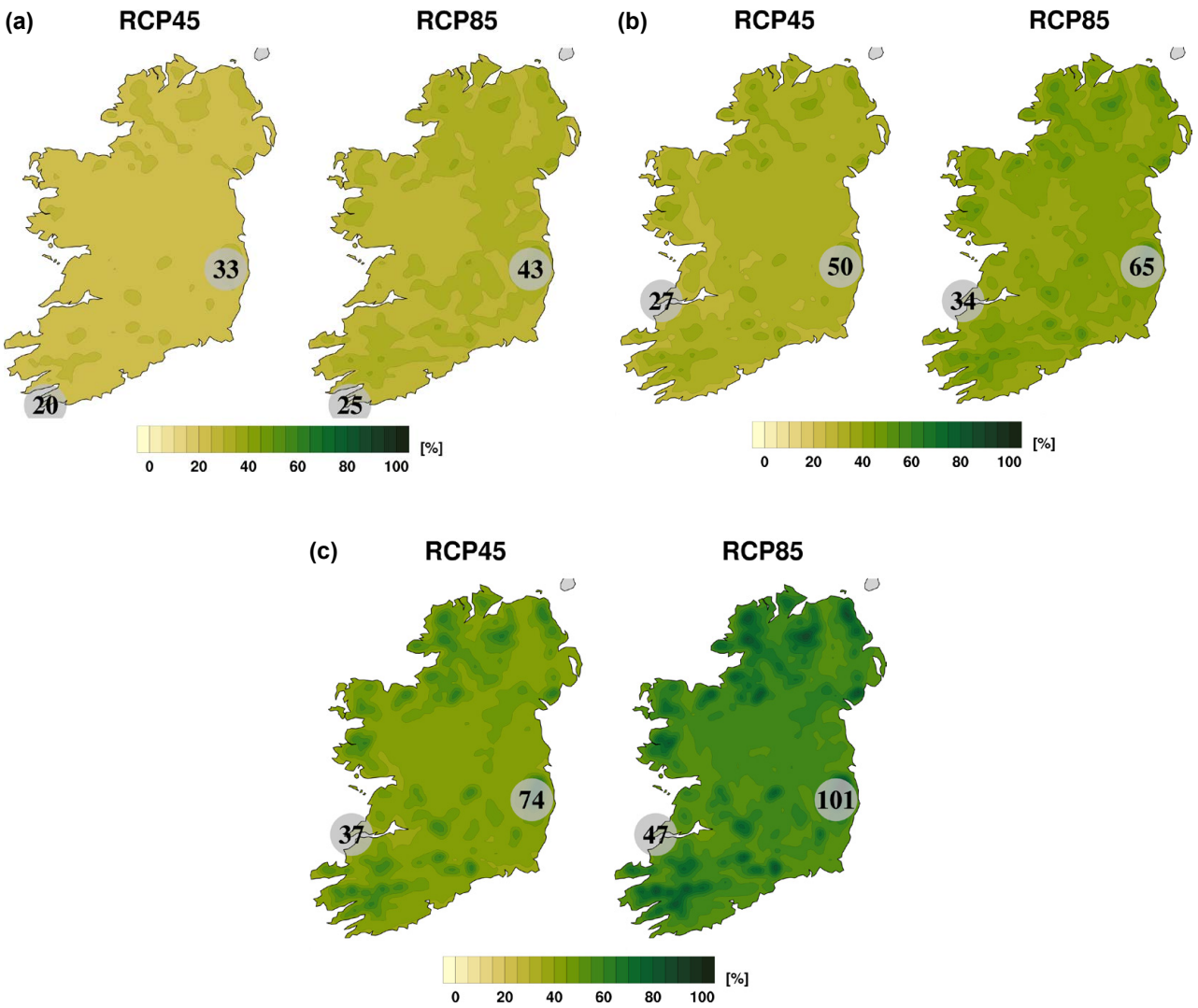

Figure 3.13. Mid-century projected changes (%) in GDDs for "crop base temperatures": (a) T_b = 5.5°C (wheat, barley, rye, oats and lettuce), (b) T_b = 8°C (sunflower and potato) and (c) T_b = 10°C (American maize, rice, corn and tomato). In each case, the future period, 2041–2060, is compared with the past period, 1981–2000. The numbers included on each plot are the minimum and maximum projected changes, displayed at their locations.

at 30°C; no growth occurs below 10°C and growth peaks at 30°C and declines thereafter. The minimum (or night-time) relationship uses 4.4°C as the base temperature, with the response above this being linear; Y_{min} does not specify an optimum temperature because night-time minimum temperatures very seldom exceed 25°C. Mean annual OCHU values for May to September are calculated using daily values as follows:

$$\text{Daily OCHU} = \frac{Y_{max} + Y_{min}}{2} \quad (3.4)$$

where

$$Y_{max} = \max\{3.33(T_{max} - 10) - 0.084(T_{max} - 10)^2, 0\}, \quad (3.5)$$

$$Y_{min} = \max\{1.8(T_{min} - 4.44), 0\} \quad (3.6)$$

and T_{min} and T_{max} are the daily minimum and maximum temperatures, respectively.

Figure 3.15 shows that, by the middle of the century, OCHUs (May to September) are projected to increase by 18–38% and 23–49% for the RCP4.5 and RCP8.5 scenarios, respectively. Averaged over the whole country, OCHUs are projected to increase by 23% and 29% for the RCP4.5 and RCP8.5 scenarios, respectively.

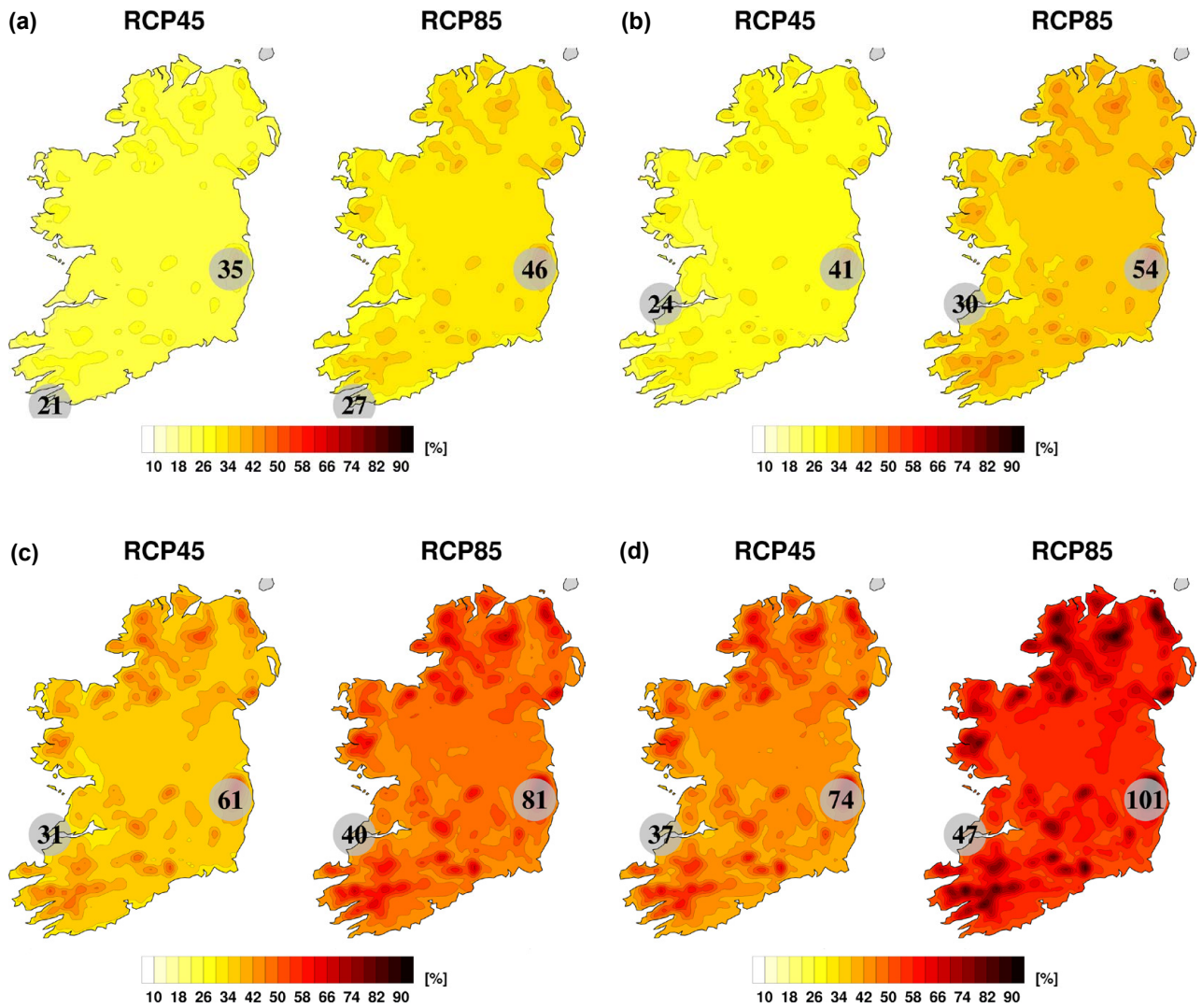

Figure 3.14. Mid-century projected changes (%) in GDDs for "pest base temperatures": (a) T_b = 6°C (stalk borer), (b) T_b = 7°C (corn rootworm), (c) T_b = 9°C (Lucerne weevil) and (d) T_b = 10°C (black cutworm, European corn borer and standard baseline for insect and mite pests of woody plants). In each case, the future period, 2041–2060, is compared with the past period, 1981–2000. The numbers included on each plot are the minimum and maximum projected changes, displayed at their locations.

3.9 Mid-century Precipitation Projections

Figure 3.16 presents the mean annual percentage change in precipitation for the RCP4.5 and RCP8.5 scenarios. There is an indication of a slight reduction in the annual precipitation of ≈0–6% for the RCP4.5 scenario. However, projected reductions are small (≈0%) over most of the country for both scenarios.

Figure 3.17a presents the seasonal change (%) in precipitation for the RCP4.5 scenario; the corresponding plots for RCP8.5 are presented in Figure 3.17b. The strongest signals are a projected decrease for summer, with the largest impacts for the RCP8.5 scenario. The summer reductions range from ≈0% to 11% for the RCP4.5 scenario and from 2% to 17% for the RCP8.5 scenario. Other seasons show a small projected change in precipitation, with the exception of winter under the RCP8.5 scenario, where precipitation is expected to increase by ≈0 to 11%.

The projected precipitation changes of the current study vary greatly between ensemble members, much more so than for the temperature projections (see section 3.1). The regional details of Figures 3.16 and 3.17 are therefore not reliable. Furthermore, the disagreement between RCM projections can result in large individual outliers skewing the mean ensemble

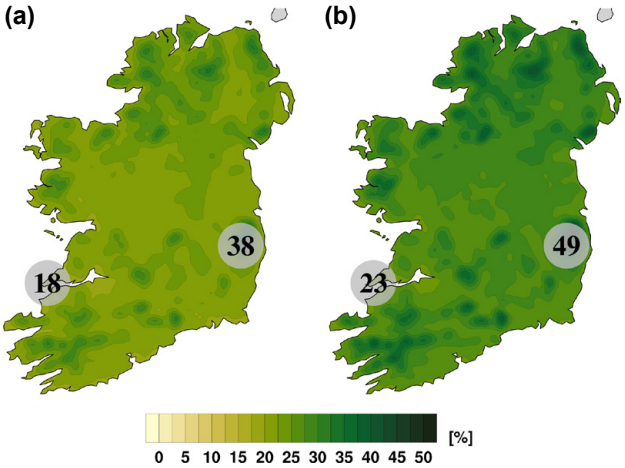

Figure 3.15. Mid-century projected changes (%) in OCHUs during May to September for the (a) RCP4.5 and (b) RCP8.5 scenarios. In each case, the future period, 2041–2060, is compared with the past period, 1981–2000. The numbers included on each plot are the minimum and maximum projected changes, displayed at their locations.

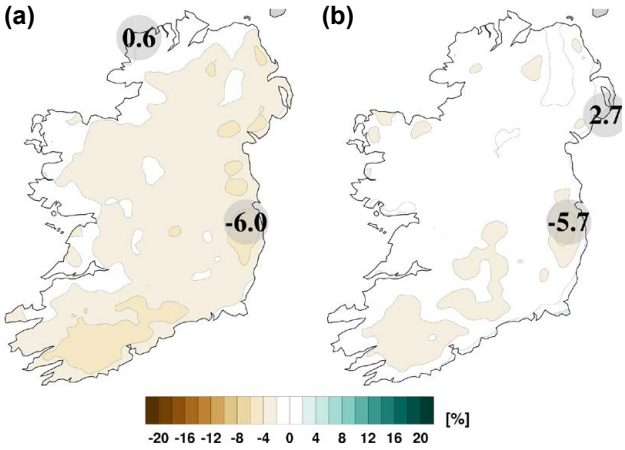

Figure 3.16. Ensemble mean of mid-century annual precipitation projections (%) for the (a) RCP4.5 and (b) RCP8.5 scenarios. In each case, the future period, 2041–2060, is compared with the past period, 1981–2000. The numbers included on each plot are the minimum and maximum projected changes, displayed at their locations.

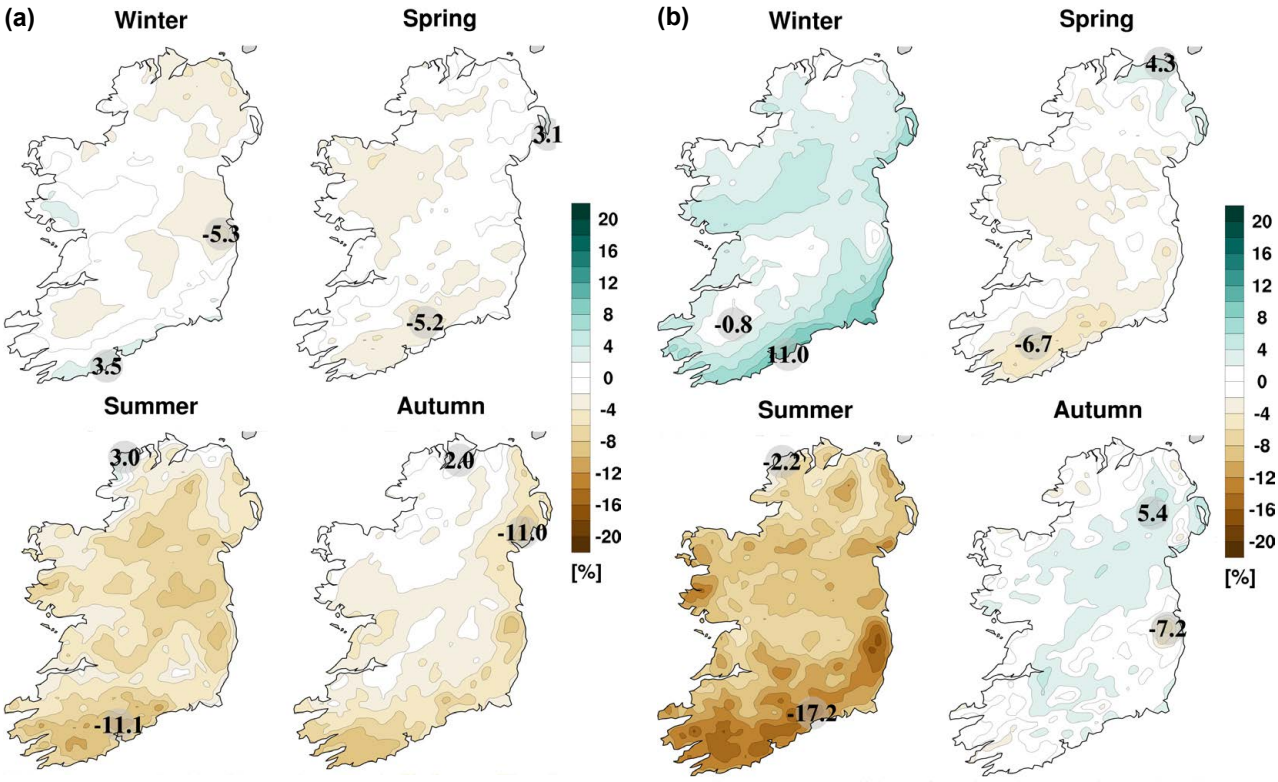

Figure 3.17. Mid-century seasonal projections of mean precipitation (%) for the (a) RCP4.5 and (b) RCP8.5 scenarios. In each case, the future period, 2041–2060, is compared with the past period, 1981–2000. The numbers included on each plot are the minimum and maximum projected changes, displayed at their locations.

projection. It is therefore more informative to consider the 33rd, 50th and 66th percentile projections as presented in Figure 3.18. The likelihood values are calculated at each grid point using the full RCM ensemble of projections, as outlined in Table 1.2. The figures show that there is large uncertainty in the projections, as demonstrated by a disagreement between the percentile projections. The exceptions

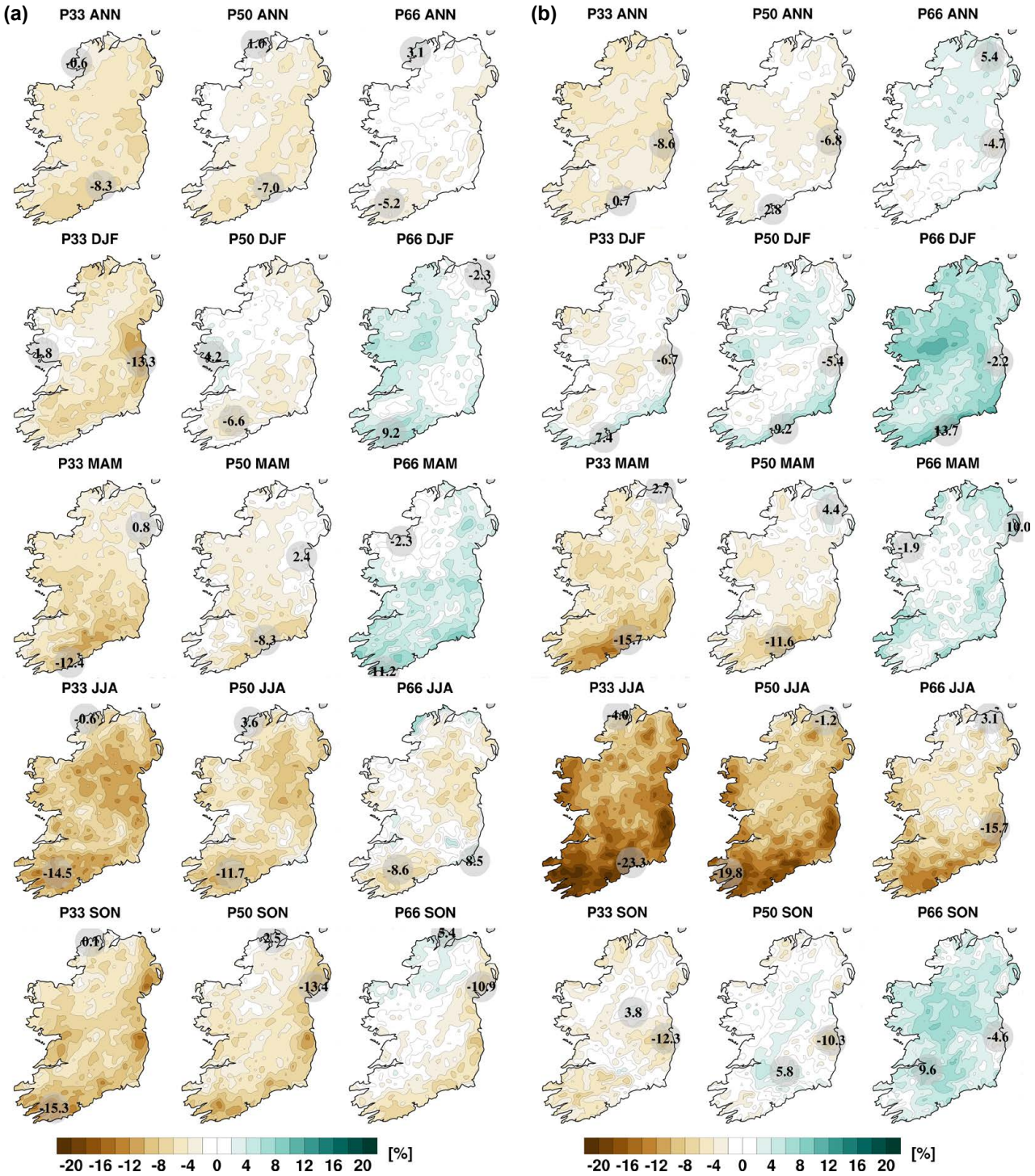

Figure 3.18. The 33rd, 50th and 66th percentiles of annual and seasonal mean precipitation projections (%) for the (a) RCP4.5 and (b) RCP8.5 scenarios. In each case, the future period, 2041–2060, is compared with the past period, 1981–2000. The numbers included on each plot are the minimum and maximum projected changes, displayed at their locations. ANN, annual; DJF, December, January, February; JJA, June, July, August; MAM, March, April, May; SON, September, October, November.

are summer (both RCP4.5 and RCP8.5 scenarios) and annual and autumn (RCP4.5 projections), when the signals are more robust. The strongest signal is for a substantial drying during summer, when there is a clear agreement between the percentiles (for both the RCP4.5 and RCP8.5 scenarios).

3.9.1 Changes in the variability of the precipitation climate

The uncertainty of the mean precipitation projections may be partly attributed to a projected increase in the variability of the future Irish precipitation climate, resulting in an increase in both dry periods and heavy rainfall events. This is clearly demonstrated in Figures 3.19 and 3.20, which present the annual and seasonal projected change in the standard deviation of 3-hour precipitation, respectively. It is noted that the standard deviation of precipitation is expected to increase substantially for all seasons by the middle of the century, with the exception of spring, when the signal is less pronounced for the RCP8.5 scenario.

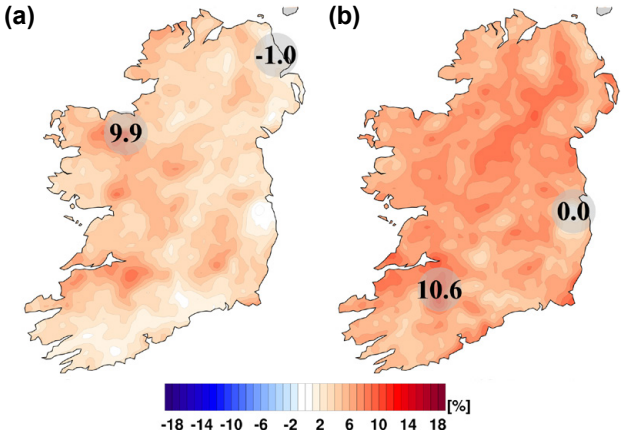

Figure 3.19. Annual projected change in the standard deviation of precipitation (%) for the (a) RCP4.5 and (b) RCP8.5 scenarios. In each case, the future period, 2041–2060, is compared with the past period, 1981–2000. The numbers included on each plot are the minimum and maximum projected changes, displayed at their locations.

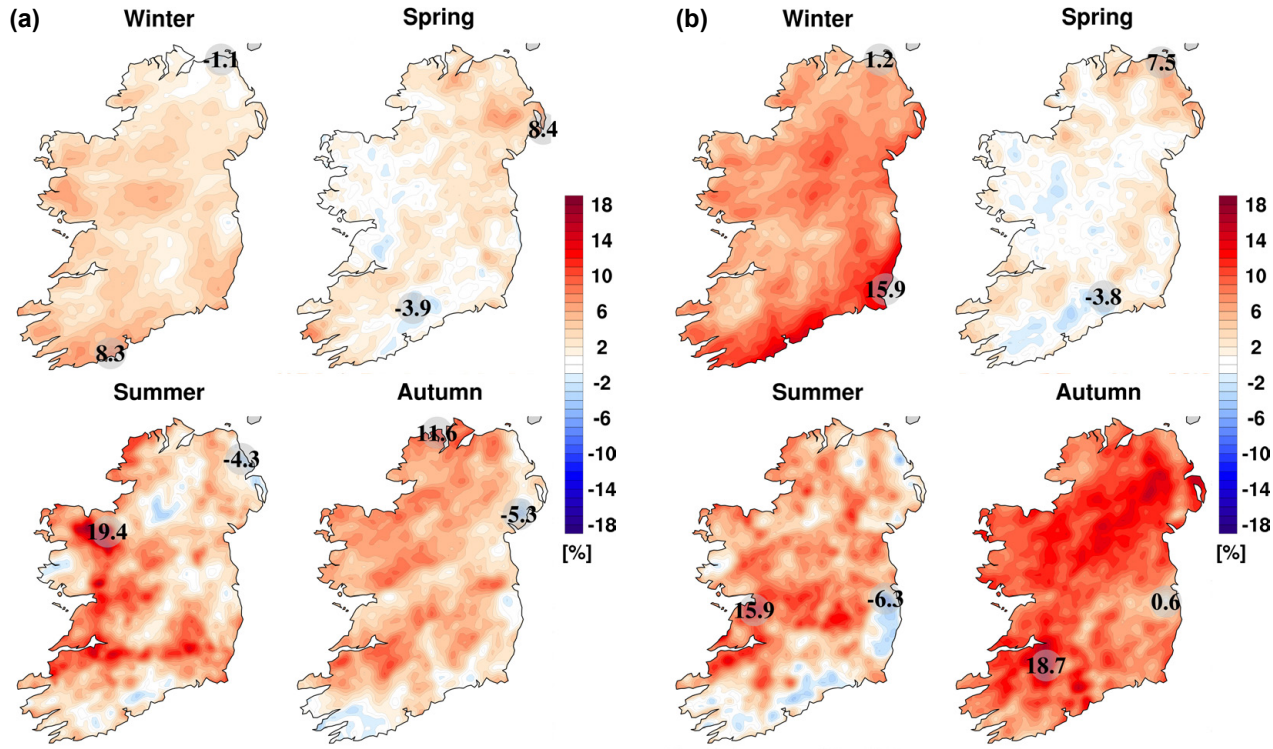

Figure 3.20. Seasonal projected change in the standard deviation of precipitation (%) for the (a) RCP4.5 and (b) RCP8.5 scenarios. In each case, the future period, 2041–2060, is compared with the past period, 1981–2000. The numbers included on each plot are the minimum and maximum projected changes, displayed at their locations.

The large projected change in the standard deviation of precipitation, coupled with small changes in the mean, imply an increase in both dry periods and heavy rainfall events (i.e. the tails of rainfall distribution will become more pronounced; see Figure 1.3b for a schematic example of such an outcome). This is confirmed by Figures 3.21 and 3.22, which show large projected changes in intense rainfall events and dry periods, respectively. The projections of increased variability of the precipitation climate will have adverse implications for society (e.g. droughts, flooding, water management and housing) and sectors of the economy, such as agriculture. Furthermore, the increase in frequency of both droughts and heavy rainfall events could be detrimental to potential gains of a warming climate to the agricultural sector, as discussed in sections 3.5–3.8.

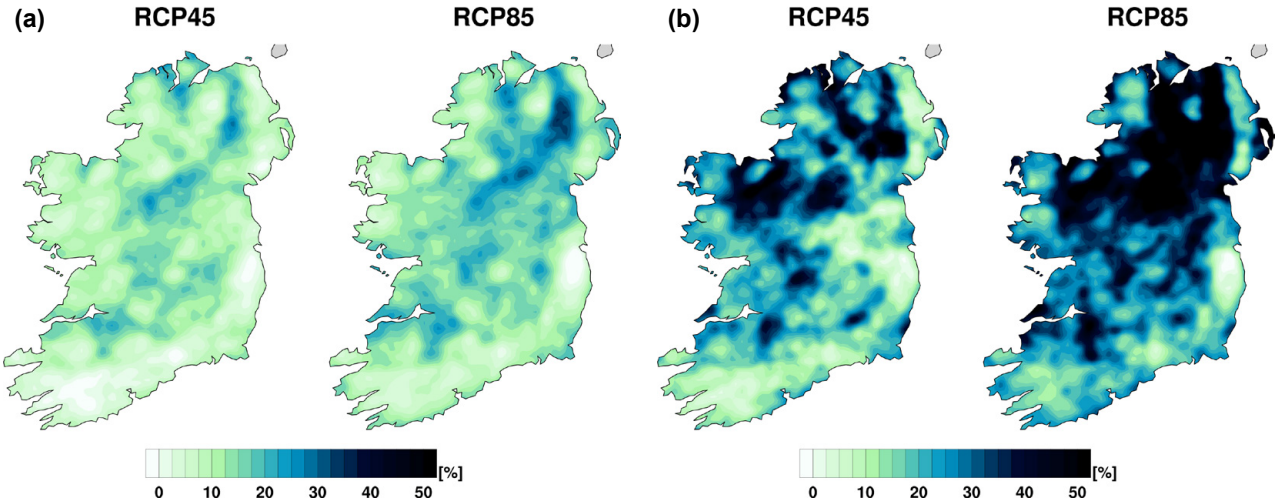

Figure 3.21. Projected changes (%) in mid-century number of annual (a) wet days (precipitation > 20 mm day^{-1}) and (b) very wet days (precipitation > 30 mm day^{-1}). In each case, the future period, 2041–2060, is compared with the past period, 1981–2000.

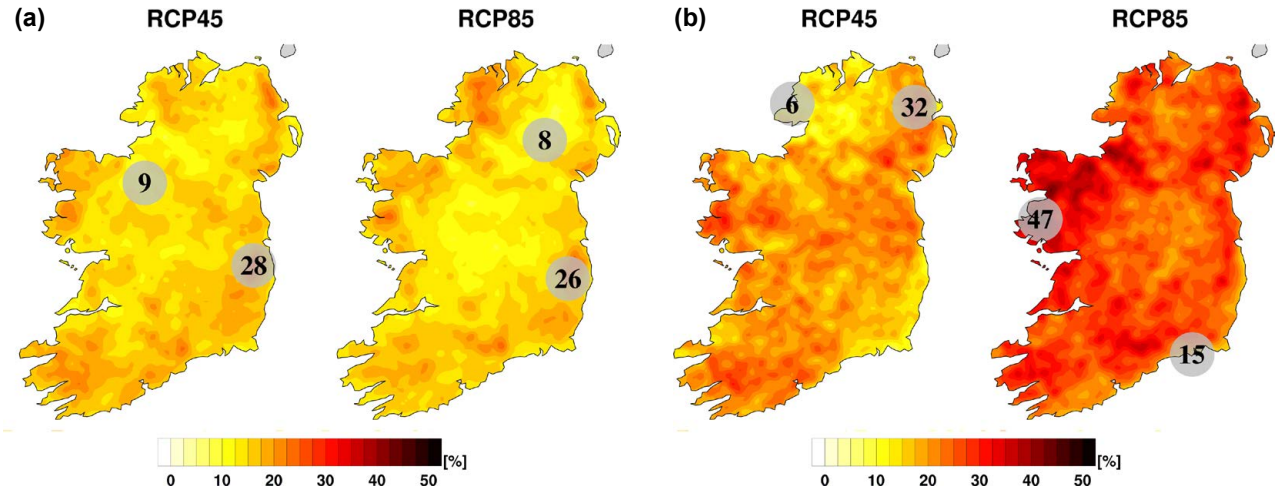

Figure 3.22. Projected changes (%) in mid-century number of dry periods (a) annually and (b) in summer. In each case, the future period, 2041–2060, is compared with the past period, 1981–2000. The numbers included on each plot are the minimum and maximum projected changes, displayed at their locations.

3.10 Heavy Precipitation Events

Changes in the occurrence of heavy rainfall events are of particular importance because of the link with flooding. In this section, mid-century projections of "wet days" and "very wet days" are presented. A "wet day" is defined as one on which the daily precipitation amount is greater than 20 mm. A "very wet day" is defined as one on which the daily precipitation is greater than 30 mm.[10] Figure 3.21a indicates an increase in the annual number of wet days for the RCP4.5 (mean value 10%) and RCP8.5 (mean value 14%) scenarios. The largest increases in wet days are expected for the autumn (9% for RCP4.5; 16% for RCP8.5) and winter (17% for RCP4.5; 26% for RCP8.5) months; a small increase is projected for summer (≈10% for both scenarios) and a mixed signal was found for spring. The projected increase in the annual number of very wet days, presented in Figure 3.21b, is substantial, with mean values of 21% and 31% for the RCP4.5 and RCP8.5 scenarios, respectively. Again, the largest increases were noted for the autumn (25% for RCP4.5; 42% for RCP8.5) and winter (33% for RCP4.5; 61% for RCP8.5) months.

A "likely" increase was also noted in the number of annual wet days (5% for RCP4.5; 8% for RCP8.5), annual very wet days (8% for RCP4.5; 19% for RCP8.5), autumn wet days (1% for RPC4.5; 6% for RCP8.5), autumn very wet days (3% for RCP4.5; 18% for RCP8.5), winter wet days (4% for RCP4.5; 12% for RCP8.5) and winter very wet days (2% for RCP4.5; 18% for RCP8.5).[11] It follows that it is "likely" that increases in heavy rainfall events will be greater than or equal to these values. The increased frequency of heavy precipitation is well marked in winter and autumn and over the full year, particularly for the RCP8.5 scenario, but regional details are not reliable because of a large spread in the ensembles. The projected increase in heavy rainfall events during autumn, winter and over the full year is consistent with the large projected change in standard deviation of the 3-hour precipitation presented in Figures 3.19 and 3.20.

The projected increase in the number of wet and very wet days should be considered in the context of historical values. Figure 3.23 presents the annual number of observed wet and very wet days, averaged

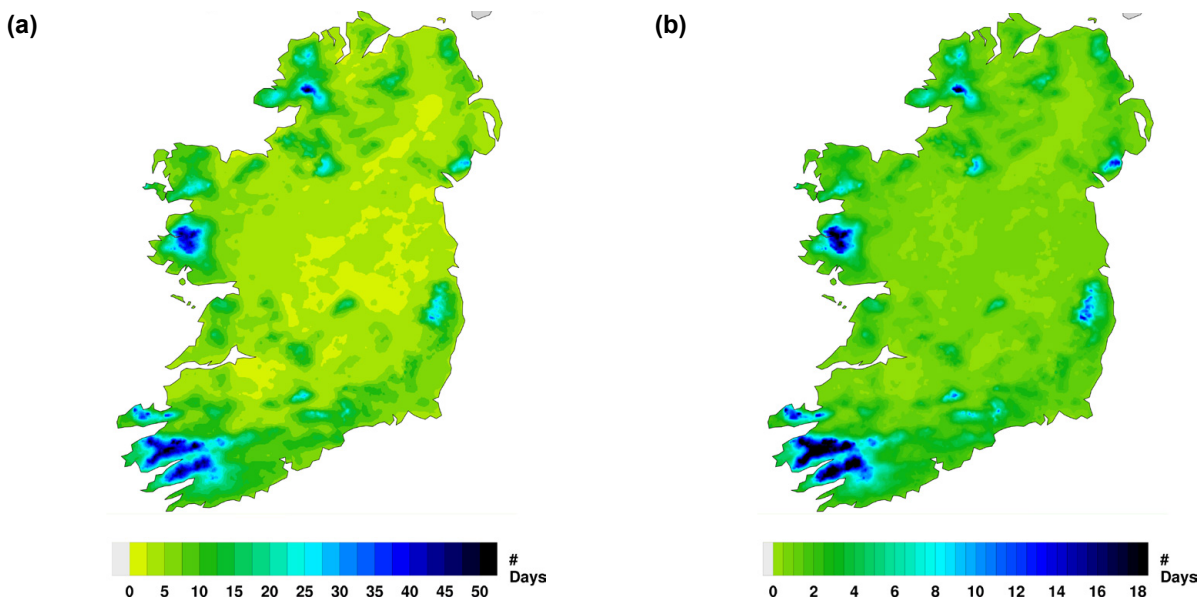

Figure 3.23. The observed number of mean annual (a) wet days (precipitation > 20 mm) and (b) very wet days (precipitation > 30 mm) averaged over the 20-year period 1981–2000. Note the different scales for each figure.

10 Note that these definitions apply only to the current study and were chosen to reflect amounts considered extreme in an Irish context. Such values would be considered less (more) extreme in wetter (dryer) regions of the planet.

11 Spatial figures are not presented for the "likely" projections of heavy precipitation events, as the regional details are highly variable and therefore not reliable. Current work focuses on reducing this regional uncertainty by increasing the RCM ensemble size and using more up-to-date RCMs to downscale CMIP6 global data.

over the 20-year period 1981–2000. Seasonal figures (not shown) present a similar geographical trend.

The projected change in heavy rainfall events are in line with previous RCM studies for Ireland, which showed large projected increases in intense rainfall by the middle of the century, particularly during the winter and autumn months (e.g. Gleeson *et al*., 2013; Nolan, 2015; Nolan *et al*., 2017).

3.11 Dry Periods

To quantify the potential impact of climate change on future drought events, the change in the number of dry periods was analysed. A dry period is defined as at least 5 consecutive days on which the daily precipitation is less than 1 mm.

Figure 3.22a indicates an increase in the annual number of dry periods for the RCP4.5 and RCP8.5 scenarios (mean value ≈16% for both RCPs). The largest increases in dry periods are expected for the summer months (20% for RCP4.5; 27% for RCP8.5 ; see Figure 3.22b). Substantial increases in dry periods are also expected for winter and autumn; projections are similar for both seasons, with an expected increase of ≈20% for both scenarios. A mixed signal was found for spring.

A "likely" increase was also noted in the number of annual (≈9% for both RCPs), winter (≈9% for both RCPs), summer (11% for RCP4.5; 18% for RCP8.5) and autumn (≈10% for both RCPs) dry periods. It follows that it is "likely" that increases in dry periods will be greater than or equal to these values. The projected increase in the frequency of dry periods is well marked in summer, winter, autumn and over the full year, but regional details are not reliable because of a large spread in the ensembles. The projected increase in dry periods during winter, summer, autumn and over the full year is consistent with the large projected change in standard deviation of precipitation (presented in Figures 3.19 and 3.20).

The projected percentage increase in the number of dry periods should be considered in the context of the historical number of dry periods. Figure 3.24 presents the observed number of dry periods annually and in autumn and summer, averaged over the 20-year period 1981–2000. The number of dry periods during winter (not shown) is similar to autumn. The projections of increased dry periods during summers are in line with observed precipitation trends. Murphy *et al*. (2017) analysed a continuous 305-year (1711–2016) monthly rainfall series and found statistically significant decreasing trends in summer rainfall.

The projected changes in dry periods are in line with previous RCM studies for Ireland, which showed large projected increases in dry events by the middle of the century, particularly during the summer and autumn months (e.g. Gleeson *et al*., 2013; Nolan, 2015; Nolan *et al*., 2017). The current study has additionally demonstrated a "likely" increase in dry periods during mid-century winter months.

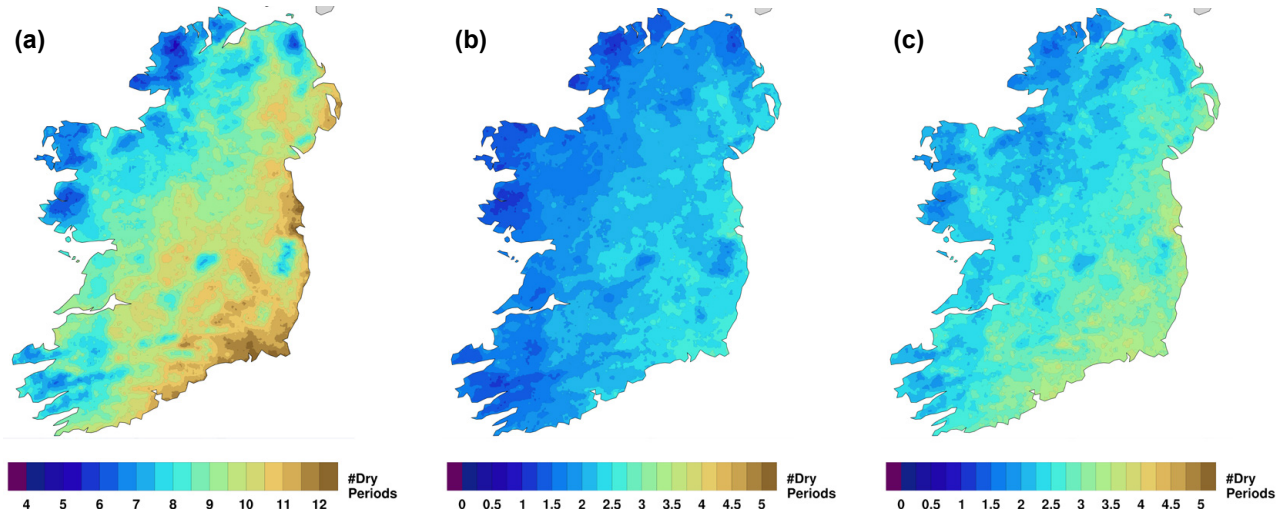

Figure 3.24. The observed number of dry periods averaged over the 20-year period 1981–2000 (a) annually, (b) in autumn and (c) in summer. Note the different scale for the annual figure.

3.12 Snowfall Projections

Figure 3.25 shows that annual snowfall is projected to decrease substantially by the middle of the century for the RCP4.5 (mean value 52%) and RCP8.5 scenarios (mean value 63%). The largest decreases are noted over low-lying regions. Figure 3.26 shows a small variation between the 33rd, 50th and 66th projection percentiles, which demonstrates good agreement (small spread) between ensemble members. Averaged over the whole country, the "likely" decreases in mid-century snowfall are 51% and 60% for the RCP4.5 and RCP8.5 scenarios, respectively.

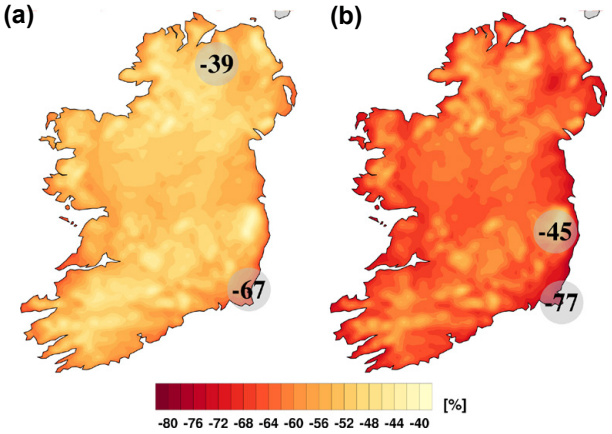

Figure 3.25. Ensemble mean of mid-century snowfall projections (%) for the (a) RCP4.5 and (b) RCP8.5 scenarios. In each case, the future period, 2041–2060, is compared with the past period, 1981–2000. The numbers included on each plot are the minimum and maximum projected changes, displayed at their locations.

3.13 10-m Wind Speed Projections

Figure 3.27 presents the mean annual percentage change in 10-m wind speed for the RCP4.5 and RCP8.5 scenarios. For the purpose of offshore wind energy and shipping applications, the analyses of wind speed cover all land points and a small portion

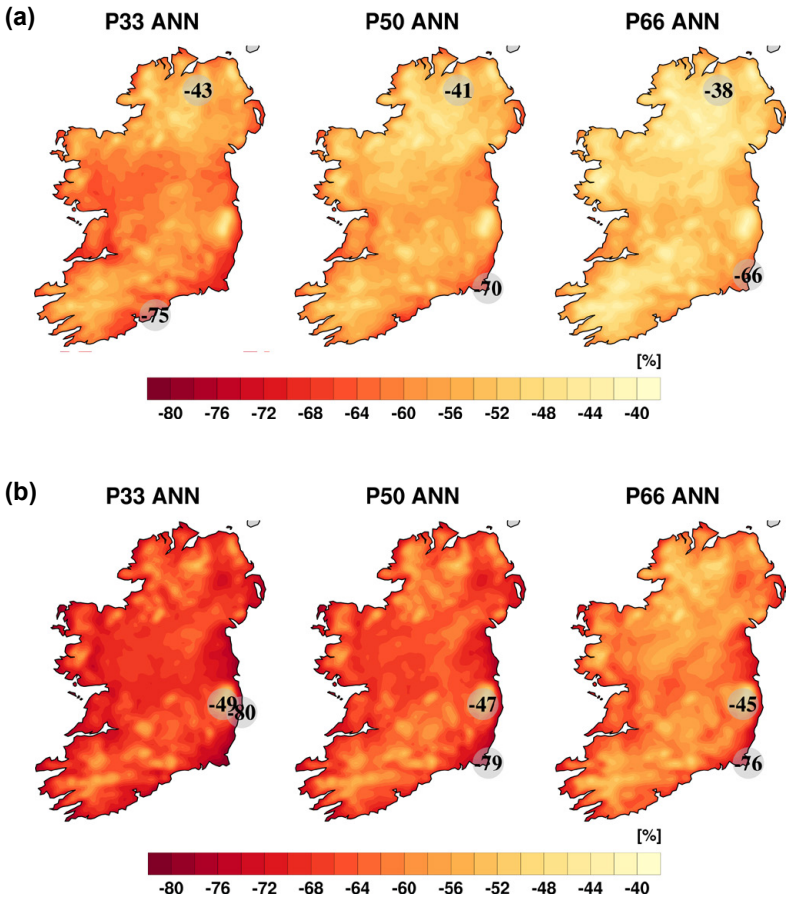

Figure 3.26. The 33rd, 50th and 66th percentiles of annual snowfall projections (%) for the (a) RCP4.5 and (b) RCP8.5 scenarios. In each case, the future period, 2041–2060, is compared with the past period, 1981–2000. The numbers included on each plot are the minimum and maximum projected changes, displayed at their locations.

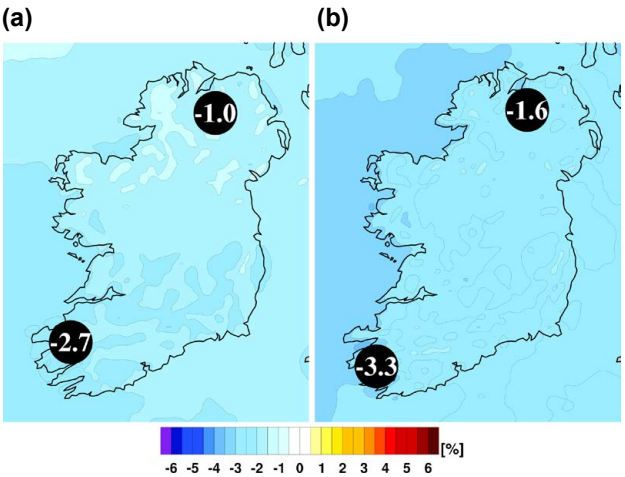

Figure 3.27. Ensemble mean of mid-century 10-m wind speed projections (%) for the (a) RCP4.5 and (b) RCP8.5 scenarios. In each case, the future period, 2041–2060, is compared with the past period, 1981–2000. The numbers included on each plot are the minimum and maximum projected changes over land, displayed at their locations.

of the surrounding sea. The projections show a slight reduction in the 10-m wind speed of 1–2.7% (mean value 1.8%) for the RCP4.5 scenario and 1.6–3.3% (mean value 2.6%) for the RCP8.5 scenario. Figure 3.28a presents the seasonal change (%) in 10-m wind speed for the RCP4.5 scenario; the corresponding plots for RCP8.5 are presented in Figure 3.28b. All seasons show a projected decrease in mean 10-m wind speed. The decreases are largest for summer under the RCP8.5 scenario. The summer reductions range from 0.3% to 3.4% for the RCP4.5 scenario and from 2% to 5.4% for the RCP8.5 scenario.

With the exception of spring and autumn under the RCP4.5 scenario, Figure 3.29 shows a small variation between the 33rd, 50th and 66th 10-m wind speed projection percentiles. This agreement adds a level of confidence to the projected reductions during summer (both RCPs), winter (both RCPs), spring (RCP8.5), autumn (RCP8.5) and over the full year (both RCPs).

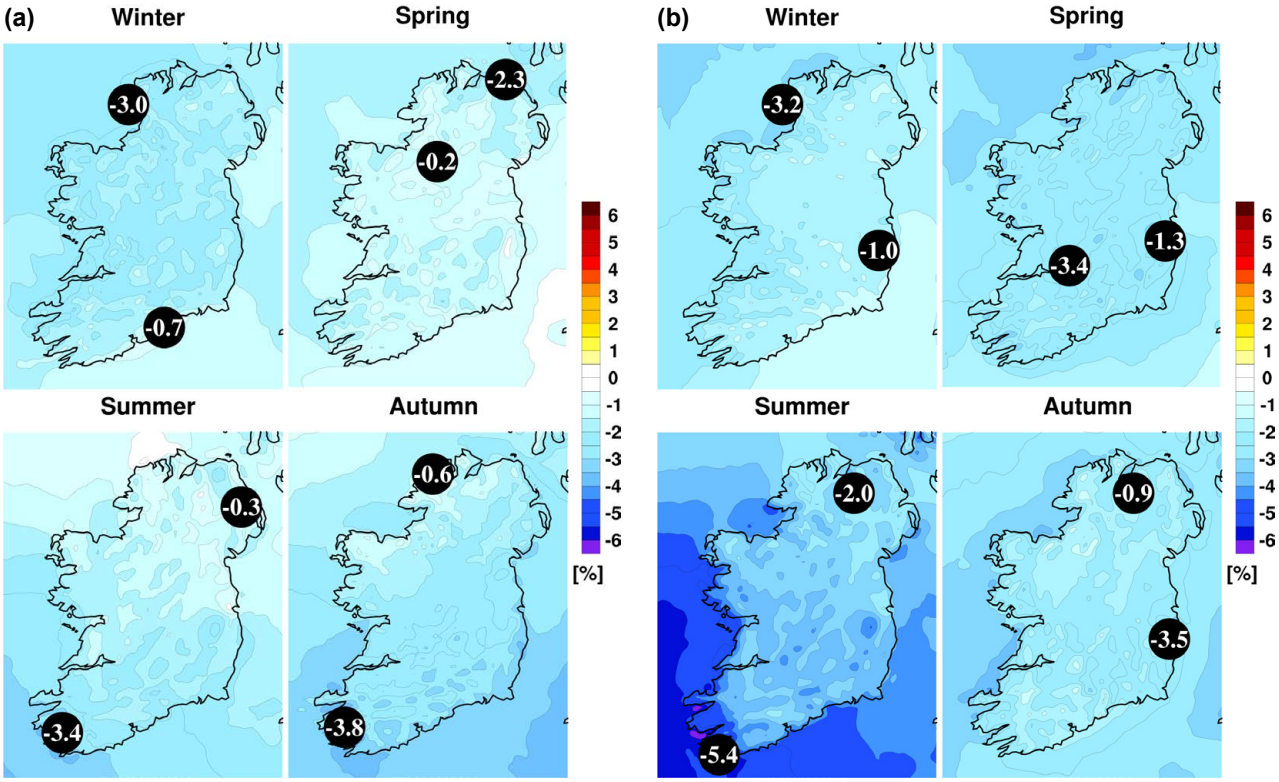

Figure 3.28. Mid-century seasonal projections of mean 10-m wind speed (%) for the (a) RCP4.5 and (b) RCP8.5 scenarios. In each case, the future period, 2041–2060, is compared with the past period, 1981–2000. The numbers included on each plot are the minimum and maximum projected changes, over land, displayed at their locations.

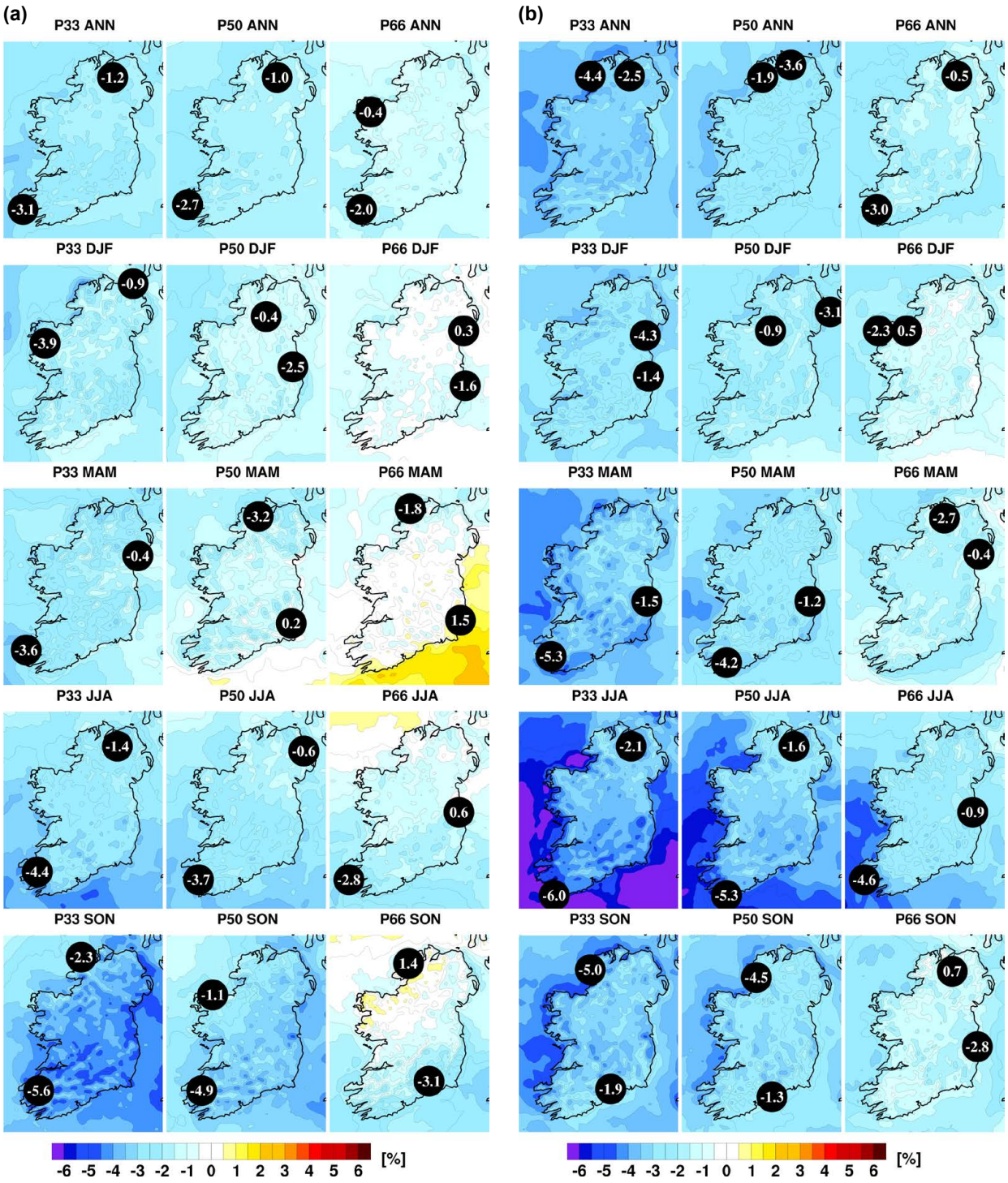

Figure 3.29. The 33rd, 50th and 66th percentiles of annual and seasonal mean 10-m wind speed projections (%) for the (a) RCP4.5 and (b) RCP8.5 scenarios. In each case, the future period, 2041–2060, is compared with the past period, 1981–2000. The numbers included on each plot are the minimum and maximum projected changes over land, displayed at their locations. ANN, annual; DJF, December, January, February; JJA, June, July, August; MAM, March, April, May; SON, September, October, November.

The annual change in the standard deviation of 10-m wind speed (Figure 3.30) shows small changes of ≈−2% to ≈0% for both the RCP4.5 and RCP8.5 scenarios. Similarly, the seasonal projected changes in the standard deviation of 10-m wind speed are small (Figure 3.31). All seasons – except winter, where small (≈0%) changes are noted – show reductions, with the largest decreases noted during summer. A reduction

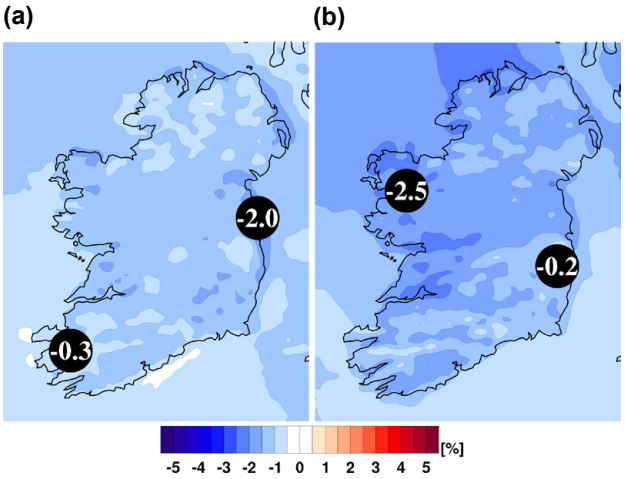

Figure 3.30. Annual projected change in the standard deviation of 10-m wind speed (%) for the (a) RCP4.5 and (b) RCP8.5 scenarios. In each case, the future period, 2041–2060, is compared with the past period, 1981–2000. The numbers included on each plot are the minimum and maximum projected changes, displayed at their locations.

in mean 10-m wind speed, coupled with a decrease in standard deviation, implies a shift to the left of the wind speed distribution and a decrease in the frequency of higher wind speeds.

3.14 Specific Humidity Projections

Figure 3.32a shows that annual specific humidity (the amount of water vapour in the atmosphere calculated as the ratio of the mass of water vapour to the total mass of the air parcel) is projected to increase substantially by the middle of the century for both the RCP4.5 (mean value 8%) and RCP8.5 (mean value 11%) scenarios. There exists a clear south-west to north-east gradient in the projections, with the largest increases in the north. For reference, the "observed" mean annual specific humidity (g kg^{-1}), as resolved by a high-resolution (1.5-km) downscaled ERA-Interim climate simulation, is presented in Figure 3.32b. Please refer to Flanagan *et al*. (2019) for an overview of the climate simulation configuration and validation results.

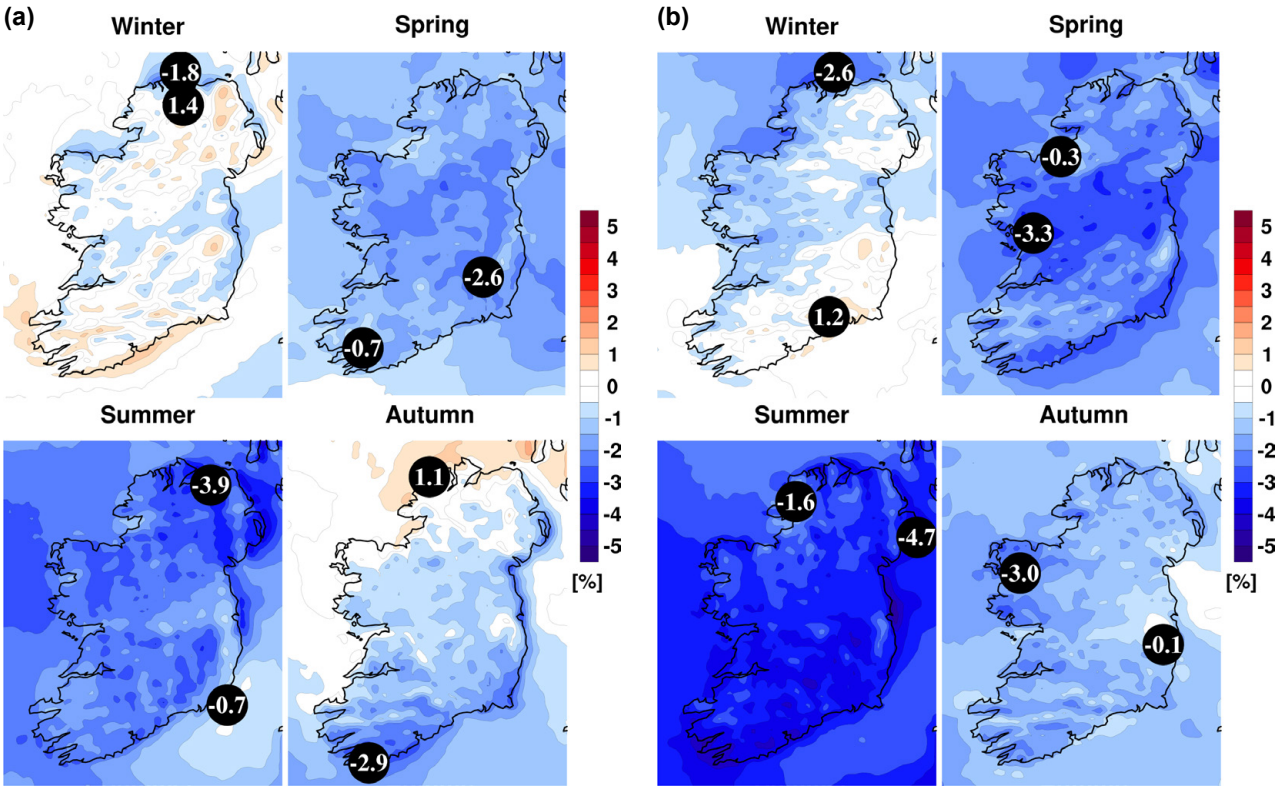

Figure 3.31. Seasonal projected change in the standard deviation of 10-m wind speed (%) for the (a) RCP4.5 and (b) RCP8.5 scenarios. In each case, the future period, 2041–2060, is compared with the past period, 1981–2000. The numbers included on each plot are the minimum and maximum projected changes, displayed at their locations.

Figure 3.33 presents the projected seasonal change (%) in specific humidity for the RCP4.5 and RCP8.5 scenarios. All seasons show a large expected increase in specific humidity. The increases are largest for autumn under the RCP8.5 scenario. Figure 3.34 shows a small variation between the 33rd, 50th and 66th projection percentiles for all seasons and both RCP scenarios. This result demonstrates

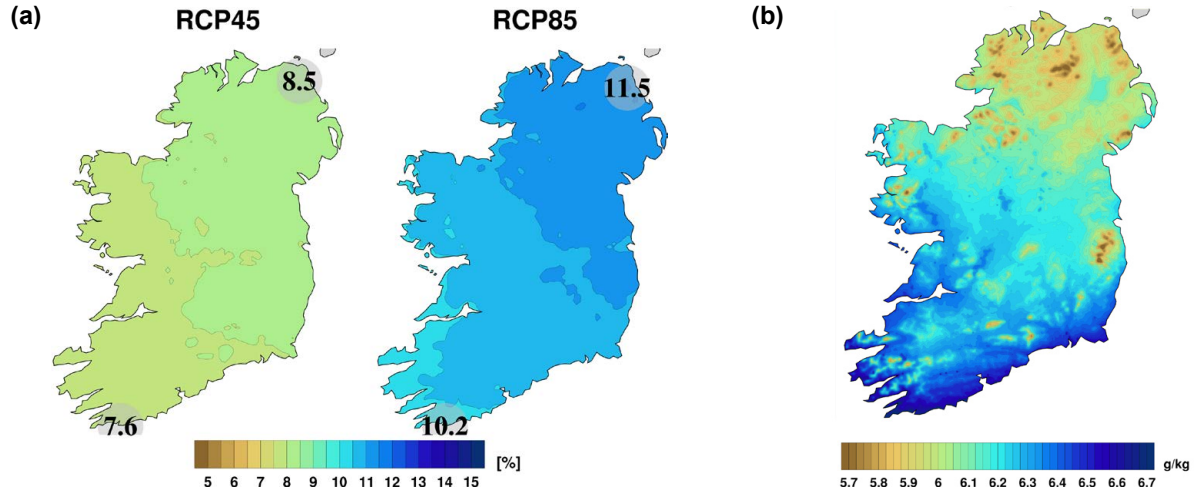

Figure 3.32. (a) Ensemble mean of mid-century specific humidity projections (%) for the RCP4.5 and RCP8.5 scenarios. In each case, the future period, 2041–2060, is compared with the past period, 1981–2000. The numbers included on each plot are the minimum and maximum projected changes, displayed at their locations. (b) Annual mean specific humidity (g kg^{-1}) as resolved by COSMO5-CLM-ERA-Interim 1.5-km data (1981–2000).

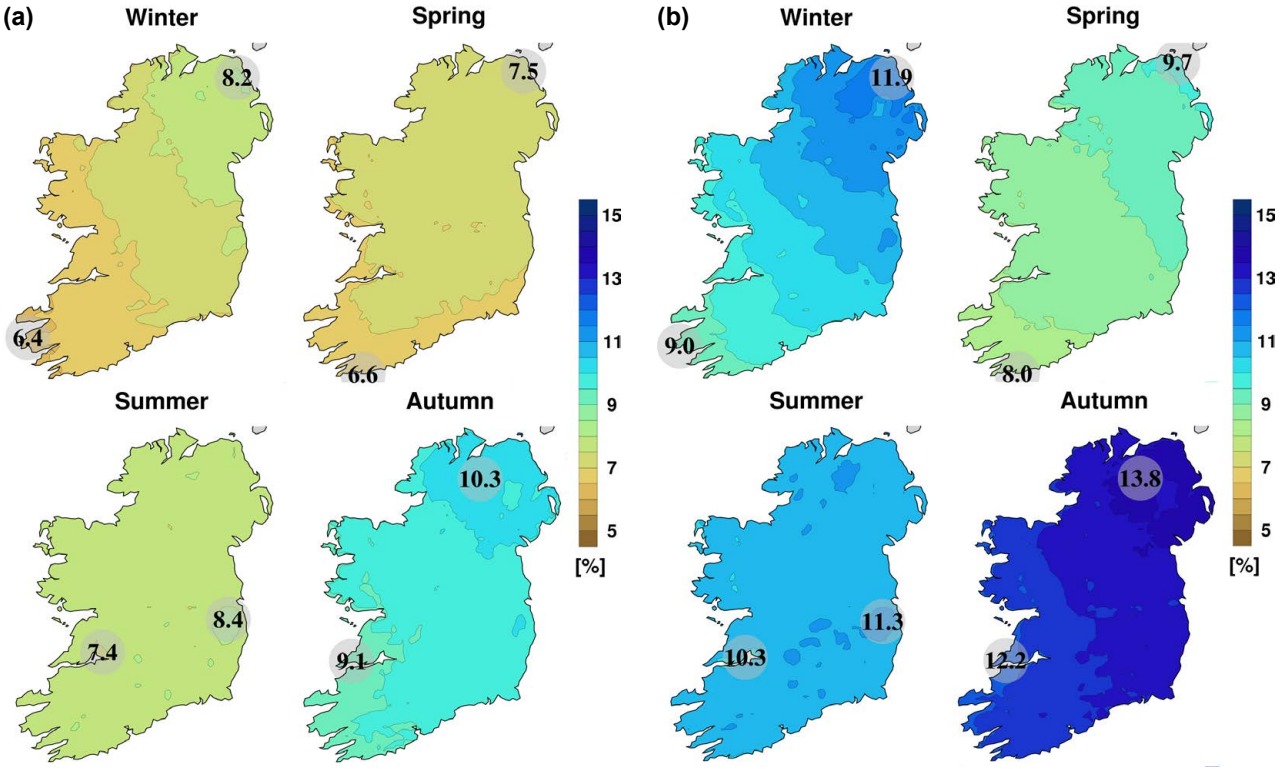

Figure 3.33. Mid-century seasonal projections of specific humidity (%) for the (a) RCP4.5 and (b) RCP8.5 scenarios. In each case, the future period, 2041–2060, is compared with the past period, 1981–2000. The numbers included on each plot are the minimum and maximum projected changes, displayed at their locations.

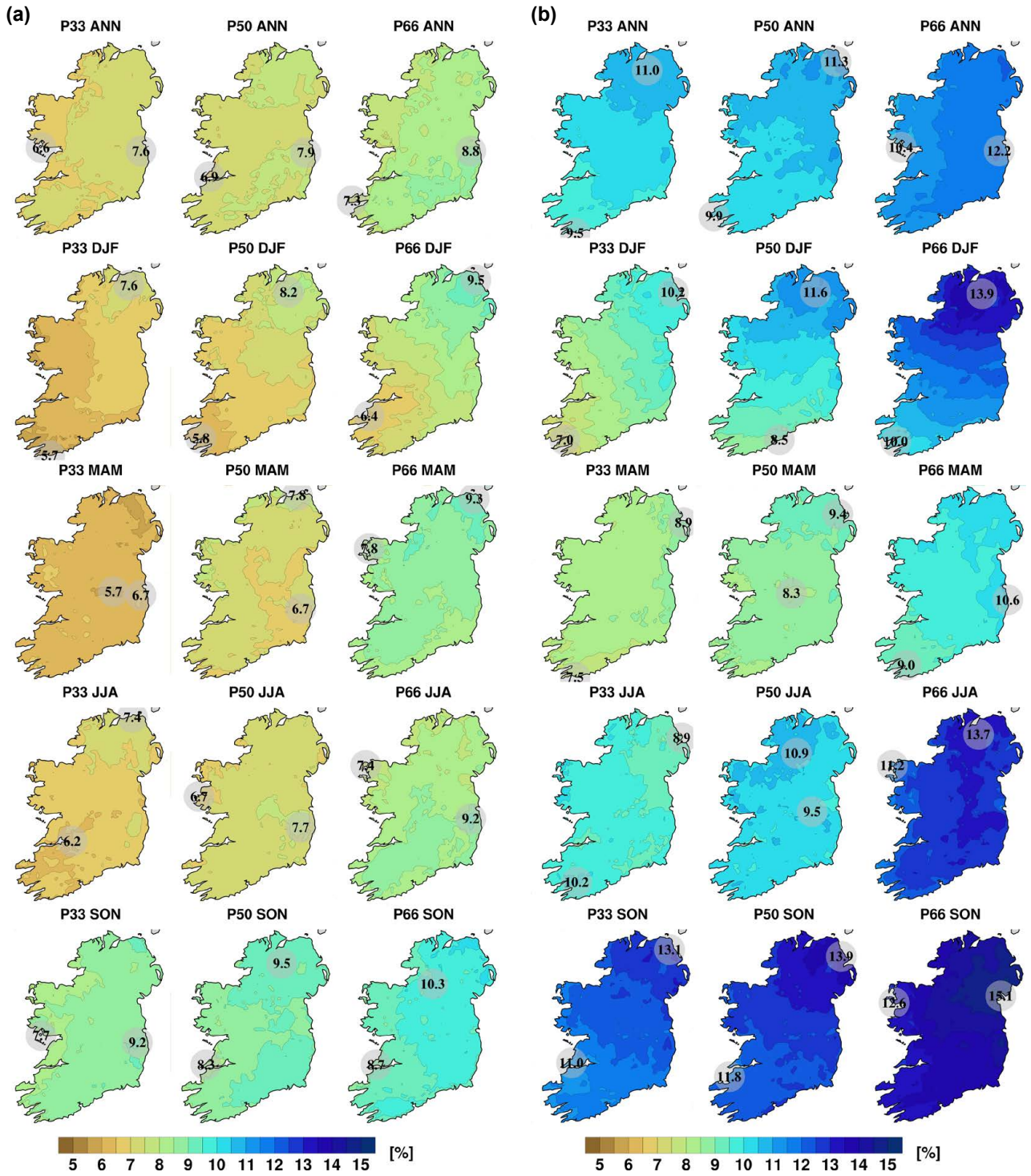

Figure 3.34. The 33rd, 50th and 66th percentiles of annual and seasonal mean specific humidity projections (%) for the (a) RCP4.5 and (b) RCP8.5 scenarios. In each case, the future period, 2041–2060, is compared with the past period, 1981–2000. The numbers included on each plot are the minimum and maximum projected changes, displayed at their locations. ANN, annual; DJF, December, January, February; JJA, June, July, August; MAM, March, April, May; SON, September, October, November.

good agreement (small spread) between ensemble members and adds a high level of confidence to the projections. Averaged over the whole country, the "likely" projected increases in mid-century specific humidity are 7% (annual RCP4.5), 10% (annual RCP8.5), 7% (winter RCP4.5), 9% (winter RCP8.5), 6% (spring RCP4.5), 8% (spring RCP8.5), 7%

(summer RCP4.5), 10% (summer RCP8.5), 9% (autumn RCP4.5) and 12% (autumn RCP8.5).

Specific humidity has direct impacts on animal and human health. Epidemiological studies indicate that low levels of specific humidity are associated with greater influenza mortality (e.g. Shaman *et al*., 2010, 2011; Tamerius *et al*., 2013). Barreca and Shimshack (2012) showed that the humidity–influenza relation is nonlinear, with lower specific humidity levels resulting "in greater influenza mortality at mean daily specific humidity levels below 6 g kg^{-1}", and that "incremental changes in humidity do not significantly affect influenza mortality when mean daily specific humidity exceeds a 6 g kg^{-1} threshold". An increase in specific humidity will amplify the adverse effects of increases in extreme temperatures (section 3.2) and heatwaves (section 3.3) and lead to higher mortality by limiting heat loss through evaporative cooling (Coffel *et al*., 2017).

3.15 Relative Humidity Projections

Relative humidity is the ratio of the amount of water vapour present in the air to the greatest amount possible at the same temperature. Warm air can hold substantially more moisture than cold air, meaning that the relative humidity of cold air is far higher than that of warm air for equal absolute humidity levels. Relative humidity is expressed as a percentage, with 0% corresponding to totally dry air and 100% to totally saturated air (leading to increased probability of precipitation).

Figure 3.35a presents the mean annual change (%)[12] in surface relative humidity for the RCP4.5 and RCP8.5 scenarios. The projections show a slight increase in relative humidity of ≈0–0.6% (mean value 0.1%) for the RCP4.5 scenario and 0–1% (mean value 0.35%) for the RCP8.5 scenario. There exists a south-east to north-west gradient in the projections, with the largest increases in the north. For reference, "observed" mean annual relative humidity (%), as resolved by a high-resolution (1.5-km) downscaled ERA-Interim climate simulation, is presented in Figure 3.35b. Please refer to Flanagan *et al*. (2019) for an overview of model configuration and validation.

Figure 3.36 presents the seasonal change (%) in relative humidity for the RCP4.5 and RCP8.5 scenarios. All seasons, with the exception of summer, show an increase (or ≈0% change) in relative humidity. The largest increases are noted for spring (both RCP scenarios) and winter (RCP8.5). For summer, relative humidity is projected to decrease in the south-east and increase in the north-west (both RCP scenarios).

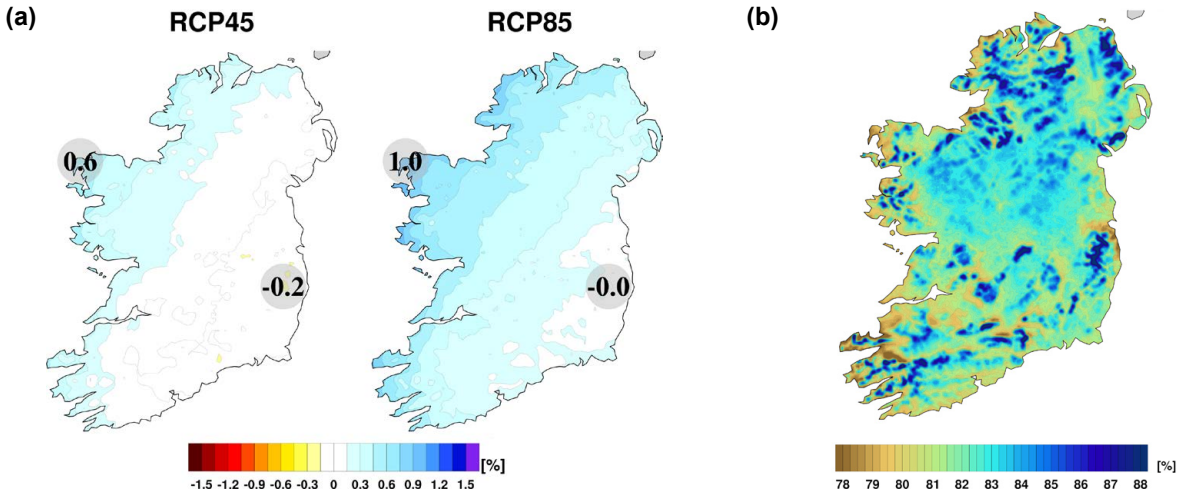

Figure 3.35. (a) Ensemble mean of mid-century relative humidity projections (%) for the RCP4.5 and RCP8.5 scenarios. In each case, the future period, 2041–2060, is compared with the past period, 1981–2000. The numbers included on each plot are the minimum and maximum projected changes, displayed at their locations. (b) Annual mean relative humidity (%) as resolved by COSMO5-CLM-ERA-Interim 1.5-km data (1981–2000).

12 For relative humidity, rather than a relative percentage change, climate projections (%) are calculated as "future (%) minus past (%)".

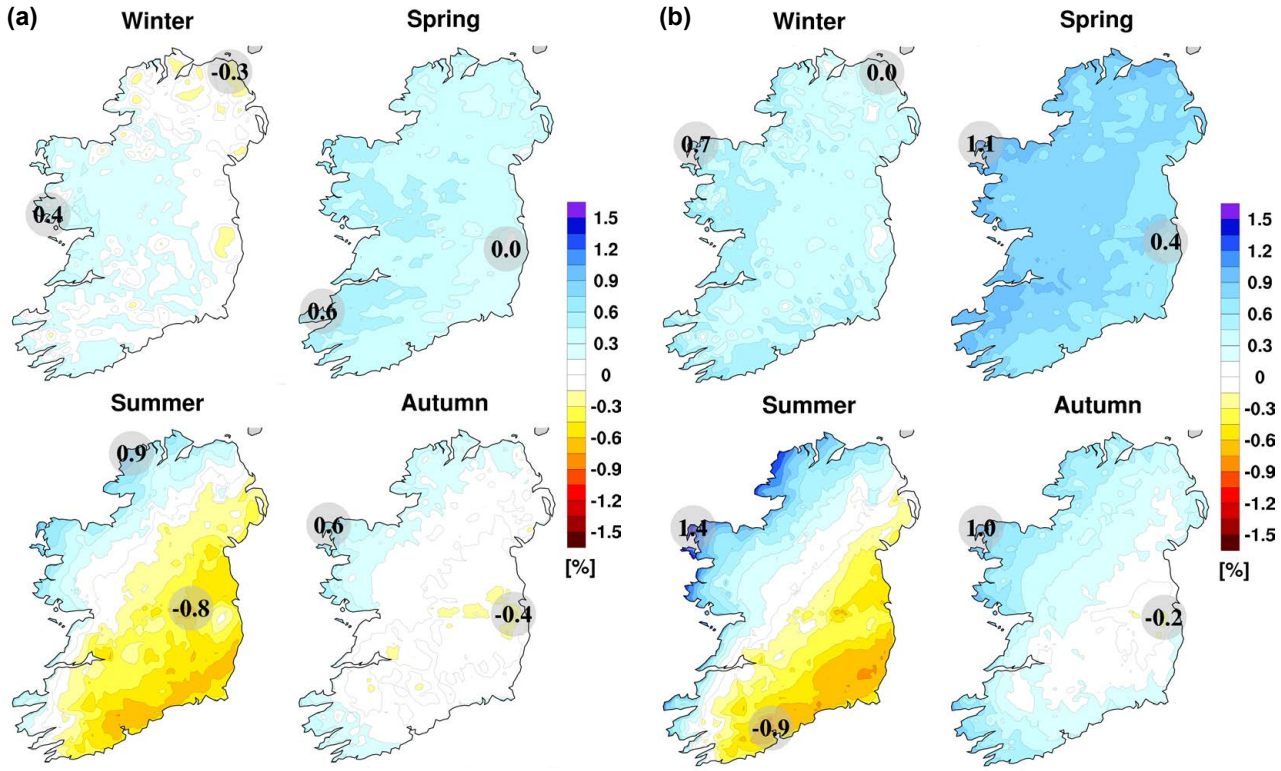

Figure 3.36. Mid-century seasonal projections of relative humidity (%) for the (a) RCP4.5 and (b) RCP8.5 scenarios. In each case, the future period, 2041–2060, is compared with the past period, 1981–2000. The numbers included on each plot are the minimum and maximum projected changes, displayed at their locations.

The percentile projection figures, presented in Figure 3.37, show a small variation between the 33rd, 50th and 66th for winter (RCP8.5), spring (both scenarios), over the full year (RCP8.5) and, to a lesser extent, during autumn (RCP8.5). The signal of decreases in the south-east and increases in the north-west during summer is evident for all percentiles and both RCPs. This agreement adds a level of confidence to the projected changes for summer (both RCPs) and the projected increases for spring (both RCPs), winter (RCP8.5), autumn (RCP8.5) and annual (RCP8.5).

The projections are somewhat contrary to the general consensus in the scientific literature that relative humidity will decrease over land in a warming climate. For example, Byrne and O'Gorman (2018) showed that in recent decades (1979–2016) the land surface has warmed substantially more than the ocean surface and, consequently, relative humidity has fallen over land. Declining relative humidity over land is also the dominant feature of future climate projections, with models predicting that future changes in surface temperature will be strongly amplified over land (Sutton *et al*., 2007; Byrne and O'Gorman, 2013) and that relative humidity will decline over land and either increase (M. Collins *et al*., 2013) or remain approximately constant (O'Gorman and Muller, 2010; Byrne and O'Gorman, 2016) over the oceans. However, the projected trend of decreasing relative humidity over land is not universal. For example, the CMIP5 ensemble of global projections show a projected increase in relative humidity in some coastal land regions, such as West Africa, the Middle East and India (e.g. Figure 1a of Byrne *et al*., 2016; Figure 12.21 of M. Collins *et al*., 2013). The projections over Ireland are small and a large projected increase is noted over the North Atlantic region directly to the north and west of Ireland (which is particularly noticeable in Figure 1a of Byrne *et al*., 2016). Sloth *et al*. (2012) analysed the ENSEMBLES dataset, a large ensemble of RCM climate projections for Europe (van der Linden *et al*., 2009), and found a mixed signal for mid-century projections of relative humidity, with a number of ensemble members showing an increase in relative humidity, particularly over Ireland and Northern Europe

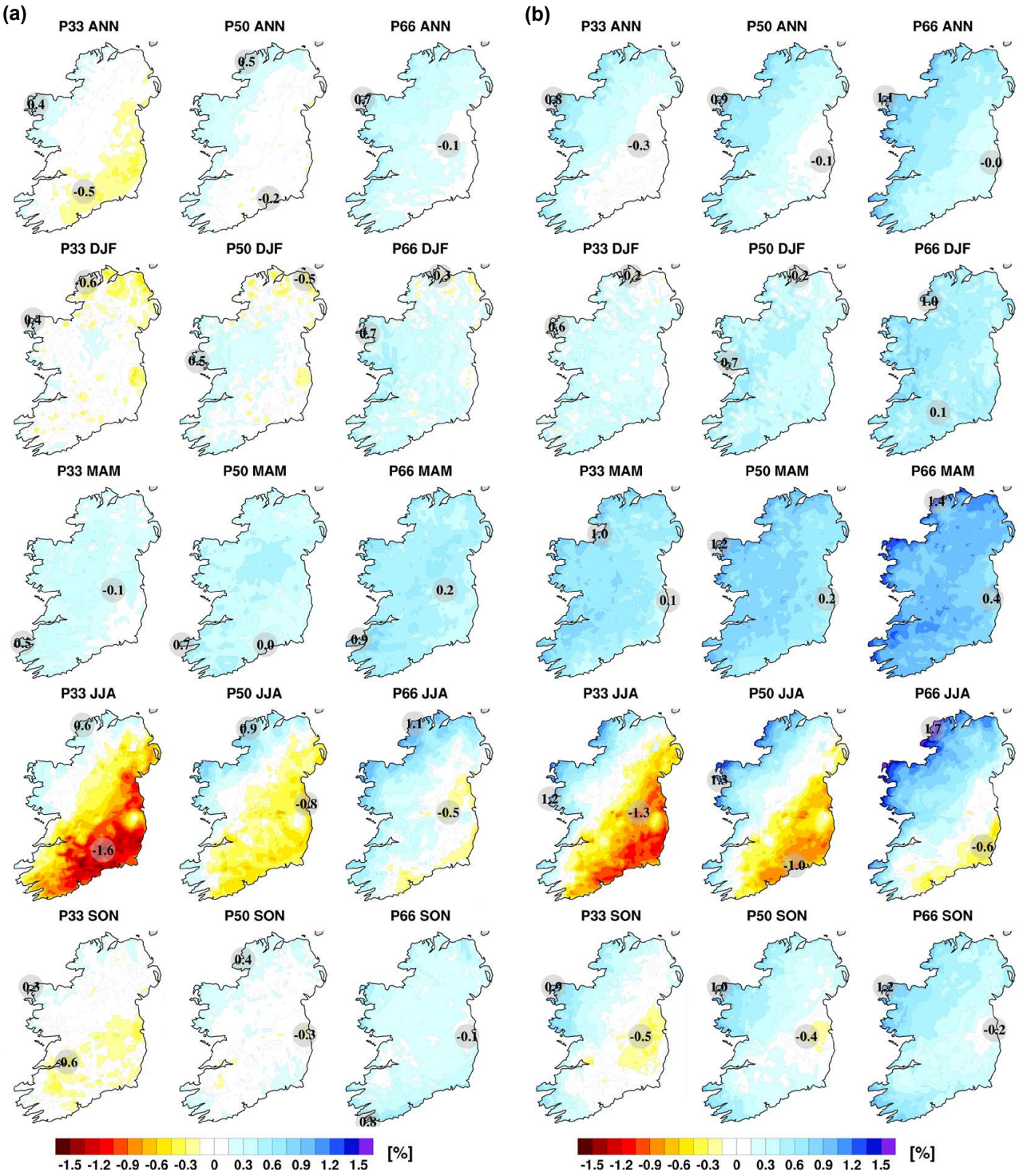

Figure 3.37. The 33rd, 50th and 66th percentiles of annual and seasonal relative humidity projections (%) for the (a) RCP4.5 and (b) RCP8.5 scenarios. In each case, the future period, 2041–2060, is compared with the past period, 1981–2000. The numbers included on each plot are the minimum and maximum projected changes, displayed at their locations. ANN, annual; DJF, December, January, February; JJA, June, July, August; MAM, March, April, May; SON, September, October, November.

(see Figure 9 of Sloth *et al*., 2012). The authors found that the regions where large changes in relative humidity are projected generally correspond to those with large projected increases in mean temperature (relative humidity decreases) or large projected increases in precipitation (relative humidity increases).

The projections of the current study, of small projected increases in relative humidity for all seasons except summer, may be partly attributed to the large influence of the North Atlantic Ocean on the Irish climate. The relative humidity projections for summer (decreases in the south-east and increases in the north-west) may be partly attributed to the temperature projections for summer; note that Figure 3.2 shows a similar south-east to north-west gradient in projected temperature increases, with enhanced warming in the south-east. However, further investigation of these factors is necessary to attribute causation to the relative humidity projections of the current study.

Relative humidity is an important climate field that has a direct impact on many sectors, including public health, agriculture and the built environment. For example, the link between low relative (and specific) humidity and greater influenza mortality is well established (e.g. Noti *et al*., 2013). The incidences of Lyme borreliosis (Lyme disease), a vector-borne illness caused by the bacterium *Borrelia* and spread by ticks, increase with high relative humidity; ticks require a minimum 80% humidity to avoid drying out during the early stages of life (Cullen, 2010) and air temperatures greater than 6°C during host questing (Süss *et al*., 2008). Potato crop failures in Ireland can result when high relative humidity and temperature combine to provide the warm, wet conditions in which the *Phytophthora infestans* fungi (potato blight) thrive (Cucak *et al*., 2019). Changes in relative humidity will have an impact on the built and archaeological heritage of Ireland, affecting deterioration mechanisms such as salt weathering, mould growth and corrosion (Daly, 2019). Relative humidity is also an important field for derived variables, such as fire risk indexes; the risk of wildfire decreases with increasing relative humidity (e.g. Dowdy *et al*., 2010).

3.16 Mean Sea Level Pressure Projections

Figure 3.38 shows that annual average mean sea level pressure (MSLP) is projected to increase by the middle of the century for both the RCP4.5 (mean value 1.4 hPa) and RCP8.5 scenarios (mean value 1.2 hPa). There exists a clear south-east to north-west gradient in the projections, with the largest increases in the north.

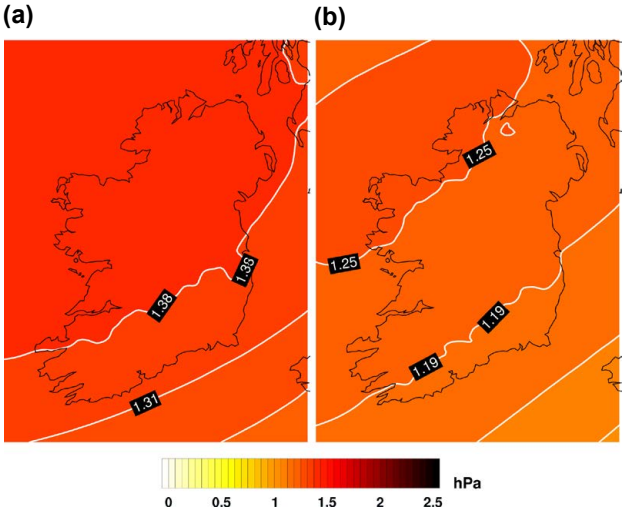

Figure 3.38. Ensemble mean of mid-century MSLP (hPa) projections for the (a) RCP4.5 and (b) RCP8.5 scenarios. In each case, the future period, 2041–2060, is compared with the past period, 1981–2000. The numbers included on each plot are the minimum and maximum projected changes, displayed at their locations.

Figure 3.39 presents the projected mean seasonal change (hPa) in MSLP for the RCP4.5 and RCP8.5 scenarios. All seasons show a large projected increase in MSLP. Figure 3.40 shows a small variation between the 33rd, 50th and 66th projection percentiles for all seasons and both RCP scenarios. This result demonstrates good agreement (small spread) between ensemble members and adds a high level of confidence to the MSLP projections. Averaged over the whole country, the "likely" projected increases in the mid-century average MSLP are 1.2 hPa (annual RCP4.5), 0.9 hPa (annual RCP8.5), 0.6 hPa (winter RCP4.5), 0.2 hPa (winter RCP8.5), 0.8 hPa (spring RCP4.5), 0.6 hPa (spring RCP8.5), 0.6 hPa (summer RCP4.5), 1.3 hPa (summer RCP8.5), 1.6 hPa (autumn RCP4.5) and 1 hPa (autumn RCP8.5).

The projected increases in MSLP are some of many possible factors that could contribute to the projections of decreases in wind speed (section 3.13) and wind power (section 3.18), and increases in dry periods (section 3.11) and heatwave (section 3.3) events.

The projected increase in MSLP may be attributed to the projected decrease in the number of overall cyclones (section 3.17). A discussion on possible mechanisms for a reduction in the number of

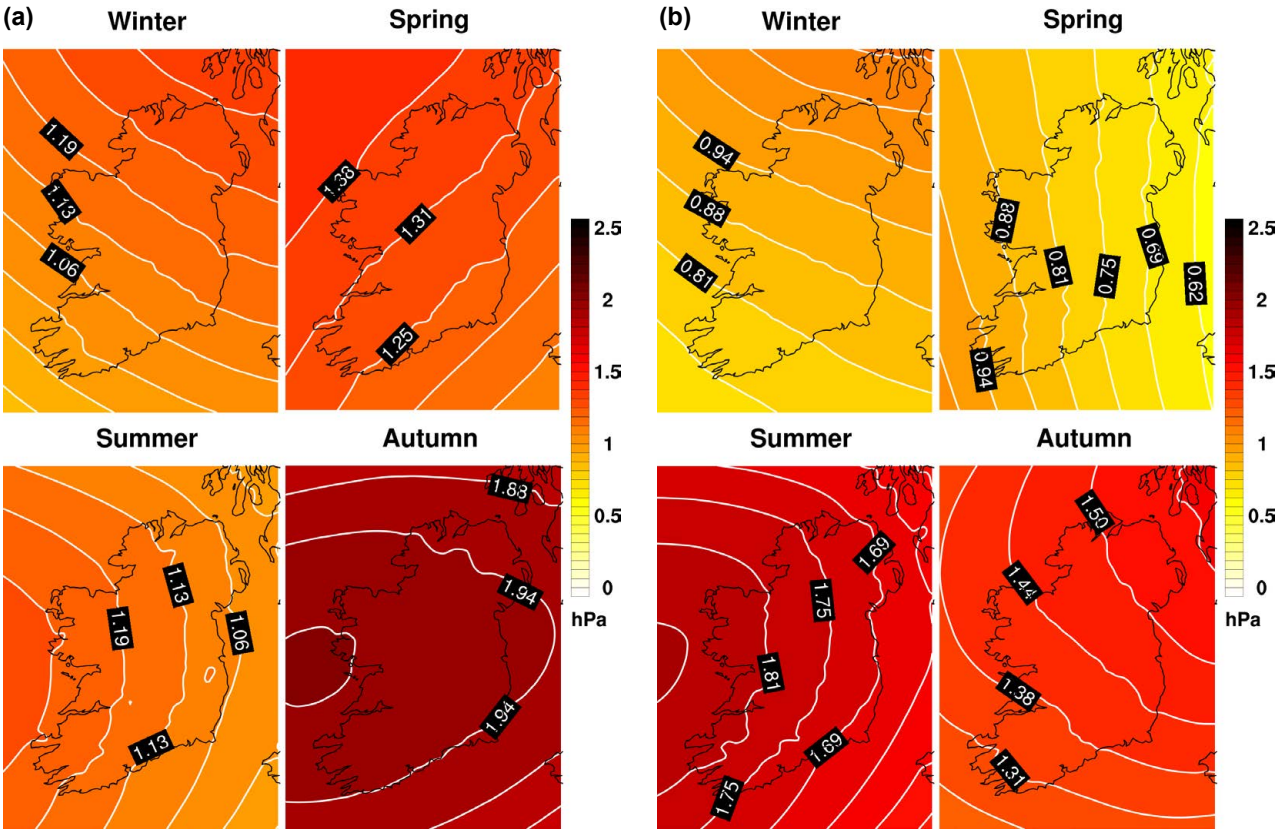

Figure 3.39. Mid-century seasonal projections of MSLP (hPa) for the (a) RCP4.5 and (b) RCP8.5 scenarios. In each case, the future period, 2041–2060, is compared with the past period, 1981–2000. The numbers included on each plot are the minimum and maximum projected changes, displayed at their locations.

mid-latitude storms in a warming world is provided in section 3.17. However, further investigation is necessary to attribute causation to the MSLP projections of the current study. Future work will attempt to address this issue by analysing a substantially larger RCM ensemble of downscaled CMIP6 data. Furthermore, the impact of changes in both the frequency and intensity of low pressure systems on MSLP will be quantified.

3.17 Storm Track Projections

Given the large societal impacts of extreme storms, there is considerable interest in the potential impact of climate change on extreme cyclonic activity in the North Atlantic. Windstorms and associated high wind speeds are a major source of natural hazard risk for Ireland and many countries across Europe. For example, Ireland and the UK were severely affected by an exceptional run of storms during the winter of 2013/2014, culminating in serious coastal damage and widespread, persistent flooding. Reports issued by the meteorological agencies of Ireland and the UK have confirmed that records for precipitation totals and extreme wind speeds were set during this period (Met Éireann, 2014; Kendon *et al.,* 2015). Matthews *et al*. (2014) found that the UK/Ireland winter of 2013/2014 was the stormiest for at least 143 years when storm frequency and intensity are considered together. In addition to the potential widespread flooding and structural damage associated with intense storms, the wind energy supply can be negatively affected, as wind turbines are shut down during periods of high wind speeds to prevent damage.

Feser *et al*. (2014) conducted a review of studies of storms over the North Atlantic and north-western Europe to identify potential long-term trends. Storm trends derived from reanalyses data and climate model data for the past were mostly limited to the last four to six decades. They found that “the majority of these studies find increasing storm activity north of about 55–60°N over the North Atlantic with a negative tendency southward” (Feser *et al*., 2014). Furthermore, “future scenarios until about the year 2100 indicate mostly an increase in winter storm intensity over the

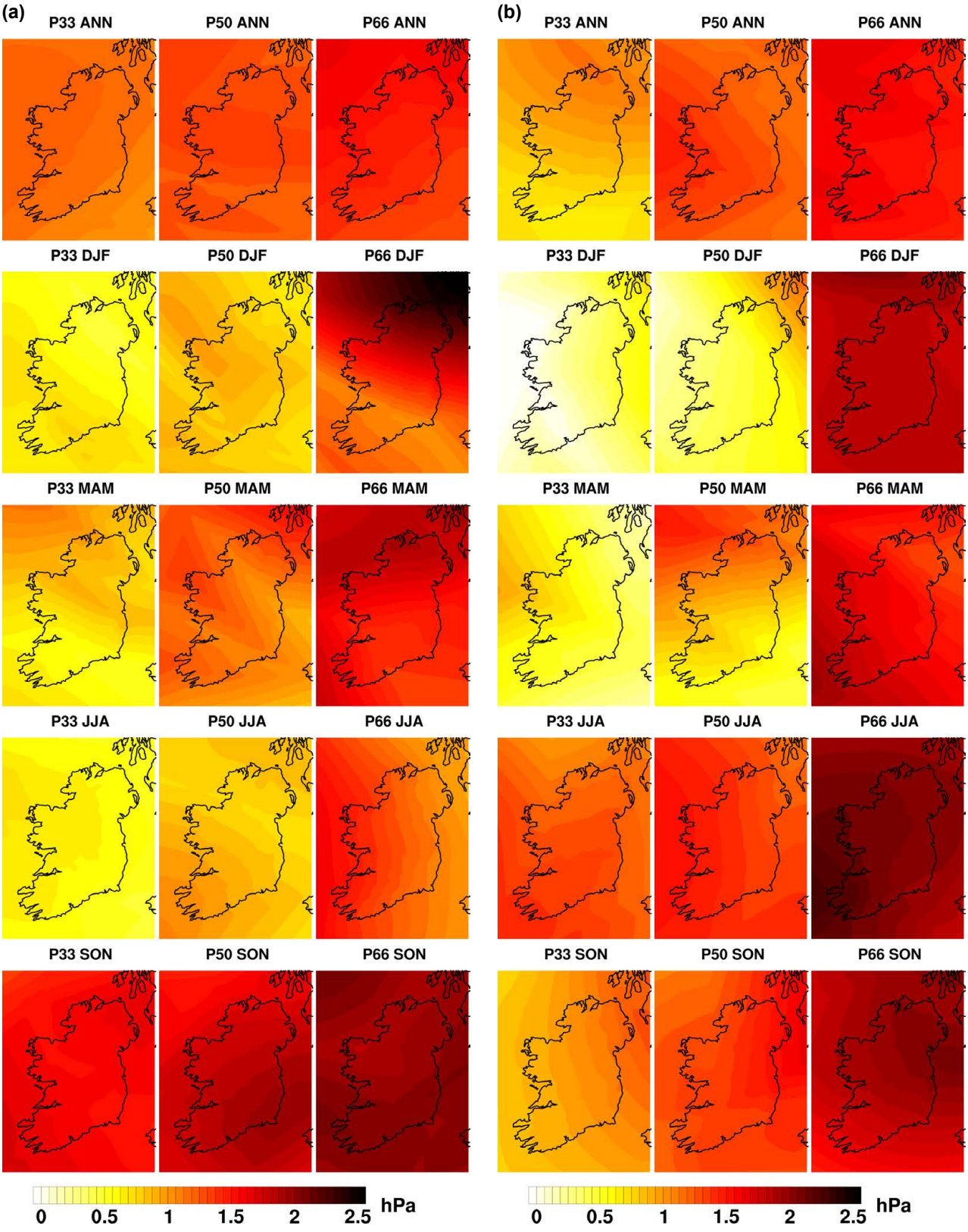

Figure 3.40. The 33rd, 50th and 66th percentiles of annual and seasonal MSLP projections (hPa) for the (a) RCP4.5 and (b) RCP8.5 scenarios. In each case, the future period, 2041–2060, is compared with the past period, 1981–2000. The numbers included on each plot are the minimum and maximum projected changes, displayed at their locations. ANN, annual; DJF, December, January, February; JJA, June, July, August; MAM, March, April, May; SON, September, October, November.

North Atlantic and western Europe. However, future trends in total storm numbers are quite heterogeneous and depend on the model generation used" (Feser *et al*., 2014). Matthews *et al*. (2016) analysed cyclone trends in the British and Irish Isles (BI) by assessing a 142-year (1871–2012) record of cyclone frequency, intensity and "storminess" derived from the 20th-century Reanalysis V2 (20CR) dataset. They found an "upward trend in cyclone intensity for the BI region, which is strongest in winter and consistent with model projections" (Matthews *et al*., 2016). Zappa *et al*. (2013) analysed a CMIP5 ensemble of 19 GCMs and found a small, but significant, increase in the number and intensity of winter cyclones associated with strong wind speeds over the UK by the end of the century. A 2013 study with a very high-resolution version of the EC-Earth model (Haarsma *et al*., 2013) suggests an increase in the frequency of extreme wind storms affecting Western Europe in future autumn seasons as a result of climate change.

As part of the current study, an algorithm was developed to identify and track cyclones. The algorithm was applied to an ensemble subset of EURO-CORDEX 12-km downscaled CMIP5 data. Results show a reduction of ≈10% in the numbers of less intense storms affecting Ireland and suggest an eastward extension of the more severe wind storms over Ireland and the UK from the middle of the century.[13] Figure 3.41 presents intense storm tracks as simulated by the European Coordinated Regional climate Downscaling Experiment (EURO-CORDEX) ensemble. Previous studies that analysed RCM projections of future extreme storm events over Ireland are in broad agreement with these results (Semmler *et al*., 2008a,b; Nolan, 2015; McGrath and Nolan, 2017). It should be noted that extreme storms, as presented in Figure 3.41, are rare events. Therefore, the storm projections should be considered with a high level of caution. Future work will focus on analysing a larger ensemble of downscaled CMIP6 data, thus allowing a robust statistical analysis of extreme storm track projections.

The warming of the climate system on account of greenhouse gas forcing is expected to change the thermal structure of the lower atmosphere; the enhanced warming of the poles, particularly in the Arctic, will reduce the equator-to-pole temperature gradient and this effect is often appealed to as a mechanism for a reduction in the number of mid-latitude storms in a warming world. For example, Geng and Sugi (2003) and Semmler *et al*. (2008b) proposed that a decreased meridional temperature gradient and the associated reduced baroclinicity in the future climate could be responsible for the decrease of the total number of cyclones. Furthermore, the higher moisture supply as a result of a generally higher sea surface temperature and the related increase in latent heat fluxes could trigger strong-intensity cyclones (Hall *et al*., 1994; Semmler *et al*., 2008b). Further work, analysing a large ensemble of downscaled CMIP6 datasets, is required to fully investigate these issues.

3.18 120-m Wind Power Projections

There is considerable interest among policymakers and the energy industry in renewable energy resources as a means of reducing carbon dioxide emissions to minimise climate change (Solomon *et al*., 2007). Within this context, the current section assesses the impacts of climate change on the future wind energy resource of Ireland. Because the energy content of the wind is proportional to the cube of the wind speed, we focus on projections of the mean cube of the wind speed.[14] Furthermore, wind energy projections at 120 m above the surface were analysed, so the results provide information at a typical turbine height.[15]

Figure 3.42 presents the mean annual percentage change in 120-m wind power for the RCP4.5 and RCP8.5 scenarios. For the purpose of onshore and offshore wind energy applications, the analyses of wind power cover all land points and a small portion of the surrounding sea. The projections show a slight reduction in the 120-m wind power of 3.1–5.8%

13 Note that because extreme storms are very rare events, a slight increase has no noticeable effect on the mean wind speed statistics presented in section 3.13. The projected decrease in less intense (very common) storms has a substantially greater effect on decreasing the frequency of higher wind speeds than the increase in very rare intense storms.

14 A more accurate measure of wind power is given by wind power = 0.5 × air density × (wind speed)^3. Because air density was not archived for all RCM ensemble members, we focus on the cube of the wind speed as a measure of wind power.

15 https://www.windawareireland.com/overview/ (accessed 31 May 2020).

(a) EURO-CORDEX, 1976–2005

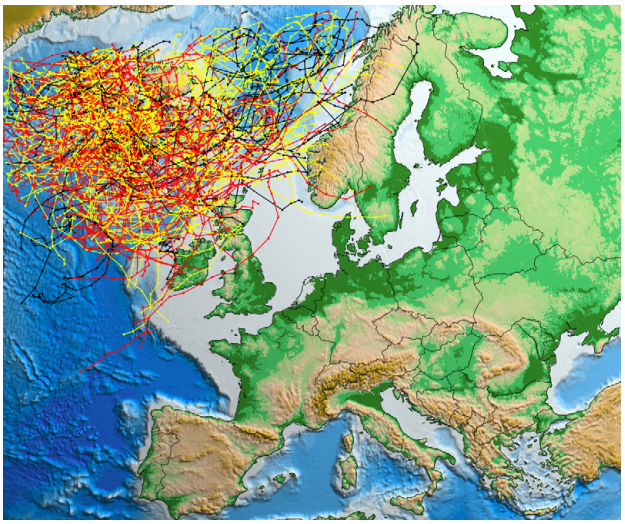

(b) EURO-CORDEX RCP4.5, 2040–2069

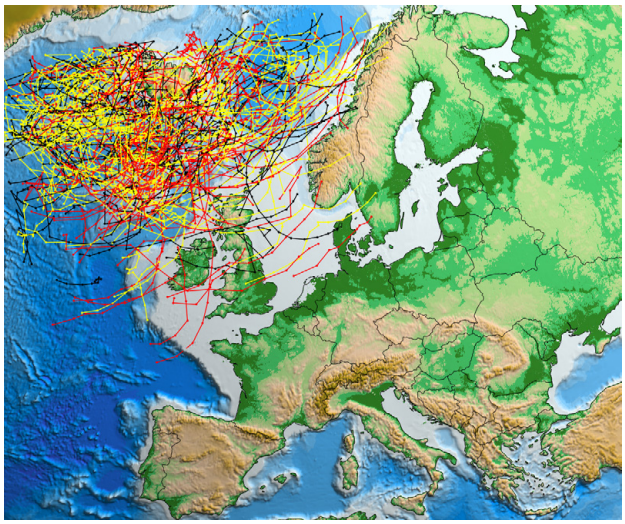

(c) EURO-CORDEX RCP8.5, 2040–2069

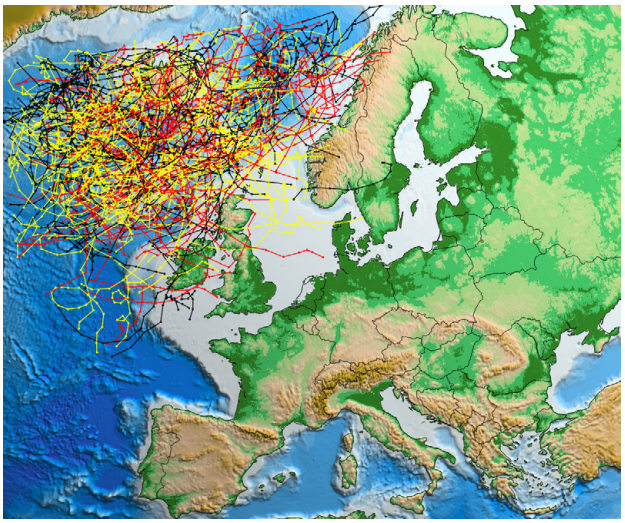

(d) EURO-CORDEX RCP4.5, 2070–2099

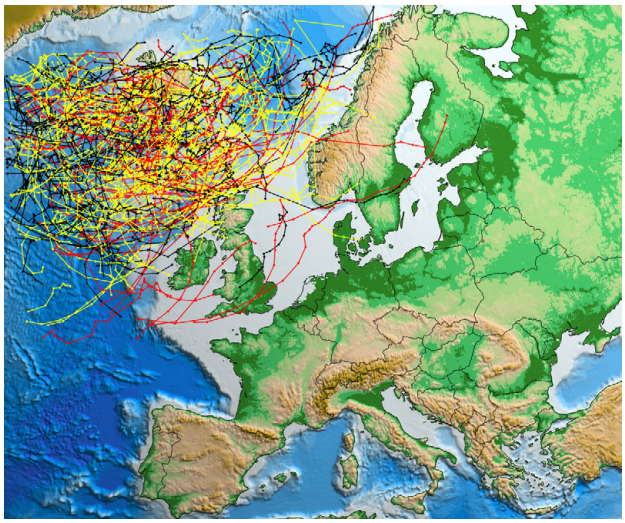

(e) EURO-CORDEX RCP8.5, 2070–2099

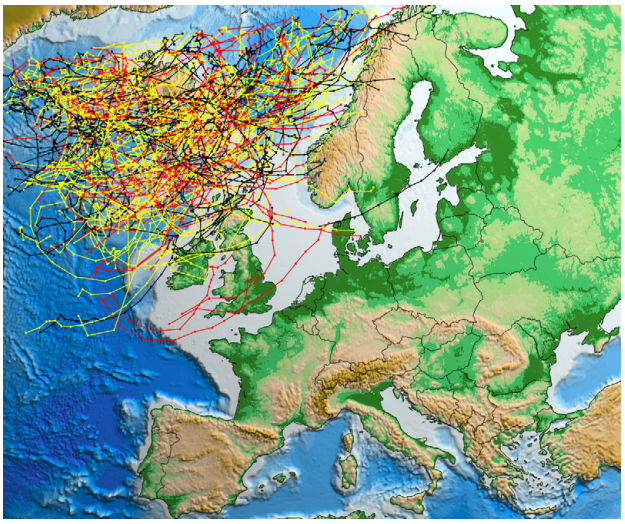

Figure 3.41. Tracks of intense storms as simulated by an ensemble of EURO-CODEX model runs. Tracks are plotted for storms with core MSLPs less than 950 hPa and that exist for at least 24 hours. In addition, storms are only considered if the maximum 10-m wind speed within 250 km of the storm centre (radius of maximum wind; denoted w_r) is greater than 24.5 m s^{-1}. Tracks are coloured black if $24.5 < w_r \leq 28.5$ m s^{-1}, yellow if $28.5 < w_r \leq 32.7$ m s^{-1} and red if $w_r > 32.7$ m s^{-1}. (a) Past simulations (1976–2005), (b) RCP4.5 (2040–2069), (c) RCP8.5 (2040–2069), (d) RCP4.5 (2070–2099) and (e) RCP8.5 (2070–2099).

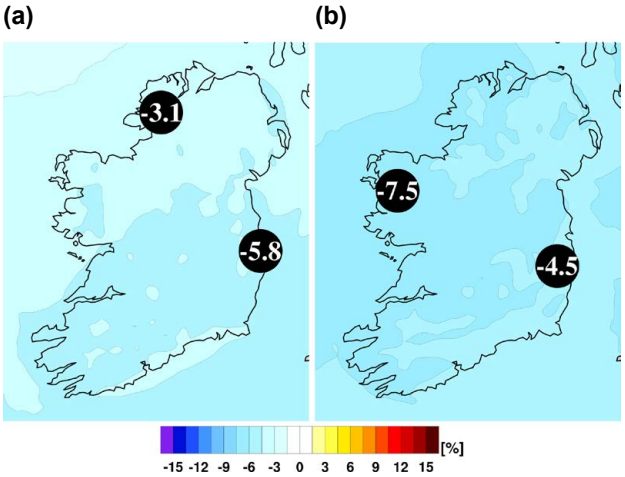

Figure 3.42. Ensemble mean of mid-century 120-m wind power projections (%) for the (a) RCP4.5 and (b) RCP8.5 scenarios. In each case, the future period, 2041–2060, is compared with the past period, 1981–2000. The numbers included on each plot are the minimum and maximum projected changes, displayed at their locations.

(mean value 4.5%) for the RCP4.5 scenario and 4.5–7.5% (mean value 6%) for the RCP8.5 scenario. Figure 3.43a presents the seasonal change (%) in 120-m wind power for the RCP4.5 scenario; the corresponding plots for RCP8.5 are presented in Figure 3.43b. All seasons show a projected decrease in mean 120-m wind power. The decreases are largest for summer under the RCP8.5 scenario. The summer reductions range from 2.8% to 8.7% for the RCP4.5 scenario and from 6.5% to 14.1% for the RCP8.5 scenario.

With the exception of spring and autumn under the RCP4.5 scenario, Figure 3.44 shows a small variation between the 33rd, 50th and 66th 120-m wind power projection percentiles. This agreement adds a level of confidence to the projected reductions in wind power during summer (both RCPs), winter (both RCPs), spring (RCP8.5), autumn (RCP8.5) and over the full year (both RCPs).

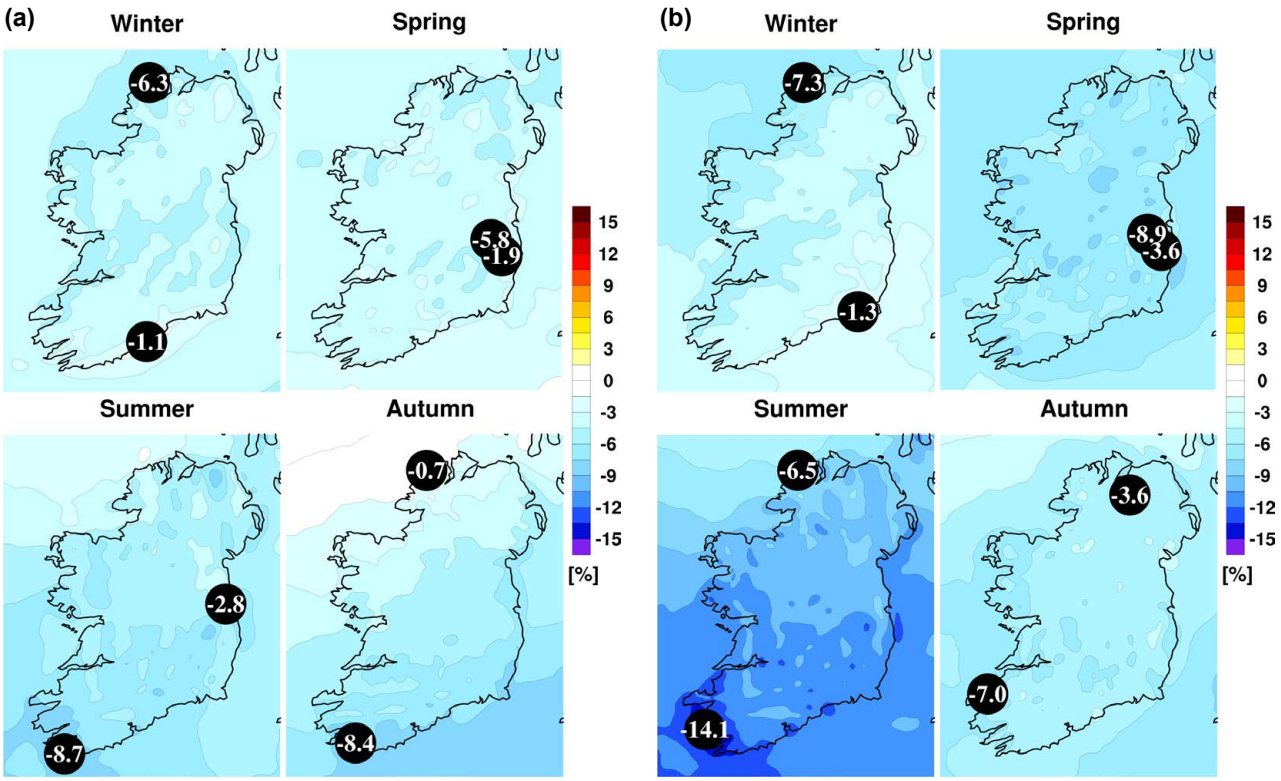

Figure 3.43. Mid-century seasonal projections of mean 120-m wind power (%) for the (a) RCP4.5 and (b) RCP8.5 scenarios. In each case, the future period, 2041–2060, is compared with the past period, 1981–2000. The numbers included on each plot are the minimum and maximum projected changes, displayed at their locations.

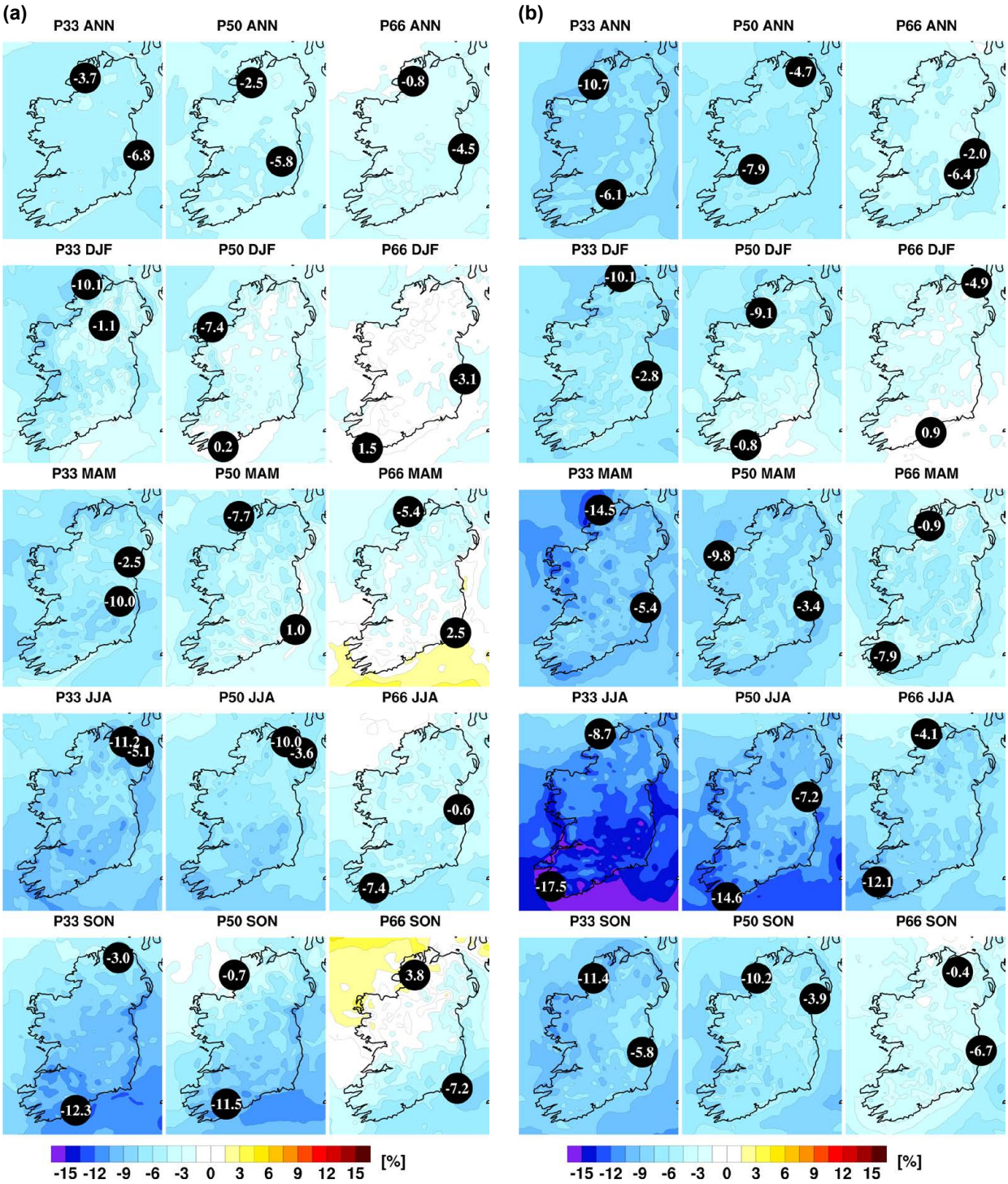

Figure 3.44. The 33rd, 50th and 66th percentiles of annual and seasonal mean 120-m wind power projections (%) for the (a) RCP4.5 and (b) RCP8.5 scenarios. In each case, the future period, 2041–2060, is compared with the past period, 1981–2000. The numbers included on each plot are the minimum and maximum projected changes, displayed at their locations. ANN, annual; DJF, December, January, February; JJA, June, July, August; MAM, March, April, May; SON, September, October, November.

The annual change in the standard deviation of 120-m wind power (Figure 3.45) shows small changes of between ≈−5.5% and −0.6% for both the RCP4.5 and RCP8.5 scenarios. All seasons – except winter and autumn (RCP4.5), when small (≈0%) changes are noted – show reductions, with the largest decreases noted during summer (Figure 3.46). A reduction in 120-m wind power, coupled with a decrease in

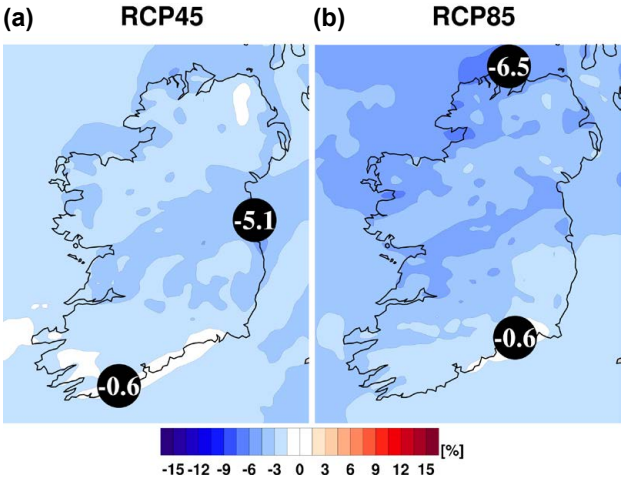

Figure 3.45. Annual projected change in the standard deviation of 120-m wind power (%) for the (a) RCP4.5 and (b) RCP8.5 scenarios. In each case, the future period, 2041–2060, is compared with the past period, 1981–2000. The numbers included on each plot are the minimum and maximum projected changes, displayed at their locations.

standard deviation, implies a shift to the left of the wind power distribution and an enhanced decrease in wind power in the more energetically useful range.

The projected changes in wind power are in line with previous RCM studies for Ireland, which showed projected decreases in wind power by the middle of the century during summer, spring and over the full year (e.g. Nolan *et al*., 2014; Nolan, 2015).

3.19 Surface Shortwave Radiation and Solar Photovoltaic Power

Figure 3.47a, the projected change in mean annual surface shortwave radiation, shows ≈0% or small decreases by the middle of the century. Small projected decreases are also noted for winter and spring, whereas summer and autumn show small increases, particularly in the south (not shown). However, the projected changes are small and so will have minimal effect on solar energy, agricultural and health impacts (e.g. skin cancer and vitamin D deficiency).

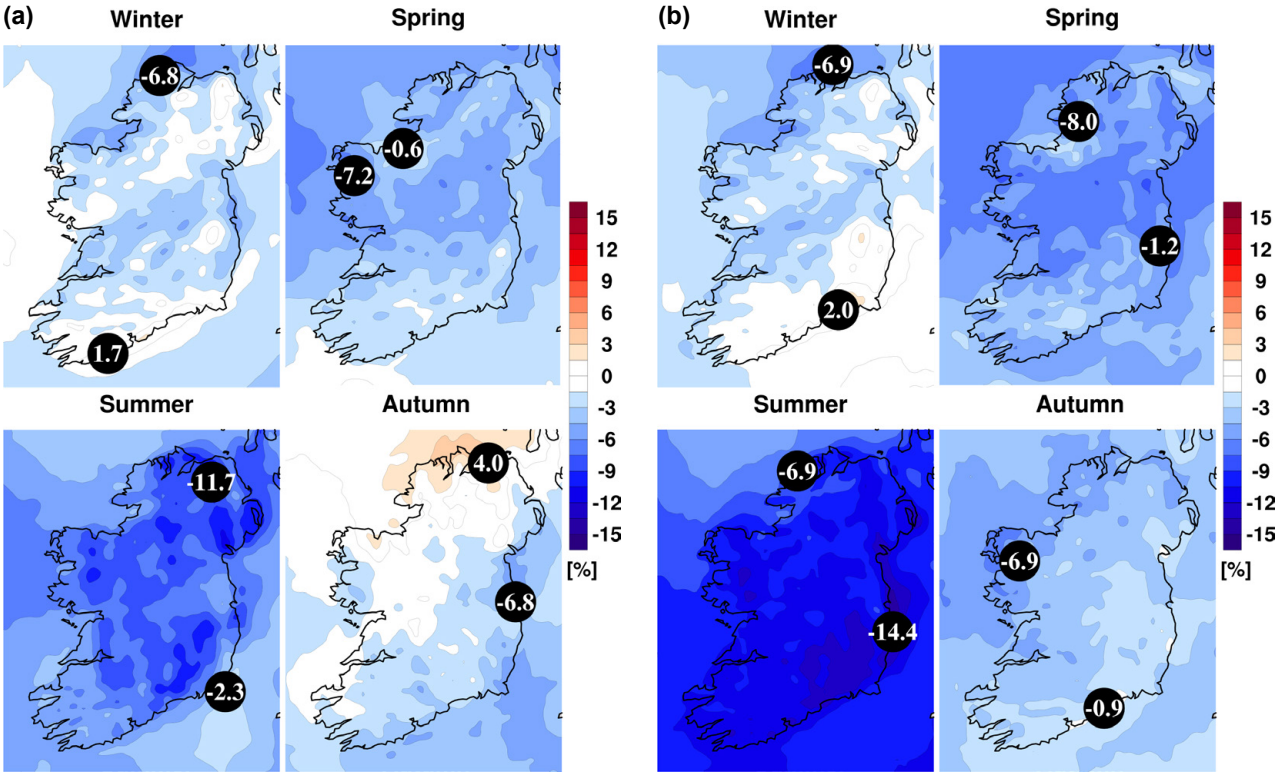

Figure 3.46. Seasonal projected change in the standard deviation of 120-m wind power (%) for the (a) RCP4.5 and (b) RCP8.5 scenarios. In each case, the future period, 2041–2060, is compared with the past period, 1981–2000. The numbers included on each plot are the minimum and maximum projected changes, displayed at their locations.

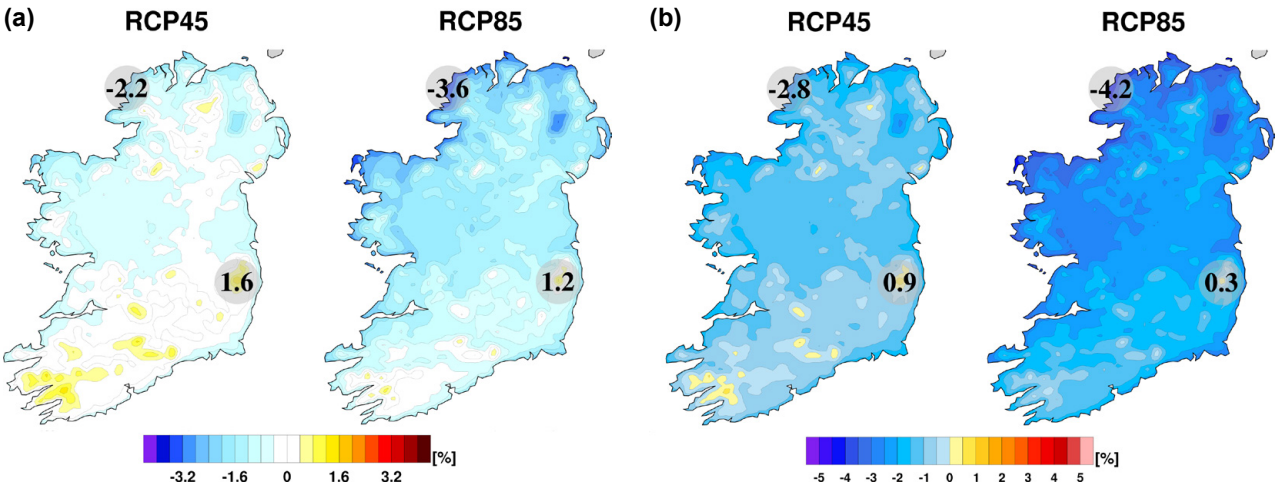

Figure 3.47. Mid-century projected changes (%) in mean annual (a) surface shortwave radiation and (b) solar PV power.

The radiation projections are in line with similar European studies. Jerez *et al*. (2015) analysed an ensemble of EURO-CORDEX RCM projections and found the ensemble mean pattern of change for mean surface-downwelling shortwave radiation (2070–2099 vs 1970–1999 climatologies under RCP8.5) shows "positive signals (about 5 W m^{-2}) in Southern Mediterranean regions" and "negative signals northwards (about −10 W m^{-2}, down to −20 W m^{-2} in the northernmost areas)". Bartók *et al*. (2017) also analysed a EURO-CORDEX RCP85 ensemble and found that "the multi-model mean of RCMs indicates a decrease in surface solar radiation of −0.60 W m^{-2} per decade over Europe" for the period 2006–2100. The authors proposed that the reduction of surface solar radiation in the RCMs "can be attributed to increasing atmospheric absorption in line with the increase of water vapor content" (Bartók *et al*., 2017).

A more comprehensive analysis of the impacts of climate change on solar photovoltaic (PV) power in Ireland was evaluated using the following method outlined in Jerez *et al*. (2015) and Mavromatakis *et al*. (2010):

$$PV(t) = P_R(t)\frac{SW(t)}{SW_S} \tag{3.7}$$

where SW refers to surface-downwelling shortwave radiation (W m^{-2}) and SW_S refers to surface-downwelling shortwave radiation at standard test conditions ($SW_S = 1000$ W m^{-2}), for which the nominal capacity of a PV device is determined as its measured power output. P_R is the "performance ratio", formulated to account for changes of the PV cells, efficiency as a result of changes in their temperature as:

$$P_R(t) = 1 + \gamma\left(T_{cell}(t) - T_s\right) \tag{3.8}$$

where T_{cell} is the PV cell temperature, $T_s = 25$°C (standard test conditions) and $\gamma = -0.005$°C^{-1}, considering the typical response of monocrystalline silicon solar panels (Tonui *et al*., 2008). T_{cell} is modelled considering the effects of surface temperature, T (°C), SW (W m^{-2}) and wind speed, W (m s^{-1}), on it as:

$$T_{cell}(t) = c_1 + c_2 T + c_3 SW + c_4 W \tag{3.9}$$

with $c_1 = 4.3$°C, $c_2 = 0.943$, $c_3 = 0.028$°C m^2 W^{-1} and $c_4 = -1.528$°C s m^{-1}, as recommended by Jerez *et al*. (2015) and Tonui *et al*. (2008).

The projected change in PV, presented in Figure 3.47b, shows a small expected decrease in PV by the middle of the century, ranging from ≈0 to 4%. The largest decreases are noted in the north of the country and for the RCP8.5 scenario. The results are consistent with Jerez *et al*. (2015), who analysed the effects of climate change on PV in Europe using an ensemble of Euro-CORDEX datasets.

3.20 Heating Degree Days

A degree day, an estimate of accumulated heat, is defined as the deviation (°C) from a base temperature value (Fraisse *et al*., 2010; Kalogirou, 2013; Project Team ECA&D, 2013; Kendon *et al*., 2015). Heating

degree days (HDDs) are used by power companies and consumers to estimate the amount of energy required for residential or commercial space heating during the cold season. Conversely, cooling degree days (CDDs) are used to estimate the amount of air conditioning usage during the warm season.

The HDD was computed using a base temperature of 15.5°C (i.e. a temperate below which heating is required) and the daily mean temperature (T_M), as described by Spinoni *et al*. (2015) and Project Team ECA&D (2013):

$$HDD_{daily} = \max\{(15.5°C - T_M), 0\} \quad (3.10)$$

$$HDD = \Sigma HDD_{daily} \quad (3.11)$$

Conversely, CDD was computed using a base temperature of 22°C (i.e. a temperate above which air conditioning is required) and the daily mean temperature (T_M):

$$CDD_{daily} = \max\{(T_M - 22°C), 0\} \quad (3.12)$$

$$CDD = \Sigma CDD_{daily} \quad (3.13)$$

Figure 3.48, the projected change in HDDs, shows that by the middle of the century there will be a greatly reduced requirement for heating in Ireland, with HDDs projected to decrease by 12–17% and 15–21% for the RCP4.5 and RCP8.5 scenarios, respectively. A clear north-to-south gradient is evident for both RCP scenarios. Averaged over the whole country, the expected decreases in HDDs are 14% and 18% for the RCP4.5 and RCP8.5 scenarios, respectively. The projections show that CDDs are projected to slightly increase (not shown), particularly over the east and midlands, suggesting a very small increase in air conditioning requirements by the middle of the century. However, the amounts are small compared with HDD and therefore have a negligible effect on the projected changes in the total energy demand (EDD = HDD + CDD).

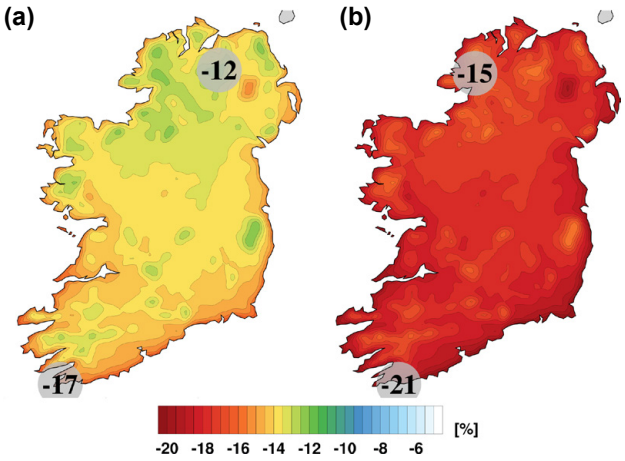

Figure 3.48. Mid-century projected changes (%) in HDDs for the (a) RCP4.5 and (b) RCP8.5 scenarios.

The projected changes in heating and cooling energy demand are in line with previous RCM studies for Ireland. Semmler *et al*. (2010) found that the mid-century (2021–2060) heating demand is projected to decrease by ≈10% for the A1B and A2 emissions scenarios. The authors found a small projected increase in summer CDDs, which may intensify a weak demand for air conditioning towards the end of the century (Semmler *et al*., 2010). However, the "main influence of a warming climate will be reflected in a decrease in energy requirements for commercial and domestic heating in Ireland" (Semmler *et al*., 2010).

3.21 Driving Rain

The "driving rain" metric ($m^2 s^{-1} year^{-1}$) can be approximated from the following equation (Collins and Cummins, 1996; Met Éireann, 2010):

$$DR = W \cdot R \quad (3.14)$$

where W is the mean annual 10-m wind speed ($m s^{-1}$) and R is the mean annual rainfall ($m year^{-1}$).

The driving rain metric is a useful parameter for agriculture, construction and transport applications.

Figure 3.49a shows that by the middle of the century, "driving rain" is projected to decrease by 1–7% and 0–8% for the RCP4.5 (mean decrease 4.5%) and RCP8.5 (mean decrease 4%) scenarios, respectively. Decreases are projected for all seasons (except winter under the RCP8.5 scenario). The largest decreases are noted for summer, with overall mean decreases of 7% (RCP4.5) and 12% (RCP8.5). Increases in driving rain are projected for winter under the RCP8.5 scenario, with the largest increases noted near the south and east coastlines (see Figure 3.49b).

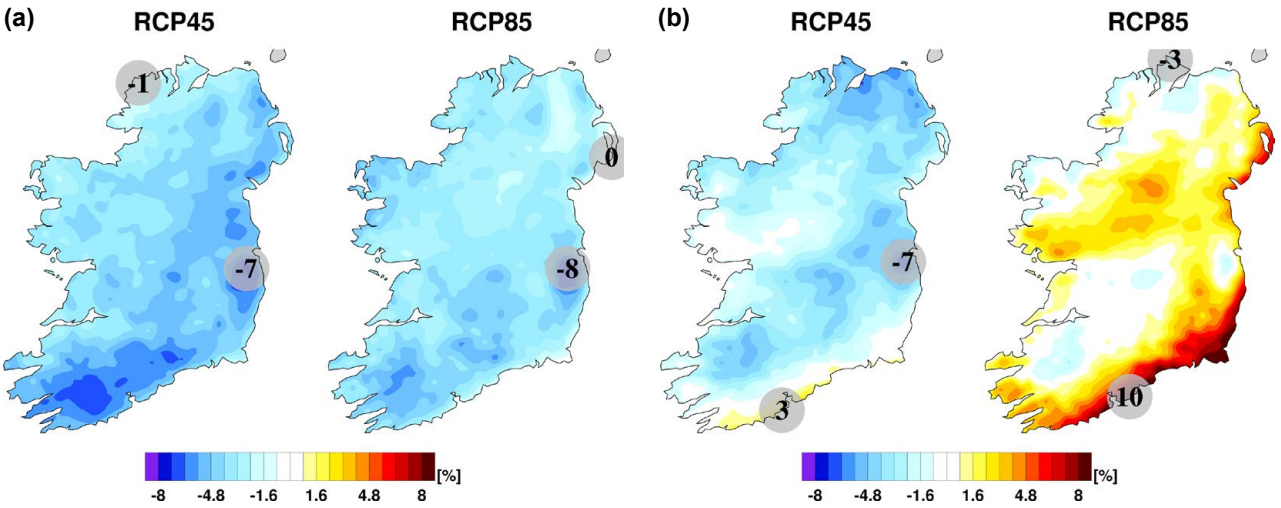

Figure 3.49. Projected changes (%) in mid-century "driving rain" (a) annually and (b) in winter. In each case, the future period, 2041–2060, is compared with the past period, 1981–2000. The numbers included on each plot are the minimum and maximum projected changes, displayed at their locations.

3.22 Evapotranspiration

Projections of evapotranspiration are presented in Figure 3.50a. The projections show that by the middle of the century, evapotranspiration is projected to increase by 2.3–7% and 1.8–8% for the RCP4.5 and RCP8.5 scenarios, respectively. The largest increases are noted in the east. All seasons show increases in evapotranspiration by the middle of the century, with the largest increases noted for summer and autumn. The projected increase in evapotranspiration may offset flooding events arising from the expected increases in heavy rainfall events (see section 3.10). For reference, "observed" annual evapotranspiration (mm day^{-1}), derived from a high-resolution (1.5-km) downscaled ERA-Interim climate simulation, is presented in Figure 3.50b. Please refer to Werner *et al*. (2019) for validations and additional maps and information.[16]

Evapotranspiration was calculated using the output of RCMs (see Table 1.1). The Penman–Monteith FAO-56 method of Zotarelli *et al*. (2010) was followed. A mathematical description is provided below.

$$ET_{sz} = \frac{0.408\Delta\left(R_n - G\right) + \gamma \frac{C_n}{T_{mean} + 273} u_2 \left(e_s - e_a\right)}{\Delta + \gamma\left(1 + C_d u_2\right)} \quad (3.15)$$

- ET_{sz} is the reference evaporation, mm day^{-1};
- R_n is the net surface radiation, MJ m^{-2} day^{-1} (see equation 3.16);
- G is the surface sensible heat flux, MJ m^{-2} day^{-1} (see equation 3.17);
- T_{mean} is the mean daily 2-m temperature,°C;
- u_2 is the mean daily 2-m wind speed, m s^{-1} (see equation 3.18);
- e_s is the saturation vapour pressure (daily average), kPa (see equation 3.19);
- e_a is the actual vapour pressure (daily average), kPa (see equation 3.20);
- Δ is the slope of the vapour pressure curve, kPa°C^{-1} (see equation 3.21);
- γ is the psychrometric constant, kPa°C^{-1} (see equation 3.22);
- C_n is the reference crop type constant numerator;
- C_d is the reference crop type constant denominator.

For the calculation above, $C_n = 900$ and $C_d = 0.34$ were used.

$$R_n = 0.0864(R_{ns} - R_{nl}) \quad (3.16)$$

R_{ns} and R_{nl} are the mean daily surface shortwave and longwave net radiation in units of W m^{-2}

16 In summary, Werner *et al*. (2019) compared modelled evapotranspiration with observational data at 22 stations spanning Ireland and found that the COSMO-CLM RCM resolved evapotranspiration to "within 10% of values calculated from station measurements for all stations analysed".

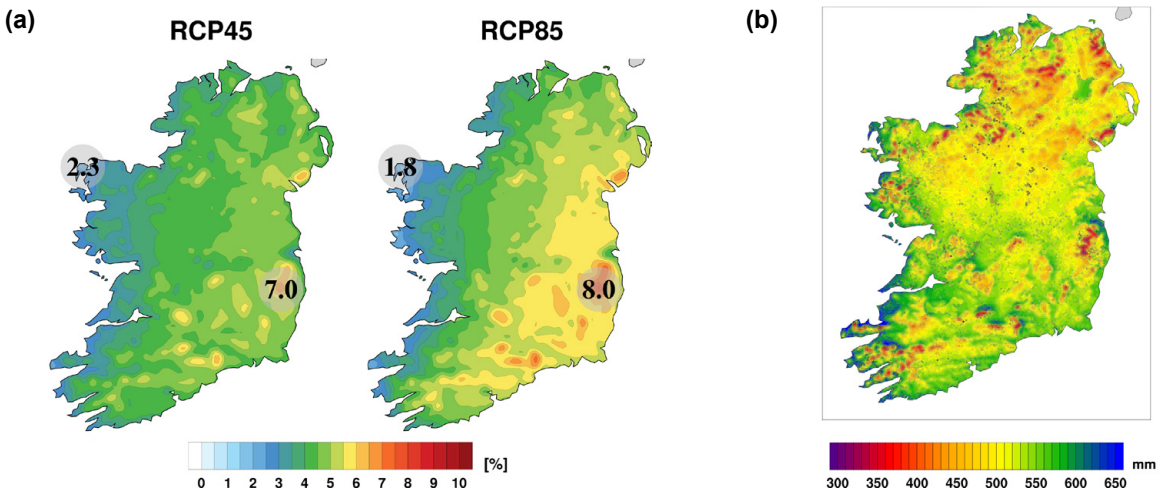

Figure 3.50. (a) Mid-century projected changes (%) in evapotranspiration. (b) "Observed" annual evapotranspiration FAO-56, 1981–2015

$$G = 0.0864\,SH \tag{3.17}$$

SH is the mean daily surface sensible heat flux in units of $W\,m^{-2}$

$$u_2 = u_{10}\frac{4.87}{\ln\left(67.8\times 10 - 5.42\right)} \tag{3.18}$$

u_{10} is the 10-m wind speed, $m\,s^{-1}$

$$e_s = 0.6108e^{\left(\frac{17.27T}{T+237.3}\right)} \tag{3.19}$$

T is the 2-m temperature,°C

$$e_a = 0.6108e^{\left(\frac{17.27T_d}{T_d+237.3}\right)} \tag{3.20}$$

T_d is the 2-m dew point temperature,°C

$$\Delta = \frac{4098.2e_s}{\left(T_{mean}+237.3\right)^2} \tag{3.21}$$

$$\gamma = 0.000000665\,P \tag{3.22}$$

where *P* is the mean daily surface pressure, Pa.

4 Recommendations

There is higher confidence in the temperature (and derived variables related to temperature) projections than in the rainfall projections. This is reflected in a rather large spread, particularly at a regional level, in the rainfall projections between the individual RCM ensemble members. Current RCM research aims to reduce climate change projection uncertainty and provide sharper estimates of expected climate change in the decades ahead. This is being achieved by running a large ensemble of high-resolution downscaled simulations using the most up-to-date RCMs (both standard and coupled atmosphere–ocean–wave), additional CMIP5 GCM datasets including the RCP2.6 and RCP6.0 scenarios and recently completed CMIP6 GCM simulations (e.g. Nolan and McKinstry, 2020) under the full range of ScenarioMIP "tier 1" SSPs: SSP1-2.6, SSP2-4.5, SSP3-7.0 and SSP5-8.5 (Riahi *et al*., 2017). Additionally, the accuracy and usefulness of the model predictions will be enhanced by increasing the model resolution (≈3 km) and using fully coupled atmosphere–ocean–wave RCMs. Preliminary RCM projection results are in line with previous work showing, for example, enhanced temperature rises by

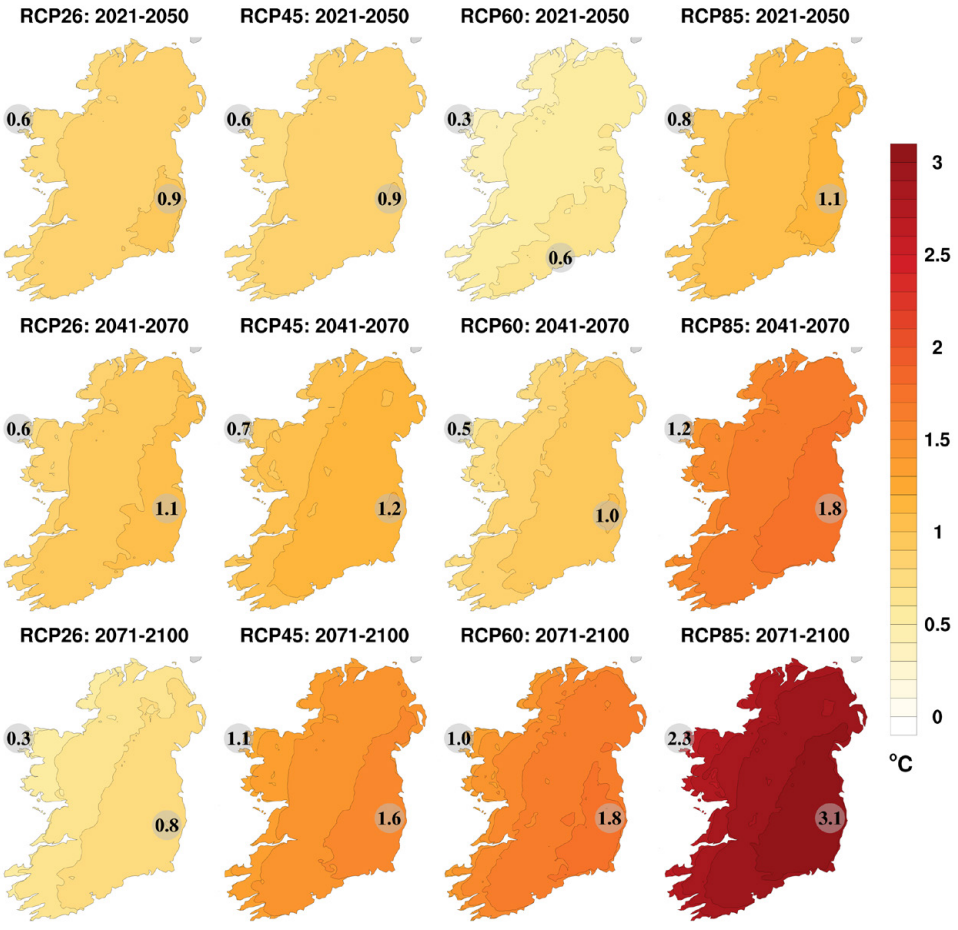

Figure 4.1. Updated RCM ensemble projections of mean annual 2-m temperature. All RCM ensemble members were run with 4-km grid spacing. In each case, the future 30-year period is compared with the past period, 1976–2005. The relatively low RCP6.0 temperature increase for early to mid-century can be attributed to a difference in RCP ensemble size. The preliminary results shown were obtained from analysing four RCP2.6, six RCP4.5, two RCP6.0 and six RCP8.5 RCM simulations. Current work is focusing on greatly increasing the ensemble size.

the end of the century (Figure 4.1), wetter winters with a clear north-west to south-east gradient (Figure 4.2) and a general decrease in wind speeds during summer. The preliminary results shown in Figures 4.1 and 4.2 were obtained by extending the COSMO5-CLM and WRF simulations outlined in Table 1.2 to cover the period 1975–2100 and inclusion of the RCP2.6 and RCP6.0 scenarios in the simulation of the future climate.

It is also important to stress that the likelihood values presented in the current study are derived from the most up-to-date evidence available. Therefore, the "likelihood" values only apply to the specific sets of high-resolution models and experimental design of the current study. It is expected that future improvements in modelling will alter the projections, as uncertainty is expected to be gradually reduced.

As extreme storm events are rare, the storm-tracking research needs to be extended. Future work will focus on analysing a larger ensemble, thus allowing a robust statistical analysis of extreme storm track projections.

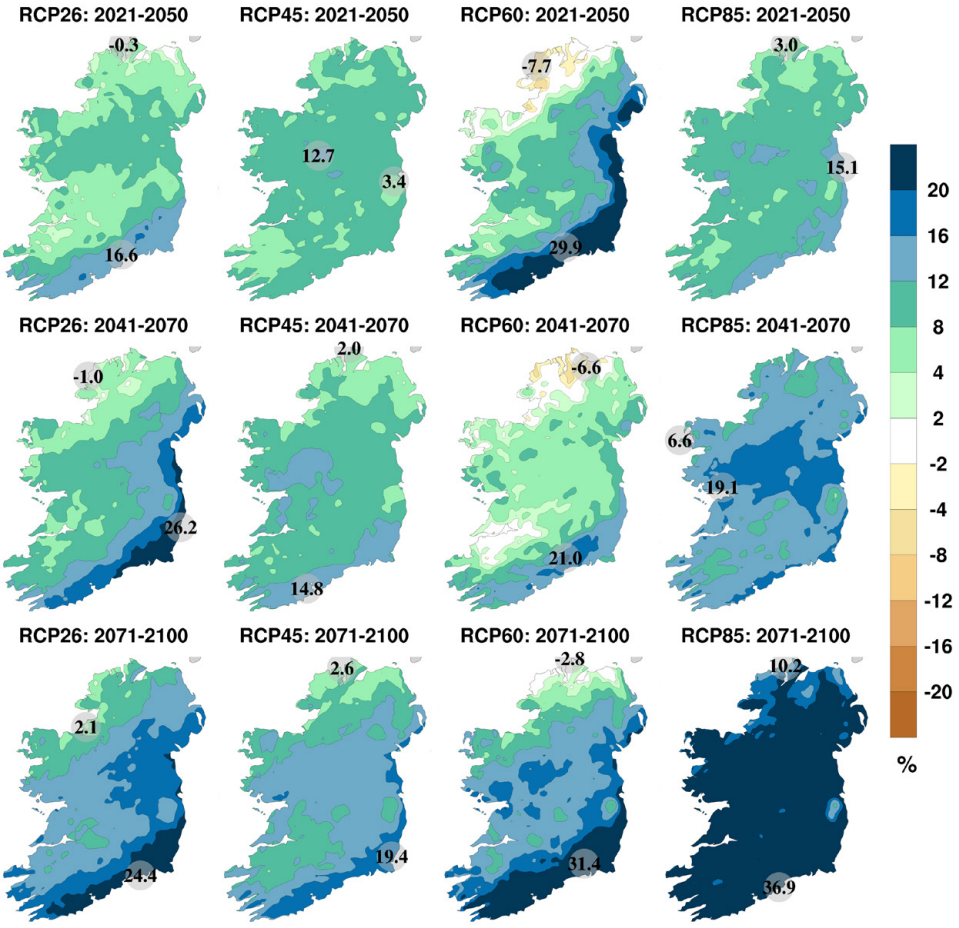

Figure 4.2. Updated RCM ensemble projections of mean winter precipitation (%). All RCM ensemble members were run with 4-km grid spacing. In each case, the future 30-year period is compared with the past period, 1976–2005.

References

Antic, S., Laprise, R., Denis, B. and De Elía, R., 2006. Testing the downscaling ability of a one-way nested regional climate model in regions of complex topography. *Climate Dynamics* 26(2–3): 305–325.

Barreca, A.I. and Shimshack, J.P., 2012. Absolute humidity, temperature, and influenza mortality: 30 years of county-level evidence from the United States. *American Journal of Epidemiology* 176(suppl 7): S114–S122.

Bartók, B., Wild, M., Folini, D., Lüthi, D., Kotlarski, S., Schär, C., Vautard, R., Jerez, S. and Imecs, Z., 2017. Projected changes in surface solar radiation in CMIP5 global climate models and in EURO-CORDEX regional climate models for Europe. *Climate Dynamics* 49(7–8): 2665–2683.

Bieniek, P., Bhatt, U.S., Walsh, J.E., Rupp, T.S., Zhang, J., Krieger, J.R. and Lader, R. 2015. Dynamical downscaling of ERA-Interim temperature and precipitation for Alaska. *Journal of Applied Meteorology and Climatology* 55(3): 635–654. https://doi.org/10.1175/JAMC-D-15-0153.1

Bigler, C. and Bugmann, H., 2018. Climate-induced shifts in leaf unfolding and frost risk of European trees and shrubs. *Scientific Reports* 8: 9865. https://doi.org/10.1038/s41598-018-27893-1

Bootsma, A., Tremblay, G. and Filion, P., 1999. *Risk Analyses of Heat Units Available for Corn and Soybean Production in Quebec*. Technical Bulletin. Agriculture and Agri-food Canada/Eastern Cereal and Oilseed Research Centre, Ottawa, Canada.

Bootsma, A., McKenney, D.W., Anderson, D. and Papadopol, P., 2007. A re-evaluation of crop heat units in the Maritime Provinces of Canada. *Canadian Journal of Plant Science* 87(2): 281–287.

Brisson, E., Demuzere, M. and van Lipzig, N., 2015. Modelling strategies for performing convection-permitting climate simulations. *Meteorologische Zeitschrift* 25(2): 149–163.

Byrne, M.P. and O'Gorman, P.A., 2013. Link between land–ocean warming contrast and surface relative humidities in simulations with coupled climate models. *Geophysical Research Letters* 40: 5223–5227.

Byrne, M.P. and O'Gorman, P.A., 2016. Understanding decreases in land relative humidity with global warming: conceptual model and GCM simulations. *Journal of Climate* 29: 9045–9061.

Byrne, M.P. and O'Gorman, P.A., 2018. Trends in continental temperature and humidity directly linked to ocean warming. *Proceedings of the National Academy of Sciences* 115(19): 4863–4868.

C3S (Copernicus Climate Change Service), 2017. *ERA5: Fifth Generation of ECMWF Atmospheric Reanalyses of the Global Climate*. Copernicus Climate Change Service Climate Data Store (CDS). Available online: https://confluence.ecmwf.int/display/CKB/ERA5%3A+data+documentation#ERA5:datadocumentation-HowtociteERA5 (accessed 17 March 2020).

Camargo, S., 2013. Global and regional aspects of tropical cyclone activity in the CMIP5 models. *Journal of Climate* 26(4): 9880–9902.

Cavicchia, L. and von Storch, H., 2011. The simulation of medicanes in a high-resolution regional climate model. *Climate Dynamics* 39: 2273–2290.

Coffel, E.D., Horton, R.M. and de Sherbinin, A., 2017. Temperature and humidity based projections of a rapid rise in global heat stress exposure during the 21st century. *Environmental Research Letters* 13: 014001.

Collins, J.F. and Cummins, T., 1996. *Agroclimatic Atlas of Ireland*. AGMET, Dublin.

Collins, M., Knutti, R., Arblaster, J., Dufresne, J.-L., Fichefet, T., Friedlingstein, P., *et al*., 2013. Long-term climate change: projections, commitments and irreversibility. In Stocker, T.F., Qin, D., Plattner, G.-K., Tignor, M., Allen, S.K., Boschung, J., Nauels, A., Xia, Y., Bex, V. and Midgley, P.M. (eds), *Climate Change 2013: The Physical Science Basis*. Contribution of Working Group I to the Fifth Assessment Report of the Intergovernmental Panel on Climate Change. Cambridge University Press, Cambridge, UK.

Collins, W.J., Bellouin, N., Doutriaux-Boucher, M., Gedney, N., Halloran, P., Hinton, T., *et al*., 2011. Development and evaluation of an Earth-system model: HadGEM2. *Geoscientific Model Development* 4: 1051–1075.

Cucak, M., Sparks, A., Moral, R.D.A., Kildea, S., Lambkin, K. and Fealy, R., 2019. Evaluation of the 'Irish rules': the potato late blight forecasting model and its operational use in the Republic of Ireland. *Agronomy* 9(9): 515.

Cullen, E., 2010. Lyme disease and climate change. *Irish Medical Journal* 103(4): 101–102.

Daloz, A.S., Camargo, S.J., Kossin, J.P., Emanuel, K., Horn, M., Jonas, J.A., Kim, D., LaRow, T., Lim, Y.K., Patricola, C.M. and Roberts, M., 2015. Cluster analysis of downscaled and explicitly simulated North Atlantic tropical cyclone tracks. *Journal of Climate* 28(4): 1333–1361.

Daly, C., 2019. *Built & Archaeological Heritage: Climate Change Sectoral Adaptation Plan*. Available online: https://www.chg.gov.ie/app/uploads/2019/10/ccsap-built-archaeological-heritage-final-main-report-low-res.pdf (accessed 1 June 2020).

Dee, D.P., Uppala, S.M., Simmons, A.J., Berrisford, P., Poli, P., Kobayashi, S., Andrae, U., Balmaseda, M.A., Balsamo, G., Bauer, P. and Bechtold, P., 2011. The ERA-interim reanalysis: configuration and performance of the data assimilation system. *Quarterly Journal of the Royal Meteorological Society* 137(656): 553–597.

Denis, B., Laprise, R. and Caya, D., 2003. Sensitivity of a regional climate model to the resolution of the lateral boundary conditions. *Climate Dynamics* 20(2–3): 107–126.

Déqué, M., Rowell, D.P., Lüthi, D., Giorgi, F., Christensen, J.H., Rockel, B., Jacob, D., Kjellström, E., De Castro, M. and van den Hurk, B.J.J.M., 2007. An intercomparison of regional climate simulations for Europe: assessing uncertainties in model projections. *Climatic Change* 81(1): 53–70.

Di Luca, A., Argüeso, D., Evans, J.P., de Elía, R. and Laprise, R., 2016. Quantifying the overall added value of dynamical downscaling and the contribution from different spatial scales. *Journal of Geophysical Research: Atmospheres* 121(4): 1575–1590.

Doms, G. and Schättler, U., 2002. *A Description of the Nonhydrostatic Regional Model LM. Part I: Dynamics and Numerics*. Deutscher Wetterdienst, Offenbach, Germany.

Donat, M., Leckebusch, G., Wild, S. and Ulbrich, U., 2010. Benefits and limitations of regional multi-model ensembles for storm loss estimations. *Climate Research* 44: 211–225.

Dowdy, A.J., Mills, G.A., Finkele, K. and de Groot, W., 2010. Index sensitivity analysis applied to the Canadian forest fire weather index and the McArthur forest fire danger index. *Meteorological Applications* 17(3): 298–312.

Dwyer, N., 2013. *The Status of Ireland's Climate, 2012*. Environmental Protection Agency, Johnstown Castle, Ireland. Available online: https://cora.ucc.ie/bitstream/handle/10468/2969/CCRP26_-_Status_of_Ireland's_Climate_2012.pdf (accessed 1 June 2020).

Easterling, D.R., Meehl, G.A., Parmesan, C., Changnon, S.A., Karl, T.R. and Mearns, L.O., 2000. Climate extremes: observations, modeling, and impacts. *Science* 289: 2068–2074.

Feser, F., 2006. Enhanced detectability of added value in limited-area model results separated into different spatial scales. *Monthly Weather Review* 134: 2180–2190.

Feser, F. and Barcikowska, M., 2012. The influence of spectral nudging on typhoon formation in regional climate models. *Environmental Research Letters* 7: 014024.

Feser, F., Rockel, B., von Storch, H., Winterfeldt, J. and Zahn, M., 2011. Regional climate models add value to global model data: a review and selected examples. *Bulletin of the American Meteorological Society* 92(9): 1181–1192.

Feser, F., Barcikowska, M., Krueger, O., Schenk, F., Weisse, R. and Xia, L., 2014. Storminess over the North Atlantic and northwestern Europe – a review. *Quarterly Journal of the Royal Meteorological Society* 141(687): 350–382. https://doi.org/10.1002/qj.2364

Flanagan, J., Nolan, P., McGrath, R. and Werner, C., 2019. Towards a definitive historical high-resolution climate dataset for Ireland – promoting climate research in Ireland. *Advances in Science and Research* 15: 263–276.

Fraisse, J., Bellow, J. and Brown, C., 2010. Degree days: heating, cooling, and growing. Document ABE 381. University of Florida IFAS Extension, Gainesville, FL. Available online: http://edis.ifas.ufl.edu/ae428 (accessed 1 June 2020).

Fronzek, S., Carter, T.R. and Jylhä, K., 2012. Representing two centuries of past and future climate for assessing risks to biodiversity in Europe. *Global Ecology and Biogeography* 21(1): 19–35.

Geng, Q. and Sugi, M., 2003. Possible change of extratropical cyclone activity due to enhanced greenhouse gases and sulphate aerosols: study with a high-resolution AGCM. *Journal of Climate* 16: 2262–2274.

Giorgetta, M.A., Jungclaus, J., Reick, C.H., Legutke, S., Bader, J., Böttinger, M., Brovkin, V., Crueger, T., Esch, M., Fieg, K. and Glushak, K., 2013. Climate and carbon cycle changes from 1850 to 2100 in MPI-ESM simulations for the Coupled Model Intercomparison Project phase 5. *Journal of Advances in Modeling Earth Systems* 5(3): 572–597.

Gleeson, E., McGrath, R. and Treanor, M. (eds), 2013. *Ireland's Climate: The Road Ahead*. Met Éireann, Dublin.

Haarsma, R.J., Hazeleger, W., Severijns, C., de Vries, H., Sterl, A., Bintanja, R., van Oldenborgh, G.J. and van den Brink, H.W., 2013. More hurricanes to hit Western Europe due to global warming. *Geophysical Research Letters* 40(9): 1783–1788. https://doi.org/10.1002/grl.50360.

Hall, N.M.J., Hoskins, B.J., Valdes, P.J. and Senior, C.A., 1994. Storm tracks in a high resolution GCM with doubled carbon dioxide. *Quarterly Journal of the Royal Meteorological Society* 120: 1209–1230.

Hazeleger, W., Wang, X., Severijns, C., Ştefănescu, S., Bintanja, R., Sterl, A., *et al*., 2011. EC-Earth V2.2: description and validation of a new seamless earth system prediction model. *Climate Dynamics* 39: 2611–2629.

IPCC (Intergovernmental Panel on Climate Change), 2013a. *Climate Change 2013: The Physical Science Basis*. Contribution of Working Group I to the Fifth Assessment Report of the Intergovernmental Panel on Climate Change. Stocker, T.F., Qin, D., Plattner, G.-K., Tignor, M., Allen, S.K., Boschung, J., Nauels, A., Xia, Y., Bex, V. and Midgley, P.M. (eds). Cambridge University Press, Cambridge, UK.

IPCC (Intergovernmental Panel on Climate Change), 2013b. Near-term climate change: projections and predictability. In Stocker, T.F., Qin, D., Plattner, G.-K., Tignor, M., Allen, S.K., Boschung, J., Nauels, A., Xia, Y., Bex, V. and Midgley, P.M. (eds), *Climate Change 2013: The Physical Science Basis*. Contribution of Working Group I to the Fifth Assessment Report of the Intergovernmental Panel on Climate Change. Cambridge University Press: Cambridge, UK.

Jacob, D., Petersen, J., Eggert, B., Alias, A., Christensen, O.B., Bouwer, L.M., *et al*., 2014. EURO-CORDEX: new high-resolution climate change projections for European impact research. *Regional Environmental Change* 14(2): 563–578.

Jerez, S., Tobin, I., Vautard, R., Montávez, J.P., López-Romero, J.M., Thais, F., Bartok, B., Christensen, O.B., Colette, A., Déqué, M. and Nikulin, G., 2015. The impact of climate change on photovoltaic power generation in Europe. *Nature Communications* 6(1): 1–8.

Jimenez, P. and Dudhia, J., 2012. Improving the representation of resolved and unresolved topographic effects on surface wind in the WRF Model. *Journal of Applied Meteorology and Climatology* 51: 300–316.

Johnson, D., Bessin, R. and Townsend, L., 1998. Predicting insect development using degree days. Entfact 123. University of Kentucky, Lexington, KY.

Kalogirou, S.A., 2013. *Solar Energy Engineering: Processes and Systems*. Academic Press, Cambridge, MA.

Kanada, S., Nakano, M., Hayashi, S., Kato, T., Nakamura, M., Kurihara, K. and Kitoh, A., 2008. Reproducibility of maximum daily precipitation amount over Japan by a high-resolution non-hydrostatic model. *Sola* 4: 105–108.

Kanamaru, H. and Kanamitsu, M., 2007. Fifty-seven-year California reanalysis downscaling at 10 km (CaRD10). Part II: comparison with North American regional reanalysis. *Journal of Climate* 20: 5572–5592.

Kendon, E., Roberts, N., Senior, C. and Roberts, M., 2012. Realism of rainfall in a very high-resolution regional climate model. *Journal of Climate* 25: 5791–5806.

Kendon, E.J., Roberts, N.M., Fowler, H.J., Roberts, M.J., Chan, S.C. and Senior, C.A., 2014. Heavier summer downpours with climate change revealed by weather forecast resolution model. *Nature Climate Change* 4(7): 570–576.

Kendon, M., MacCarthy, M. and Jevrejeva, S., 2015. *State of the UK Climate 2014*. Met Office, Exeter, UK.

Lowe, J.A., Bernie, D., Bett, P.E., Bricheno, L., Brown, S., Calvert, D., *et al*., 2018. *UKCP18 Science Overview Report*. Met Office, Exeter, UK.

Lucas-Picher, P., Wulff-Nielsen, M., Christensen, J.H., Aðalgeirsdóttir, G., Mottram, R. and Simonsen, S.B., 2012. Very high resolution regional climate model simulations over Greenland: identifying added value. *Journal of Geophysical Research* 117(D2).

McGrath, R. and Lynch, P. (eds), 2008. *Ireland in a Warmer World: Scientific Predictions of the Irish Climate in the Twenty-first Century*. Community Climate Change Consortium for Ireland (C4I). Available online: https://www.epa.ie/pubs/reports/research/climate/EPA_climate_change_regional_models_ERTDI36.pdf (accessed 1 June 2020).

McGrath, R. and Nolan, P., 2017. Irish storminess: what does the future hold? Expert statement: Royal Irish Academy Climate Change and Environmental Sciences Committee, May 2017. Available online: https://www.ria.ie/sites/default/files/climate-change-storminess.pdf (accessed 1 June 2020).

McGrath, R., Nishimura, E., Nolan, P., Semmler, T., Sweeney, C. and Wang, S., 2005. *Climate Change: Regional Climate Model Predictions for Ireland*. Environmental Protection Agency, Johnstown Castle, Ireland.

McMaster, G.S. and Wilhelm, W., 1997. Growing degree-days: one equation, two interpretations. *Agricultural and Forest Meteorology* 87: 291–300.

Matthews, T., Murphy, C., Wilby, R.L. and Harrigan, S., 2014. Stormiest winter on record for Ireland and UK. *Nature Climate Change* 4(9): 738–740.

Matthews, T., Mullan, D., Wilby, R.L., Broderick, C. and Murphy, C., 2016. Past and future climate change in the context of memorable seasonal extremes. *Climate Risk Management* 11(1): 37–52.

Mavromatakis, F., Makrides, G., Georghiou, G., Pothrakis, A., Franghiadakis, Y., Drakakis, E. and Koudoumas, E., 2010. Modeling the photovoltaic potential of a site. *Renewable Energy* 35: 1387–1390.

Met Éireann, 2010. *Distribution of Driving Rain in Ireland*. Met Éireann, Dublin. Available online: http://www.tara.tcd.ie/bitstream/handle/2262/70489/Climatological%20Note%20No.%2013.pdf (accessed 1 June 2020).

Met Éireann, 2014. Winter 2013/2014. Available online: https://www.met.ie/cms/assets/uploads/2017/08/WinterStorms13_14.pdf (accessed 1 June 2020).

Miller, P., Lanier, W. and Brandt, S., 2001. *Using Growing Degree Days to Predict Plant Stages*. Montana State University, Bozeman, MO.

Moss, R.H., Edmonds, J.A., Hibbard, K.A., Manning, M.R., Rose, S.K., van Vuuren, D.P., *et al*., 2010. The next generation of scenarios for climate change research and assessment. *Nature* 463(7282): 747–756.

Murphy, J.M., Sexton, D.M.H., Jenkins, G.J., Boorman, P.M., Booth, B.B.B., Brown, C.C., Clark, R.T., Collins, M., Harris, G.R., Kendon, E.J., Betts, R.A., Brown, S.J., Howard, T. P., Humphrey, K.A., McCarthy, M.P., McDonald, R.E., Stephens, A., Wallace, C., Warren, R., Wilby, R. and Wood, R.A., 2009. *UK Climate Projections Science Report: Climate Change Projections*. Met Office Hadley Centre, Exeter, UK.

Murphy, C., Broderick, C., Burt, T.P., Curley, M., Duffy, C., Hall, J., Harrigan, S., Matthews, T.K., Macdonald, N., McCarthy, G. and McCarthy, M.P., 2018. A 305-year continuous monthly rainfall series for the island of Ireland (1711–2016). *Climate of the Past* 14(3): 413–440.

Nolan, P., 2015. *Ensemble of Regional Climate Model Projections for Ireland*. Environmental Protection Agency, Johnstown Castle, Ireland.

Nolan P. and McKinstry, A., 2020. *EC-Earth Global Climate Simulations: Ireland's Contributions to CMIP6*. Environmental Protection Agency, Johnstown Castle, Ireland. Available online: http://www.epa.ie/pubs/reports/research/tech/researchreport310/ (accessed 12 July 2020).

Nolan, P., Lynch, P., McGrath, R., Semmler, T. and Wang, S., 2012. Simulating climate change and its effects on the wind energy resource of Ireland. *Wind Energy* 15(4): 593–608.

Nolan, P., Lynch, P. and Sweeney, C., 2014. Simulating the future wind energy resource of Ireland using the COSMO-CLM model. *Wind Energy* 17: 19–37.

Nolan, P., O'Sullivan, J. and McGrath, R., 2017. Impacts of climate change on mid-twenty-first-century rainfall in Ireland: a high-resolution regional climate model ensemble approach. *International Journal of Climatology* 37(12): 4347–4363.

Noti, J.D., Blachere, F.M., McMillen, C.M., Lindsley, W.G., Kashon, M.L., Slaughter, D.R. and Beezhold, D.H., 2013. High humidity leads to loss of infectious influenza virus from simulated coughs. *PLOS One* 8(2): e57485.

O'Gorman, P.A. and Muller, C.J., 2010. How closely do changes in surface and column water vapor follow Clausius–Clapeyron scaling in climate-change simulations? *Environmental Research Letters* 5(2): 025207.

OMAFRA (Ontario Ministry of Agriculture, Food and Rural Affairs), 2017. *Agronomy Guide for Field Crops*. Publication 811. OMAFRA, Guelph, Canada.

O'Sullivan, J., Sweeney, C., Nolan, P. and Gleeson, E., 2015. A high-resolution, multi-model analysis of Irish temperatures for the mid-21st century. *International Journal of Climatology* 36(3): 1256–1267. https://doi.org/10.1002/joc.4419.

Powers, J.G., Klemp, J.B., Skamarock, W.C., Davis, C.A., Dudhia, J., Gill, D.O., Coen, J.L., Gochis, D.J., Ahmadov, R., Peckham, S.E. and Grell, G.A., 2017. The weather research and forecasting (wrf) model: overview, system efforts, and future directions. *Bulletin of the American Meteorological Society* 98(8): 1717–1737.

Prein, A.F., Gobiet, A., Suklitsch, M., Truhetz, H., Awan, N.K., Keuler, K. and Georgievski, G., 2013. Added value of convection permitting seasonal simulations. *Climate Dynamics* 41: 2655–2677.

Project Team ECA&D (Project Team European Climate Assessment & Dataset), 2013. Royal Netherlands Meteorological Institute (KNMI) – European Climate Assessment & Dataset (ECA&D) – Algorithm Theoretical Basis Document (ATBD) Version 10.7. Available online: http://eca.knmi.nl/documents/atbd.pdf (accessed 1 June 2020).

Rauscher, S.A., Coppola, E., Piani, C. and Giorgi, F., 2010. Resolution effects on regional climate model simulations of seasonal precipitation over Europe. *Climate Dynamics* 35(4): 685–711.

Riahi, K., van Vuuren, D.P., Kriegler, E., Edmonds, J., O'Neill, B.C., Fujimori, S., *et al*., 2017. The shared socioeconomic pathways and their energy, land use, and greenhouse gas emissions implications: an overview. *Global Environmental Change* 42: 153–168.

Rockel, B., Will, A. and Hense, A., 2008. Special issue regional climate modelling with COSMO-CLM (CCLM). *Meteorologische Zeitschrift* 17: 347–348.

Rummukainen, M., 2010. State-of-the-art with regional climate models. *WIREs Climate Change* 1: 82–96.

Semmler, T., Varghese, S., McGrath, R., Nolan, P., Wang, S., Lynch, P. and O'Dowd, C., 2008a. Regional climate model simulations of North Atlantic cyclones: frequency and intensity changes. *Climate Research* 36: 1–16.

Semmler, T., McGrath, R., Nolan, P., Wang, S. and Lynch, P., 2008b. Regional model simulation of North Atlantic cyclones: present climate and idealized response to increased sea surface temperature. *Journal of Geophysical Research Atmospheres* 113: D02107.

Semmler, T., McGrath, R., Steele-Dunne, S., Hanafin, J., Nolan, P. and Wang, S., 2010. Influence of climate change on heating and cooling energy demand in Ireland. *International Journal of Climatology* 30(10): 1502–1511.

Shaman, J., Pitzer, V.E., Viboud, C., Grenfell, B.T. and Lipsitch, M., 2010. Absolute humidity and the seasonal onset of influenza in the continental United States. *PLOS Biology* 8: e1000316.

Shaman, J., Goldstein, E. and Lipsitch, M., 2011. Absolute humidity and pandemic versus epidemic influenza. *American Journal of Epidemiology* 173(2): 127–135. https://doi.org/10.1093/aje/kwq347

Shkol'nik, I., Meleshko, V., Efimov, S. and Stafeeva E., 2012. Changes in climate extremes on the territory of Siberia by the middle of the 21st century: an ensemble forecast based on the MGO regional climate model. *Russian Meteorology and Hydrology* 37: 71–84.

Skamarock, W.C., Klemp, J.B., Dudhia, J., Gill, D.O., Barker, D.M., Duda, M.G., Huang, X.Y., Wang, W. and Powers, J.G., 2008. *A Description of the Advanced Research WRF Version 3*. NCAR Tech. Note TN-475_STR. Available online: https://opensky.ucar.edu/islandora/object/technotes%3A500/datastream/PDF/download/citation.pdf (accessed 1 June 2020).

Sloth, M.M., Maule, C.F., MacKellar, N., Olesen, J.E. and Christensen, J.H., 2012. Selection of climate change scenario data for impact modelling. *Food Additives & Contaminants: Part A* 29(10): 1502–1513.

Smith, L.P., 1976. The agricultural climate of England and Wales. MAFF Technical Bulletin 35. Her Majesty's Stationery Office, London.

Solomon, S., Qin, D., Manning, M., Chen, Z., Marquis, M., Averyt, K., Tignor, M.M.B. and Miller, H.L. Jr (eds), 2007. *Climate Change 2007: The Physical Science Basis*. Cambridge University Press, Cambridge, UK.

Spinoni, J., Vogt, J. and Barbosa, P., 2015. European degree-day climatologies and trends for the period 1951–2011. *International Journal of Climatology* 35: 25–36.

Steppeler, J., Doms, G., Schättler, U., Bitzer, H.W., Gassmann, A., Damrath, U. and Gregoric, G., 2003. Meso-gamma scale forecasts using the nonhydrostatic model LM. *Meteorology and Atmospheric Physics* 82: 75–96.

Süss, J., Klaus, C., Gerstengarbe, F.-W. and P.C. Werner, 2008. What makes ticks tick? Climate change, ticks, and tick-borne diseases. *Journal of Travel Medicine* 15: 39–45.

Sutton, R.T., Dong, B. and Gregory, J.M., 2007. Land/sea warming ratio in response to climate change: IPCC AR4 model results and comparison with observations. *Geophysical Research Letters* 34: L02701.

Tamerius, J.D., Shaman, J., Alonso, W.J., Bloom-Feshbach, K., Uejio, C.K., Comrie, A. and Viboud, C., 2013. Environmental predictors of seasonal influenza epidemics across temperate and tropical climates. *PLOS Pathogens* 9(3): e. e1003194.

Tanguy, M., Dixon, H., Prosdocimi, I., Morris, D.G. and Keller, V.D.J., 2016. Gridded estimates of daily and monthly areal rainfall for the United Kingdom (1890–2015) [CEH-GEAR]. NERC Environmental Information Data Centre. https://doi.org/10.5285/33604ea0-c238-4488-813d-0ad9ab7c51ca

Taylor, K.E., Stouffer, R.J. and Meehl, G.A., 2012. An overview of CMIP5 and the experiment design. *Bulletin of the American Meteorological Society* 93(4): 485–498.

Tonui, J.K. and Tripanagnostopoulos, Y., 2008. Performance improvement of PV/T solar collectors with natural air flow operation. *Solar Energy* 82: 1–12.

van der Linden, P. and Mitchell, J.F.B., 2009. *ENSEMBLES: Climate Change and Its Impacts: Summary of Research and Results from the ENSEMBLES Project*. Met Office Hadley Centre, Exeter, UK.

van Vuuren, D.P., Edmonds, J., Kainuma, M.L.T., Riahi, K., Thomson, A., Matsui, T., *et al*., 2011. The representative concentration pathways: an overview. *Climatic Change* 109(11): 5–31.

Voldoire, A., Sanchez-Gomez, E., y Mélia, D.S., Decharme, B., Cassou, C., Sénési, S., Valcke, S., Beau, I., Alias, A., Chevallier, M. and Déqué, M., 2013. The CNRM-CM5.1 global climate model: description and basic evaluation. *Climate Dynamics* 40(9–10): 2091–2121.

Walsh, S., 2012. *A Summary of Climate Averages for Ireland 1981–2010*. Climatological Note No14. Met Éireann, Dublin. Available online: www.met.ie/climate-ireland/SummaryClimAvgs.pdf (accessed 15 October 2019).

Watanabe, M., Suzuki, T., O'ishi, R., Komuro, Y., Watanabe, S., Emori, S., *et al*., 2010. Improved climate simulation by MIROC5: mean states, variability, and climate sensitivity. *Journal of Climate* 23: 6312–6335. https://doi.org/10.1175/2010JCLI3679.1

Werner C., Nolan P. and Naughton, O., 2019. *High-resolution Gridded Datasets of Hydro-climate Indices for Ireland*. Environmental Protection Agency, Johnstown Castle, Ireland.

Williams, C.M., Henry, H.A. and Sinclair, B.J., 2015. Cold truths: how winter drives responses of terrestrial organisms to climate change. *Biological Reviews* 90: 214–235.

Winterfeldt, J., Geyer, B. and Weisse, R., 2011. Using QuikSCAT in the added value assessment of dynamically downscaled wind speed. *International Journal of Climatology* 31(7): 1028–1039.

Zängl, G., Reinert, D., Rípodas, P. and Baldauf, M., 2015. The ICON (ICOsahedral Non-hydrostatic) modelling framework of DWD and MPI-M: description of the non-hydrostatic dynamical core. *Quarterly Journal of the Royal Meteorological Society* 141(687): 563–579.

Zappa, G., Shaffrey, L.C., Hodges, K.I., Sansom, P.G. and Stephenson, D.B., 2013. A multimodel assessment of future projections of North Atlantic and European extratropical cyclones in the CMIP5 climate models. *Journal of Climate* 26(16): 5846–5862.

Zhao, M., Held, I.M., Lin, S.J. and Vecchi, G.A., 2009. Simulations of global hurricane climatology, interannual variability, and response to global warming using a 50-km resolution GCM. *Journal of Climate* 22(24): 6653–6678.

Zotarelli, L., Dukes, M.D., Romero, C.C., Migliaccio, K.W. and Morgan, K.T., 2010. Step by step calculation of the Penman–Monteith Evapotranspiration (FAO-56 Method). Institute of Food and Agricultural Sciences, University of Florida, Gainesville, FL. Available online: http://edis.ifas.ufl.edu/pdffiles/ae/ae45900.pdf (accessed 1 June 2020).

Abbreviations

BI	British and Irish Isles
CDD	Cooling degree day
CHU	Crop heat unit
CLM	Climate Limited-area Modelling
CMIP	Coupled Model Intercomparison Project
CORDEX	Coordinated Regional climate Downscaling Experiment
COSMO	Consortium for Small-scale Modeling
ECMWF	European Centre for Medium-Range Weather Forecast
ERA-Interim	ECMWF global atmospheric reanalysis
GCM	Global climate model (or alternatively, “General Circulation Model”)
GDD	Growing degree day
HadGEM2-ES	Hadley Centre Global Environment Model version 2 Earth System
HDD	Heating degree day
ICHEC	Irish Centre for High-End Computing
IPCC	Intergovernmental Panel on Climate Change
MAE	Mean absolute error
MIROC	Model for Interdisciplinary Research on Climate
MSLP	Mean sea level pressure
OCHU	Ontario Crop Heat Unit
pdf	Probability density function
PV	Photovoltaic
RCM	Regional climate model
RCP	Representative Concentration Pathway
RMSE	Root mean square error
ScenarioMIP	Scenario Model Intercomparison Project
SSP	Shared Socioeconomic Pathway
WRF	Weather Research and Forecasting

AN GHNÍOMHAIREACHT UM CHAOMHNÚ COMHSHAOIL
Tá an Ghníomhaireacht um Chaomhnú Comhshaoil (GCC) freagrach as an gcomhshaol a chaomhnú agus a fheabhsú mar shócmhainn luachmhar do mhuintir na hÉireann. Táimid tiomanta do dhaoine agus don chomhshaol a chosaint ó éifeachtaí díobhálacha na radaíochta agus an truaillithe.

Is féidir obair na Gníomhaireachta a roinnt ina trí phríomhréimse:

Rialú: *Déanaimid córais éifeachtacha rialaithe agus comhlíonta comhshaoil a chur i bhfeidhm chun torthaí maithe comhshaoil a sholáthar agus chun díriú orthu siúd nach gcloíonn leis na córais sin.*

Eolas: *Soláthraímid sonraí, faisnéis agus measúnú comhshaoil atá ar ardchaighdeán, spriocdhírithe agus tráthúil chun bonn eolais a chur faoin gcinnteoireacht ar gach leibhéal.*

Tacaíocht: *Bímid ag saothrú i gcomhar le grúpaí eile chun tacú le comhshaol atá glan, táirgiúil agus cosanta go maith, agus le hiompar a chuirfidh le comhshaol inbhuanaithe.*

Ár bhFreagrachtaí

Ceadúnú
Déanaimid na gníomhaíochtaí seo a leanas a rialú ionas nach ndéanann siad dochar do shláinte an phobail ná don chomhshaol:
- saoráidí dramhaíola *(m.sh. láithreáin líonta talún, loisceoirí, stáisiúin aistrithe dramhaíola)*;
- gníomhaíochtaí tionsclaíocha ar scála mór *(m.sh. déantúsaíocht cógaisíochta, déantúsaíocht stroighne, stáisiúin chumhachta)*;
- an diantalmhaíocht *(m.sh. muca, éanlaith)*;
- úsáid shrianta agus scaoileadh rialaithe Orgánach Géinmhodhnaithe *(OGM)*;
- foinsí radaíochta ianúcháin *(m.sh. trealamh x-gha agus radaiteiripe, foinsí tionsclaíocha)*;
- áiseanna móra stórála peitril;
- scardadh dramhuisce;
- gníomhaíochtaí dumpála ar farraige.

Forfheidhmiú Náisiúnta i leith Cúrsaí Comhshaoil
- Clár náisiúnta iniúchtaí agus cigireachtaí a dhéanamh gach bliain ar shaoráidí a bhfuil ceadúnas ón nGníomhaireacht acu.
- Maoirseacht a dhéanamh ar fhreagrachtaí cosanta comhshaoil na n-údarás áitiúil.
- Caighdeán an uisce óil, arna sholáthar ag soláthraithe uisce phoiblí, a mhaoirsiú.
- Obair le húdaráis áitiúla agus le gníomhaireachtaí eile chun dul i ngleic le coireanna comhshaoil trí chomhordú a dhéanamh ar líonra forfheidhmiúcháin náisiúnta, trí dhíriú ar chiontóirí, agus trí mhaoirsiú a dhéanamh ar leasúchán.
- Cur i bhfeidhm rialachán ar nós na Rialachán um Dhramhthrealamh Leictreach agus Leictreonach (DTLL), um Shrian ar Shubstaintí Guaiseacha agus na Rialachán um rialú ar shubstaintí a ídíonn an ciseal ózóin.
- An dlí a chur orthu siúd a bhriseann dlí an chomhshaoil agus a dhéanann dochar don chomhshaol.

Bainistíocht Uisce
- Monatóireacht agus tuairisciú a dhéanamh ar cháilíocht aibhneacha, lochanna, uiscí idirchriosacha agus cósta na hÉireann, agus screamhuiscí; leibhéil uisce agus sruthanna aibhneacha a thomhas.
- Comhordú náisiúnta agus maoirsiú a dhéanamh ar an gCreat-Treoir Uisce.
- Monatóireacht agus tuairisciú a dhéanamh ar Cháilíocht an Uisce Snámha.

Monatóireacht, Anailís agus Tuairisciú ar an gComhshaol
- Monatóireacht a dhéanamh ar cháilíocht an aeir agus Treoir an AE maidir le hAer Glan don Eoraip (CAFÉ) a chur chun feidhme.
- Tuairisciú neamhspleách le cabhrú le cinnteoireacht an rialtais náisiúnta agus na n-údarás áitiúil *(m.sh. tuairisciú tréimhsiúil ar staid Chomhshaol na hÉireann agus Tuarascálacha ar Tháscairí)*.

Rialú Astaíochtaí na nGás Ceaptha Teasa in Éirinn
- Fardail agus réamh-mheastacháin na hÉireann maidir le gáis cheaptha teasa a ullmhú.
- An Treoir maidir le Trádáil Astaíochtaí a chur chun feidhme i gcomhair breis agus 100 de na táirgeoirí dé-ocsaíde carbóin is mó in Éirinn.

Taighde agus Forbairt Comhshaoil
- Taighde comhshaoil a chistiú chun brúnna a shainaithint, bonn eolais a chur faoi bheartais, agus réitigh a sholáthar i réimsí na haeráide, an uisce agus na hinbhuanaitheachta.

Measúnacht Straitéiseach Timpeallachta
- Measúnacht a dhéanamh ar thionchar pleananna agus clár beartaithe ar an gcomhshaol in Éirinn *(m.sh. mórphleananna forbartha)*.

Cosaint Raideolaíoch
- Monatóireacht a dhéanamh ar leibhéil radaíochta, measúnacht a dhéanamh ar nochtadh mhuintir na hÉireann don radaíocht ianúcháin.
- Cabhrú le pleananna náisiúnta a fhorbairt le haghaidh éigeandálaí ag eascairt as taismí núicléacha.
- Monatóireacht a dhéanamh ar fhorbairtí thar lear a bhaineann le saoráidí núicléacha agus leis an tsábháilteacht raideolaíochta.
- Sainseirbhísí cosanta ar an radaíocht a sholáthar, nó maoirsiú a dhéanamh ar sholáthar na seirbhísí sin.

Treoir, Faisnéis Inrochtana agus Oideachas
- Comhairle agus treoir a chur ar fáil d'earnáil na tionsclaíochta agus don phobal maidir le hábhair a bhaineann le caomhnú an chomhshaoil agus leis an gcosaint raideolaíoch.
- Faisnéis thráthúil ar an gcomhshaol ar a bhfuil fáil éasca a chur ar fáil chun rannpháirtíocht an phobail a spreagadh sa chinnteoireacht i ndáil leis an gcomhshaol *(m.sh. Timpeall an Tí, léarscáileanna radóin)*.
- Comhairle a chur ar fáil don Rialtas maidir le hábhair a bhaineann leis an tsábháilteacht raideolaíoch agus le cúrsaí práinnfhreagartha.
- Plean Náisiúnta Bainistíochta Dramhaíola Guaisí a fhorbairt chun dramhaíl ghuaiseach a chosc agus a bhainistiú.

Múscailt Feasachta agus Athrú Iompraíochta
- Feasacht chomhshaoil níos fearr a ghiniúint agus dul i bhfeidhm ar athrú iompraíochta dearfach trí thacú le gnóthais, le pobail agus le teaghlaigh a bheith níos éifeachtúla ar acmhainní.
- Tástáil le haghaidh radóin a chur chun cinn i dtithe agus in ionaid oibre, agus gníomhartha leasúcháin a spreagadh nuair is gá.

Bainistíocht agus struchtúr na Gníomhaireachta um Chaomhnú Comhshaoil
Tá an ghníomhaíocht á bainistiú ag Bord lánaimseartha, ar a bhfuil Ard-Stiúrthóir agus cúigear Stiúrthóirí. Déantar an obair ar fud cúig cinn d'Oifigí:
- An Oifig um Inmharthanacht Comhshaoil
- An Oifig Forfheidhmithe i leith cúrsaí Comhshaoil
- An Oifig um Fianaise is Measúnú
- Oifig um Chosaint Radaíochta agus Monatóireachta Comhshaoil
- An Oifig Cumarsáide agus Seirbhísí Corparáideacha

Tá Coiste Comhairleach ag an nGníomhaireacht le cabhrú léi. Tá dáréag comhaltaí air agus tagann siad le chéile go rialta le plé a dhéanamh ar ábhair imní agus le comhairle a chur ar an mBord.

EPA Research Report 339

High-resolution Climate Projections for Ireland – A Multi-model Ensemble Approach

Authors: Paul Nolan and Jason Flanagan

Regional climate models (RCMs) take the outputs from global climate models (GCMs) to produce more refined projections of the potential local and regional impacts of climate change. The current study used RCMs to simulate the mid-21st-century climate of Ireland. The projections were run at high spatial resolution (4 km), allowing a more realistic representation of important physical processes and enabling a more accurate evaluation of the local impacts. To address the uncertainty inherent in climate model projections, different RCMs were used to downscale outputs from a number of different CMIP5 (Coupled Model Intercomparison Project – Phase 5) GCMs. A statistical analysis of the resulting multi-model ensemble of downscaled datasets was completed allowing for the uncertainty in the projections to be partially quantified. To address the uncertainty in future emissions and changing land use, and how the world will come together to response to the challenge of climate change, the future climate was simulated under both Representative Concentration Pathway 4.5 (RCP4.5) and RCP8.5 scenarios. The climate projections of the current report are in broad agreement with previous research, which adds a measure of confidence to the projections.

Identifying Pressures

Ireland's climate is changing, resulting in higher temperatures, changing precipitation patterns and increases in the frequency and intensity of extreme events, with these changes expected to continue and intensify into the future. Ongoing and projected climate change impacts pose significant risks to all aspects of Ireland's economy, society and environment. Accurate climate projections, produced by high-resolution RCMs, can assist national policymakers to plan for, and adapt to, the adverse effects of climate change.

Informing Policy

This research will inform national climate policy and further the understanding of the potential impacts of climate change in Ireland. Furthermore, the research will inform the climate change adaptation action that various governmental departments and local authorities are mandated to undertake under the National Adaptation Framework. Selected findings from this study indicate that by the middle of this century (2041–2060):

- temperatures are projected to increase by 1–1.6°C compared with the baseline period (1981–2000), with the largest increases in the east;
- warming will be enhanced at the extremes (i.e. hot days and cold nights), with summer daytime and winter night-time temperatures projected to increase by 1–2.4°C;
- substantial decreases of approximately 50% are projected in the number of frost and ice days;
- summer heatwave events are expected to occur more frequently, with the largest increases in the south;
- precipitation is expected to become more variable, with substantial projected increases in the occurrence of both dry periods and heavy precipitation events.

The research presents projections of additional climate fields and derived variables that are of importance to sectors including agriculture, health, energy, biodiversity and transport.

Developing Solutions

The research provides Ireland with a data resource to explore Ireland's future climate and enables the assessment of the scale of impacts across sectors, at regional and local scales. This report provides an outline of the regional climate modelling undertaken to assess the impacts of climate change in Ireland, based on a number of possible future scenarios, and highlights the key findings. The project has also provided a large database that can be interrogated for various meteorological parameters, essential for detailed analysis across a diverse range of sectoral concerns.

EPA Research: McCumiskey House, Richiew, Clonskeagh, Dublin 14.

Phone: 01 268 0100
Twitter: @EPAResearchNews
Email: research@epa.ie